Series in Materials Science and Engineering

High-Pressure Surface Science and Engineering

Edited by

Yury Gogotsi and Vladislav Domnich

Department of Materials Science and Engineering, Drexel University, USA

IoP

Institute of Physics Publishing
Bristol and Philadelphia

Chapter 3

Continuum mechanical fundamentals of mechanochemistry

Valery I Levitas

Notation

SC	Structural changes
SMA	Shape memory alloys
CRs	Chemical reactions
PTs	Phase transitions
TRIP	Transformation-induced plasticity
RIP	Reaction-induced plasticity
RDAC	Rotational diamond anvil cell
G	Graphite
D	Diamond
Vectors and tensors are denoted in boldface type	
$\boldsymbol{A} \cdot \boldsymbol{B} = (A_{ij}B_{jk})$	Contraction of tensors over one nearest index
$\boldsymbol{A} : \boldsymbol{B} = A_{ij}B_{ji}$	Contraction of tensors over two nearest indices
$\boldsymbol{I}$	Unit tensor
-1	Superscript which denotes inverse operation
$:=$	Equals per definition
s	Subscript which designates symmetrization of the tensors
the indices 1 and 2 denote the values before and after the SC	
V	Region of multiphase material
S	Boundary of a region V
V_{n}	Region undergoing the SC
Σ_{n}	Boundary of region V_{n}
σ_y	Yield stress
τ_y	Yield stress in shear
$f(\boldsymbol{T}, \ldots, \xi) = 0$	Yield condition

M_s	Martensite start temperature
$\boldsymbol{\varepsilon}$	Total strain tensor
$\boldsymbol{\varepsilon}_t$	Transformation strain
$\boldsymbol{\varepsilon}_e$	Elastic strain
$\boldsymbol{\varepsilon}_p$	Plastic strain
ξ	Order parameter
s	Entropy
ψ	Helmholtz free energy
$\boldsymbol{g}$	Set of internal variables
θ	Temperature
θ_{ef}	Effective temperature
$\Delta\psi$	Difference in thermal parts of free energy
$\boldsymbol{r}$	Position vector
$\mathcal{D}$	Dissipation rate in the entire transforming volume (nucleus) due to SC only
X_v	Generalized (driving) force for SC
$\dot{\chi}$	Generalized rate
t_s	SC duration
$\boldsymbol{X}_p$	Dissipative force conjugated to dissipative rate $\dot{\boldsymbol{\varepsilon}}_p$
$\boldsymbol{X}_g$	Dissipative force conjugated to dissipative rate $\dot{\boldsymbol{g}}$
$*$	Superscript which denotes all virtual (not actual) parameters
X	Local driving force for structural changes
K	Dissipative threshold
K^0	A thermal threshold for SC
E_a	Activation energy per unit mass when $X = K^0$
n	Number of atoms in volume V_n which undergo thermal fluctuations
$N = 6.02 \times 10^{23}$	Avogadro's number
φ	Transformation work
$\boldsymbol{u}_s$	Tangential displacements
σ_n	Normal stress
τ	Shear stress
σ_c	Critical value of normal stresses
τ_s	Critical values of shear stresses
ε_0	Volumetric transformation strain
$\boldsymbol{u}$	Displacements
$\boldsymbol{p}$	Traction vector
E	Young's modulus
k	Compression modulus
μ	Shear modulus
ν	Poisson's ratio
θ_m	Melting temperature
r	Radius of spherical nucleus
t_{ob}	Accepted observation time

γ	Plastic shear
τ	Shear stress
ΔU_0	Jump in the reference internal energy per unit volume in the reference configuration
t_d	Time of deformation in the shear band
τ_e	Remote shear stress
$\gamma_{\mathrm{t}y}$	Value of γ_t at which plastic flow starts
u^*	Vertical displacement
P	External axial stress
u	Normal displacement
q	Accumulated plastic strain (Odqvist parameter)
F	Net thermodynamic driving force for SC
Γ	Surface energy per unit area
l	Length of the dislocation pile-up
$2L$, $2c$ and b	The lengths of a pill-box nucleus
$\boldsymbol{T}$	Stress tensor
$\boldsymbol{\sigma}$, $\boldsymbol{\sigma}_\mathrm{es}$ and $\boldsymbol{\sigma}_\mathrm{d}$	Contributions to total stress $\boldsymbol{T}$ from external stress, internal stresses due to transformation strain (Eshelby inclusion stress), and dislocation pile-up, respectively
τ_l and σ	Shear and normal stresses along sides L and c due to dislocation pile-up
N	Number of dislocations in a pile-up
$\boldsymbol{b}$	Burger's vector
Q	Activation energy
R	Radius of the anvil
h	Current thickness of the disc sample
c	Volume fraction of phase 2
$\boldsymbol{d}_\mathrm{p}$	Plastic strain rate
ΔX_d	Maximal microscopic contribution to transformation work
a, χ and ζ	Parameters
k, b and m	Parameters
p	Macroscopic hydrostatic pressure
p_e	SC equilibrium pressure
p_ε^d	Lowest possible pressure, below which strain-induced SC is impossible
p_h^d	Pressure, under which direct SC can occur under hydrostatic condition without a strain-induced contribution
p_h^r	Pressure, under which the reverse SC can occur under hydrostatic condition without a strain-induced contribution
p_ε^r	Maximal pressure under which the reverse SC can start with infinitesimal rate
h_0	Thickness at which rotation starts
ω_a	Angular velocity of an anvil
φ_a	Angle of rotation of an anvil

ω	Angular velocity of the deformed material
$\bar{\varphi}$	Angle of the relative sliding of an anvil with respect to the material
V_{r}	Radial velocity
τ_{r}	Radial component of the shear frictional stress $\boldsymbol{\tau}$ on the boundary S between the anvils and a disc
σ_0	Pressure at $r = R$
$\boldsymbol{v}_{\mathrm{s}}$	Velocity of relative sliding
e_z, e_r and e_θ	Normal components of the deformation rate tensor
$\hat{\gamma}$	Shear components of the deformation rate tensor
R	Radius of anvil
r_0	Radius of cBN phase
σ_{zi}	PT start pressure
h_{i}	Initial thickness
m	Mass of small transforming particle
σ_{ef}	Effective stress

3.1 Introduction

Mechanochemistry studies the effect of non-hydrostatic stresses and plastic strains on various structural changes (SCs), which include solid–solid, solid–liquid, and solid–gas chemical reactions (CRs) and phase transitions (PTs). SCs under high pressure and plastic shear are widespread in nature, physical experiments and modern technologies. Interpretation of a number of geophysical experiments and other phenomena is related to the analysis of various SCs under pressure and shear. In particular, one of the mechanisms of deep earthquakes is related to the instability caused by shear strain-induced PT [1–3]. Shear ignition of energetic materials [4–6] is subject to intensive study with the goal to assess safety issues. Mechanosynthesis (or mechanical alloying), i.e. strain-induced synthesis of various chemical compounds by ball milling, is another example [7, 8]. We also mention the importance of mechanochemical processes for understanding friction and wear, shear-induced metallization and oxidation.

The most fundamental results in strain-induced SCs were obtained in rotating Bridgman or diamond anvils (figure 3.28), see section 3.5.2. After compression of the materials in Bridgman or diamond anvils, a very high pressure is produced in the centre of the specimen which leads to a number of PTs and CRs. It is known, from numerous experiments that the addition of plastic shear, due to the rotation of an anvil, leads to findings that have both fundamental and applied importance. In particular, it leads to the following results: (a) a significant (by a factor of 3–5) reduction in SC pressure and pressure hysteresis; (b) the appearance of new phases, which could not be obtained without additional shear; (c) the substitution of a reversible PT by an irreversible PT; and (d) strain-controlled kinetics. These experimental results are discussed in detail in section 3.5.

Table 3.1. Typical values of transformation strains.

	Shear	Volumetric
Steels	0.2	−(0.02–0.05)
Shape Memory Alloys	0.1–0.2	∼0
Graphite → Diamond	0.31	0.54
hBN → cBN	0.31	0.54
Plutonium $\delta \rightarrow \alpha$	0.27	0.20
Twinning in bcc and fcc	0.71	0

As the main geometrical characteristic of SCs we consider the transformation strain. For a martensitic PT, the transformation strain (Bain strain) transforms the crystal lattice of the parent phase (austenite) into the crystal lattice of the product phase (martensite). The transformation strain cannot be arbitrary (as elastic or plastic strain). For each PT it is some fixed tensor within the symmetry operations. All intermediate values of the transformation strain are unstable and cannot exist in an equilibrium. For a solid–solid SC, including reconstructive PTs and CRs, the transformation strain, $\boldsymbol{\varepsilon}_{\mathrm{t}}$, transforms an infinitesimal volume or unit cell of the stress-free parent phase into an infinitesimal volume of the stress-free product phase. We neglect all internal atomic displacements (e.g. shuffles) inside the volume under consideration. The stress tensor does not produce work on these displacements and we assume that they are expressed in terms of the transformation strain by energy minimization.

Consequently we define the SC as a thermomechanical deformation process as the transformation strain $\boldsymbol{\varepsilon}_{\mathrm{t}}$ goes from $\boldsymbol{\varepsilon}_{\mathrm{t1}}$ in the initial phase to the final value $\boldsymbol{\varepsilon}_{\mathrm{t2}}$ in the product phase, which is accompanied by a jump in all the thermomechanical properties.

Typical values of components of transformation strain are shown in table 3.1. For comparison, the maximum elastic shear strain (the yield strain) is equal to the yield stress divided by the elastic modulus, and is of order 0.001 for steels and 0.01 for shape memory alloys (SMA). The transformation strains are significantly larger than the elastic strains. A list of the transformation strain tensors for various PTs can be found in [9, 10].

Our main goal is to study high-pressure mechanochemistry. However, we will consider some problems at normal pressure as well. There are two reasons to do this. First, the general theory has to be valid at both normal and high pressure. Second, the effect of non-hydrostatic stresses and plastic strains has been studied much more completely at normal pressure, especially for SMAs and steels. Transferring and extending some of the definitions, concepts, regularities and approaches to the high-pressure field may be very useful.

Let us refresh the classification of a martensitic PT under normal pressure. We will distinguish three types of PTs: temperature-induced, stress-induced and strain-induced. Except for some special cases (see, e.g., [11]), heterogeneous

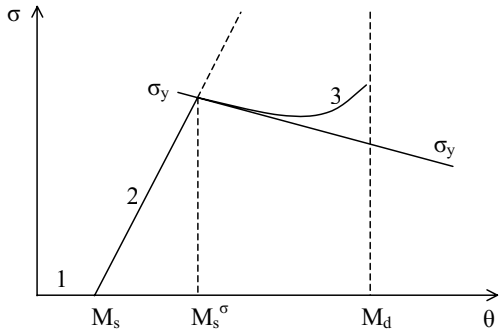

Figure 3.1. Schematic representation in stress (σ)–temperature (θ) plane of temperature-induced PTs (1), stress-induced PTs (2) and strain-induced PT (3).

nucleation takes place at pre-existing or new defects (dislocations, grain, subgrain, and twin boundaries). Temperature-induced PTs occur predominantly at pre-existing defects with no stresses at the specimen surface. Stress-induced (in particular, pressure-induced) PTs occur predominantly by nucleation at the same pre-existing defects when external stresses do not exceed the macroscopic yield limit σ_y. If the PT occurs during plastic flow, it is classified as a strain-induced PT, i.e. one that occurs by nucleation at new defects generated during plastic flow [12–15].

Temperature-induced PTs originate at the martensite start temperature M_s (figure 3.1 [13]). Strain-induced PTs occur at temperature above M_s^σ and below M_d. Above M_d, PT cannot be caused by strain at ambient pressure. Stress-induced PTs occur between the M_s^σ and M_s temperatures. Usually, the term stress-assisted PT is used [12–15] but to make this classification consistent with the term pressure-induced SCs, we will use the term stress-induced SCs.

Of course, there is some overlap between all these types of PTs; e.g., even without any external stresses, huge internal stresses exist during temperature-induced PTs, which can cause plastic flow and generate new defects (see section 3.4.5). This causes the so-called autocatalytic effect [15]. The same is true for stress- and pressure-induced PTs.

However, such a classification allows us to separate the main features from the secondary details. As will be shown in section 3.5.7, SCs in a rotational diamond anvil cell are strain-induced SCs rather than pressure-induced, which require completely different experimental and theoretical characterization.

Let us enumerate some examples of interaction between SCs and plasticity.

1. SCs, because of the transformation strain, represent an inelastic deformation process. For SMAs, a PT is the main mechanism of inelasticity. For most materials, the transformation strain is one of the contributions, along with

dislocation plasticity, twinning and others.

2. Slip represents a mechanism for lattice-invariant shear, an alternative to twinning (combination of two martensitic variants). It produces, in combination with the Bain strain and rotation of the crystal lattice, an invariant plane strain variant [16]. This significantly reduces the energy of the internal stresses and increases the driving force for nucleation and growth.
3. The appearance of large transformation strains (see table 3.1) in some regions of a body results in large stresses and accommodational inelastic strains in the transforming regions and their surroundings. Consequently, plasticity is an accommodation mechanism which reduces the internal stresses and increases the driving force for nucleation. However, stress redistribution near the growing martensitic units reduces the driving force for interface propagation. For PTs in elastic materials, the martensitic unit is arrested by a strong obstacle like a grain boundary or another martensitic unit, i.e. a plate martensite is formed. Plasticity leads to growth arrest inside the grain and to a morphological transition from the plate to the lath martensite. Analytical and numerical results illustrating these statements are presented in sections 3.3.1, 3.3.4, 3.4.1, 3.4.2, 3.4.4 and 3.4.5.
4. Plastic deformation generates defects, which serve as nucleation sites. However, the defect structure resists interface propagation. Preliminary plastic deformation suppresses martensitic PTs.
5. Plastic flow during PTs significantly promotes them. It causes a strain-induced PT which occurs by nucleation at the new defects generated during plastic flow, e.g. at slip–band intersections. For stress-induced PTs, the transformation stress increases (almost linearly) with temperature growth (figure 3.1). For strain-induced PTs, the transformation stress decreases with an increase in temperature because of a reduction in the yield stress with temperature increase.
6. The transformation strain produces huge internal stresses which, in combination with external stresses (which can be significantly smaller than the yield stress), cause plastic flow. This phenomenon is called transformation-induced plasticity (TRIP) for PTs [12, 17–20] or reaction-induced plasticity (RIP) for CRs [6]. TRIP serves as an inelastic deformation mechanism and as a mechanism of deviatoric stress relaxation. For a cyclic direct–reverse PT under an external stress which is less than the yield stress, plastic strain due to TRIP is accumulated in each cycle and can reach hundreds of percents.

We should also mention the phenomena which occur in rotating Bridgman or diamond anvils, which were described earlier and will be analysed in section 3.5. A knowledge of the influence of the plastic strain, applied and local stress fields on SCs is very important for understanding, simulating and improving technical processes, as well as for developming new technologies and materials.

We will distinguish coherent SC when displacements are continuous across the interface from semicoherent SC. For incoherent SC, the shear stress is absent at the interface and there is no lattice correspondence.

For a description of a SC in an elastic solid, the principle of a minimum of Gibbs free energy is usually used. For inelastic materials there has been no corresponding principle. It has been necessary to develop a conceptually new approach and to verify it by explanation and interpretation of a number of experimental phenomena.

This chapter is organized as follows. In section 3.2, the general theory of SC in inelastic materials, developed by the author in [21, 22], is summarized. In section 3.3, some analytical solutions based on our theory and their application to some real situations are analysed. Section 3.4 is devoted to an analysis of our published numerical solutions and their applications. In section 3.5, a new multiscale theory of strain-induced SCs under high pressure is developed and applied to interpret the numerous phenomena which occur during compression and shear of materials in a rotational diamond anvil cell.

Direct tensor notation is used throughout this chapter. Vectors and tensors are denoted in boldface type; $\boldsymbol{A} \cdot \boldsymbol{B} = (A_{ij} B_{jk})$ and $\boldsymbol{A} : \boldsymbol{B} = A_{ij} B_{ji}$ are the contraction of tensors over one and two nearest indices. A superscript -1 denotes an inverse operation, $:=$ means equals per definition, subscript s designates symmetrization of the tensors, the indices 1 and 2 denote the values before and after the SC.

3.2 Theory of structural changes in inelastic materials

We will present our theory developed over the last ten years and presented in its most current form in [21, 22]. A short overview of previous approaches and comparison with some alternative approaches will be given in section 3.2.8.

3.2.1 Problem formulation

In order to illustrate the general ideas without unnecessary formal complications, we consider the formulation for small strain. Finite strain theory and computations can be found in [21, 23–26]. Consider a region V of a multiphase material with the prescribed boundary conditions at a boundary S (figure 3.2). Assume that in some region V_n with the boundary Σ_n, due to SC during the time Δt, new nuclei appear, i.e. some material region V_n undergoes a SC. The main equations describing the SC are presented in Box 3.1.

The transformation strain $\boldsymbol{\varepsilon}_\mathrm{t}$ has to be taken into account in an additive decomposition (3.1) of a total strain tensor $\boldsymbol{\varepsilon}$, where $\boldsymbol{\varepsilon}_\mathrm{e}$ and $\boldsymbol{\varepsilon}_\mathrm{p}$ are the elastic and plastic strains. It is useful to introduce the internal dimensionless time (order parameter)

$$\xi := \frac{|\boldsymbol{\varepsilon}_\mathrm{t} - \boldsymbol{\varepsilon}_\mathrm{t1}|}{|\boldsymbol{\varepsilon}_\mathrm{t2} - \boldsymbol{\varepsilon}_\mathrm{t1}|} \qquad (0 \le \xi \le 1)$$

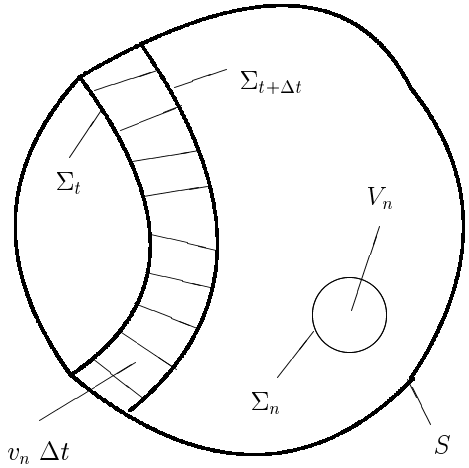

Figure 3.2. Volume with SCs.

which has the following properties: The SC starts at $\xi = 0$ and finishes at $\xi = 1$. The internal time ξ plays a similar role in the consideration of the SC in a material point as the volume fraction of the product phase for the averaged description of a SC does. All material functions (yield function f, stress $\boldsymbol{T}$, entropy s) and standard constitutive equations (3.2)–(3.4) (elasticity law, flow rule, evolution equations for internal variables and so on) are dependent on ξ and have to be given. At $\xi = 0$ and $\xi = 1$ they coincide with the functions and relations for the first and second phase, respectively. For the Helmholtz free energy we assume $\psi = \psi(\boldsymbol{\varepsilon}_\mathrm{e}, \theta, \boldsymbol{\varepsilon}_\mathrm{p}, \boldsymbol{g}, \boldsymbol{\varepsilon}_\mathrm{t}, \xi)$, where $\boldsymbol{g}$ is a set of internal variables, e.g. back stress, dislocations or point defect density and θ is the temperature.

We introduce into the nucleus the transformation strain field $\boldsymbol{\varepsilon}_\mathrm{t}(\boldsymbol{r}, \xi)$ as eigenstrains at the fixed boundary conditions and change, in some way, all the material properties from the properties of phase 1 to the properties of phase 2, where $\boldsymbol{r}$ is the position vector and ξ grows from 0 to 1. After solving the inelastic boundary value problem, we determine all fields (stress $\boldsymbol{T}$, $\boldsymbol{\varepsilon}$, θ and so on). Then we should answer three questions:

1. Is SC possible for the given boundary and initial conditions?
2. How do we define all unknown parameters which we designate as $\boldsymbol{b}$, e.g. position, volume, shape and orientation of the nucleus, actual field $\boldsymbol{\varepsilon}_\mathrm{t}(\boldsymbol{r}, \xi)$?
3. How long does such a nucleation event occur?

Note that under the term nucleus we will often understand some macroscopic region which appeared during the nucleation and growth processes. The key points of our approach are discussed in the following [22].

Using the second law of thermodynamics, the dissipation rate in the entire

transforming volume (nucleus) due to the SC only, $\mathcal{D}$, is separated from other dissipative contributions, see equations (3.9) and (3.10), with explicit expressions for the generalized (driving) force X_v and rate $\dot{\chi}$. Here Γ is the surface energy per unit area. The force is the total dissipation increment due to SC only during the complete SC in the transforming region; the rate is the inverse SC duration t_s. The local driving force for SC X can be determined as the difference between the local total dissipation and the local dissipation due to dissipative processes other than SC (in our case plastic flow and variation of internal variable), see equation (3.8). Here $\boldsymbol{X}_p$ and $\boldsymbol{X}_g$ are the dissipative forces conjugated to the dissipative rates $\dot{\boldsymbol{\varepsilon}}_p$ and $\dot{\boldsymbol{g}}$, respectively, i.e. $\boldsymbol{X}_p : \dot{\boldsymbol{\varepsilon}}_p$ and $\boldsymbol{X}_g : \dot{\boldsymbol{g}}$ is the dissipation rate due to plastic flow and variation of the internal variable.

We will distinguish two types of SC kinetics:

- athermal or rate-independent kinetics, for which real time and rate do not play a part—the SC occurs instantaneously when the SC criterion is satisfied; and
- time-dependent (true) kinetics.

3.2.2 Time-independent kinetics: SC criterion

We will start with time-independent kinetics, for which question 3 is irrelevant. Time-independent kinetics can be applied to the appearance of an arbitrary macroscopic region by nucleation and growth. To answer the first two questions, the thermomechanical SC criterion (3.11) and extremum principle (3.12) were derived, where K is the experimentally determined dissipation increments during the SC, related to the SC only (excluding plastic dissipation and dissipation due to other dissipative processes) and the superscript $*$ denotes all virtual (not actual) parameters and fields. To derive the SC criterion (3.11) the following assumptions are made [21, 22].

Box 3.1. Main equations describing phase transitions [22, 24]

---

1. Kinematic decomposition

$$\boldsymbol{\varepsilon} = \boldsymbol{\varepsilon}_e + \boldsymbol{\varepsilon}_p + \boldsymbol{\varepsilon}_t. \tag{3.1}$$

2. Constitutive equations

   2a. Elasticity law and expression for entropy

$$\boldsymbol{T} = \frac{\partial \psi(\ldots, \xi)}{\partial \boldsymbol{\varepsilon}_e} \qquad s = -\frac{\partial \psi(\ldots, \xi)}{\partial \theta}. \tag{3.2}$$

2b. Yield condition and plastic flow rule

$$f(\boldsymbol{T}, \ldots, \xi) = 0 \qquad \dot{\boldsymbol{\varepsilon}}_{\mathrm{p}} = \boldsymbol{f}_p(\boldsymbol{X}_{\mathrm{p}}, \xi) \qquad \boldsymbol{X}_{\mathrm{p}} := \boldsymbol{T} - \frac{\partial \psi}{\partial \boldsymbol{\varepsilon}_{\mathrm{p}}}. \quad (3.3)$$

2c. Evolution equation for internal variables

$$\dot{\boldsymbol{g}} = \boldsymbol{f}_g(\boldsymbol{X}_{\mathrm{g}}, \xi) \qquad \boldsymbol{X}_{\mathrm{g}} := -\frac{\partial \psi}{\partial \boldsymbol{g}^t}. \quad (3.4)$$

3. Sliding and fracture conditions at the interface

$$|\sigma_{\mathrm{n}}| < \sigma_{\mathrm{c}} \text{ or } |\tau| < \tau_{\mathrm{s}} \Rightarrow \dot{\boldsymbol{u}}^2 - \dot{\boldsymbol{u}}^1 = \boldsymbol{0} \qquad \text{(coherent interface)} \quad (3.5)$$

$$|\tau| = \tau_{\mathrm{s}} \Rightarrow \dot{\boldsymbol{u}}_s^2 - \dot{\boldsymbol{u}}_s^1 \neq \boldsymbol{0} \qquad \text{(semicoherent interface)} \quad (3.6)$$

$$|\sigma_{\mathrm{n}}| = \sigma_{\mathrm{c}} \Rightarrow \dot{\boldsymbol{u}}^2 - \dot{\boldsymbol{u}}^1 \neq \boldsymbol{0} \qquad \sigma_n = \tau = 0 \qquad \text{(fracture)}. \quad (3.7)$$

4. Local driving force for structural changes

$$X := \int_{\boldsymbol{\varepsilon}_1}^{\boldsymbol{\varepsilon}_2} \boldsymbol{T} : \mathrm{d}\boldsymbol{\varepsilon} - (\psi_2 - \psi_1) - \int_t^{t+\Delta t} (s\dot{\theta} + \boldsymbol{X}_{\mathrm{p}} : \dot{\boldsymbol{\varepsilon}}_{\mathrm{p}} + \boldsymbol{X}_{\mathrm{g}} : \dot{\boldsymbol{g}})\, \mathrm{d}t. \quad (3.8)$$

5. Global dissipation rate $\mathcal{D}$ and global driving force for structural changes X_v

$$\mathcal{D} = X_v \dot{\chi} \qquad \dot{\chi} := 1/t_{\mathrm{s}} \quad (3.9)$$

$$X_v := \bar{X} V_{\mathrm{n}} = \int_{V_{\mathrm{n}}} X \,\mathrm{d}V_{\mathrm{n}} - \int_{\Sigma_{\mathrm{n}}} \Gamma \,\mathrm{d}\Sigma_{\mathrm{n}}. \quad (3.10)$$

6. Time-independent kinetics

6a. SC criterion

$$\bar{X} = K. \quad (3.11)$$

6b. Extremum principle for the determination of all unknown parameters $\boldsymbol{b}$

$$\bar{X}(\boldsymbol{b}^*) - K(\boldsymbol{b}^*) < 0 = \bar{X}(\boldsymbol{b}) - K(\boldsymbol{b}). \quad (3.12)$$

6c. Dissipative threshold K

$$K = L\sigma_{\mathrm{y}}\varepsilon_o. \quad (3.13)$$

6d. Extremum principle for determination of stable solution (global SC criterion)

$$\int_S \int_{\boldsymbol{u}_1}^{\boldsymbol{u}_2} \boldsymbol{p} \cdot \mathrm{d}\boldsymbol{u}\, \mathrm{d}S \Rightarrow \min \qquad \text{(particular case at prescribed } \boldsymbol{u} \text{ at } S). \quad (3.14)$$

7. Thermally activated kinetics

7a. SC criterion

$$\bar{X} \geq K^0. \tag{3.15}$$

7b. Kinetic equation

$$t_s = t_0 \exp\left(-\frac{(\bar{X} - K^0 - E_a)V_n}{R\theta_{ef}}\frac{N}{n}\right) \qquad \text{at } 0 \leq \bar{X} - K^0 \leq E_a. \tag{3.16}$$

7c. Principle of the minimum of the transformation time

$$t_s = t_0 \exp -\frac{(\bar{X}(\boldsymbol{b}^*) - K^0(\boldsymbol{b}^*) - E_a(\boldsymbol{b}^*))m_n^*}{R\theta_{ef}^*}\frac{N}{n} \longrightarrow \min. \tag{3.17}$$

---

1. Instead of attempting to formulate the conditions for a finite nucleus or moving discontinuity surface (interface) immediately, we developed a local approach. This allows us to consider the SC process (variation of ξ from 0 to 1) at each material point and to try to apply a standard thermodynamic approach (as, e.g., in plasticity theory). This is done for points both in the new nucleus and a moving interface, i.e. the description of the nucleation and interface propagation is unified.
2. We do not consider the dissipation rate for each ξ (which is usual in irreversible thermodynamics) but the dissipation increment during the whole SC. In the opposite case we can, due to the choice of stress tensor or temperature, stop the SC at an arbitrary ξ which contradicts experiments and our definition of SC without a stable intermediate state [22]. At $0 < \xi < 1$, a non-equilibrium process takes place, which requires energy and stress fluctuations. We do not know any similar contradiction in the application of continuum thermodynamics. In this case, a standard thermodynamic approach cannot be applied. It is necessary to average the thermodynamic parameters, related to SC, over the SC duration t_s in order to filter off these fluctuations, which results in a consideration of the dissipation increment.
3. We assume that the SC is thermodynamically independent of other processes, e.g. plastic flow, i.e. $X > 0$ is independent of $\dot{\boldsymbol{e}}_p$ and $\dot{\boldsymbol{g}}$. Interaction between the various dissipative processes occurs only through the stress field, which is typical for micromechanical studies of, e.g., dislocation and point defect motion.
4. We assume the independence of the generalized force $\bar{X}$ of the rate $\dot{\chi}$, i.e. instantaneous kinetics. This is similar to plastic strain rate independence of stress for one-dimensional rate-independent plasticity.
5. We assume the *validity of SC condition (3.11) in a finite volume without fulfilment of the local SC criterion at each point of the nucleus*. This is a consequence of the fact that, due to allowing for surface energy, the entire

thermodynamic description and nucleation condition are non-local. This implies, in particular, that at $K = 0$ the dissipation increment may be negative at some points.

The formulation based on SC condition (3.11) and extremum principle (3.12) is consistent in the limit case with the classical description of SC in elastic materials based on the principle of minimum Gibbs free energy [21].

If ψ depends only on $\boldsymbol{\varepsilon}_{\mathrm{e}}$, θ and ξ and if the elastic properties of the phases are the same, the surface energy is negligible, for the isothermal approximation and homogeneous θ and K in the nucleus, we obtain the following SC criterion:

$$X - K = \varphi - \Delta\psi(\theta) - K = 0 \qquad \varphi := \frac{1}{V_{\mathrm{n}}} \int_{V_{\mathrm{n}}} \int_{\boldsymbol{\varepsilon}_1^t}^{\boldsymbol{\varepsilon}_2^t} \boldsymbol{\sigma} : \mathrm{d}\boldsymbol{\varepsilon}^t \, \mathrm{d}V_{\mathrm{n}} \qquad (3.18)$$

where $\Delta\psi$ is the difference in the thermal parts of the free energy. The extremum principle (3.12) results in a maximum of the transformation work φ.

It is necessary to note that the SC criterion (3.11) includes the history of stress variation $\boldsymbol{T}$ in the nucleus during the SC, i.e. we cannot define the SC condition using only the initial stresses before SC. We have to solve the elastoplastic problem and determine the variation in the stresses in the nucleus during the SC in order to calculate the transformation work φ in equation (3.18).

3.2.3 Postulate of realizability. Extremum principle

To derive extremum principle (3.12), the previously formulated postulate of realizability [21, 22, 27, 28] is applied. The main idea consists of two points:

- we prove, that if inequality $(3.12)_1$ is valid for all variable parameters, then a SC cannot occur, because the SC criterion is not satisfied; and
- we assume that if, in the course of varying the boundary conditions, the SC criterion is satisfied for the *first time* for some parameter $\boldsymbol{b}$ and SC can occur, it will occur.

The postulate of realizability represents a simple and natural assumption which expresses explicitly a concept for stability. In fact, if some dissipative process (SC, plastic flow) can occur from an energetic point of view but does not occur, then such a situation is not stable, because various fluctuations provoke the beginning of a process. Various applications of the postulate of realizability to plasticity, irreversible thermodynamics, PTs, CRs, ductile fracture, twinning, problem of plastic spin and stability analysis [6,21–25,28–32] give the impression that this postulate expresses a general essential property of dissipative systems. The mathematical study of the extremum principle for elastic materials which follows from the postulate of realizability was carried out in [33].

3.2.4 Semicoherent interface and interface with a fracture

One of the mechanisms for getting more favourable stress variation in the transforming particle is related to the possibility of displacement discontinuities on the moving or fixed (at nucleation) interface. The tangential to the jump in displacements interface produces so-called semicoherence and is connected with the generation and sliding of dislocations on the interface with the Burgers vector tangential to the interface. The jump from normal to interface displacement is a fracture. Three types of interfaces between the new and old phases are considered: coherent (with continuous displacements across the interface), semicoherent (with discontinuous tangential displacements $\boldsymbol{u}_{\mathrm{s}}$) and the interface with fracture (with a crack at the interface). The key point of our approach [21,23,27,28,34,35] is that the displacement discontinuities are treated as a *contact problem*. We assume that the SC and fracture (semicoherence) criteria are thermodynamically independent and that these processes are coupled only through the stress fields. The simplest sliding and fracture criteria are presented in equations (3.5)–(3.7), where σ_{n} and τ are normal and shear stresses at the interface; σ_{c} and τ_{s} are critical values of normal and shear stresses. If during the growth of $\boldsymbol{\varepsilon}_{\mathrm{t}}$ and variation in the material properties in a nucleus, a chosen fracture criterion is met at some point of the interface, a crack appears or grows. If, in the same process, the semicoherence criterion is satisfied, we admit sliding at this point until a value where the criterion is violated is reached. After completing the SC, we check with the SC criterion to check whether SC is thermodynamically admissible.

Note that the notion of semicoherence in continuum mechanics is related to a displacement discontinuity across the interface, which may occur both in elastic and plastic materials. In the material literature, semicoherence is related to dislocation generation which is an attribute of plastic flow.

3.2.5 Estimation of dissipative threshold K

There are a lot of sources of dissipation K due to PTs [36]:

1. interaction of a transformation strain or moving interface with various defects, e.g. point defects (solute and impurity atoms, vacancies), dislocations, grain, subgrain and twin boundaries and precipitates;
2. Emission of acoustic waves; or
3. periodic resistance force (Peierls barrier) in the crystal.

The value of K can differ for nucleation and interface propagation, as well as for direct and reverse SC and it seems to be a very complex functional of the thermomechanical deformation process and the material microstructure. At the same time we found [21,34] the surprisingly simple formula (3.13) by comparing some high-pressure experiments [37–39] with the solution of the corresponding boundary-value problem, where σ_y is the yield stress, ε_0 is the volumetric transformation strain and L is the coefficient. The values of L were determined in [21,34] for some materials and are given in table 3.2.

Table 3.2. Values of parameter L for different materials.

Materials	L
RbCl, KCl, KBr	5.89
CdS, CdSe	1.39
Ce, InSb, Bi	0.11
Steel Fe + 30% Ni	7.5
Graphite–diamond	~ 3

The physical interpretation of equation (3.13) is discussed in the following. The parameter K characterizes an interaction between a moving interface and the material's microstructure and the yield stress is an integral characteristic of the microstructure because plastic flow represents the motion of dislocations through the same obstacles (point, linear and other defects). If we assume the validity of equation (3.13) in the general case, then the dependence of K on temperature, plastic strain, plastic strain rate and history, grain size and so on is determined. At large strain, according to the regularity revealed in [40], σ_y and, consequently, K have to be strain and strain-history independent.

A linear relation between K and σ_y for SMAs follows from experimental results in [41–44], because both the stress hysteresis (which is proportional to K) and yield stress are linear functions of plastic strain.

One of the microscopic mechanisms for the appearance of threshold-type dissipation is revealed in our paper [45]. We introduced and studied a system without dissipation but with microkinetic energy which is used to simulate microscopic fluctuations. It appears that the transition from macroscopic kinetic energy to microscopic one (the thermalization phenomenon) results in macroscopic behaviour, which can be described in terms of the threshold-type dissipative term K.

3.2.6 Global SC criterion

It is possible that under a given increment in the boundary conditions the local SC criterion and extremum principle (3.12) will allow several solutions, e.g. nucleation in different places or propagation of different interfaces. At least two solutions are always possible: first, a solution without SC (because all equations of continuum mechanics can also be satisfied without SC); and second, the solution with SC. This means that, in some cases, SC will not occur despite the local SC criterion and the extremum principle (3.12) can be satisfied. Inelastic deformations due to SC and dislocation plasticity represent two competitive mechanisms of plasticity and it is necessary to find a way to describe such a competition and overcome the non-uniqueness. Such a situation was revealed for the first time in [27, 28]. It was suggested that the *best* unique solution among

all the possible ones is the *stable* one. To formulate the stability criterion, the *postulate of realizability* is applied again. Using this, the extremum principle for the whole volume is derived to obtain the stable solution. The general extremum principle [28] is too bulky. Here we will use the simplified version (3.14) of this principle with the prescribed displacements $\boldsymbol{u}$ at the boundary S of region V, where $\boldsymbol{p}$ is the traction vector, and $\boldsymbol{u}_1$ and $\boldsymbol{u}_2$ correspond to the start and end of SC. It follows from principle (3.14) that the stable solution minimizes the work of the external stresses. Consequently, fulfilling the local SC criterion is not sufficient for the occurrence of SC and only extremum principle (3.14)—which represents the global SC criterion—gives the final solution. An application of stability analysis to strain-induced nucleation at a shear-band intersection can be found in [31] and in section 3.4.3.

3.2.7 Time-dependent kinetics

As shown in [22], the time-independent model can lead to some contradictions. That is why a time-dependent kinetic equation for nucleation is necessary.

As is usual in irreversible thermodynamics, the kinetic equation between the rate and force $\dot{\chi} = f(X_v, \ldots)$ has to be given. As an example we consider *size-dependent* Arrhenius-type kinetics which includes both *thermal* activation and an *athermal* threshold K^0, see equation (3.16). Here E_a is the activation energy per unit mass at $\bar{X} - K^0 = 0$, $R = 8.314$ J K^{-1} mol^{-1} is the gas constant, t_0 some characteristic time, n the number of atoms in volume V_n which undergo thermal fluctuations, $N = 6.02 \times 10^{23}$ is Avogadro's number (number of atoms in 1 mol) and θ_ef the effective temperature. Condition $\bar{X} - K^0 \geq 0$ is the SC criterion (at $\bar{X} - K^0 < 0$, $\dot{\chi} = 0$). The last inequality in equation (3.16) means the positiveness of the actual activation energy $\bar{E}_a := E_\mathrm{a} - \bar{X} + K^0$. By introducing the effective temperature, we also take into account the fact that the temperature can vary significantly during SC. As the simplest variant we define the effective temperature as the temperature averaged over the transformation process and transforming volume. Using the postulate of realizability [22,28], *the principle of the maximum of transformation rate* or *minimum of transformation time* is derived, see equation (3.17). In most cases the characteristic size of the nucleus cannot be determinable from principle (3.17) alone, because the thermodynamic criterion of SC is violated. Then the thermodynamic restriction $\bar{X}(\boldsymbol{b}^*) - K^0(\boldsymbol{b}^*) = 0$ has to be taken into account. Allowing for this constraint in equation (3.17) results, in extremum principle, in

$$\frac{E_\mathrm{a}(\boldsymbol{b}^*) m_n^*}{\theta_\mathrm{ef}^*} \to \min \tag{3.19}$$

or, with mutually independent E_a, m_n and θ_ef, results in three principles:

$$E_\mathrm{a}(\boldsymbol{b}^*) \to \min \qquad m_n^* \to \min \qquad \theta_\mathrm{ef}^* \to \max \tag{3.20}$$

namely in *the principle of the minimum of the transforming volume mass*, *the minimum of activation energy* and *the maximum of the effective temperature*. Due to thermodynamic restriction $\bar{X}(\boldsymbol{b}^*) - K^0(\boldsymbol{b}^*) = 0$, the simplified kinetic equation

$$t_s = t_0 \exp\left(\frac{E_a m_n}{R\theta_{ef}} \frac{N}{n}\right) \tag{3.21}$$

follows from equation (3.16).

A general scheme for applying the SC criterion and extremum principle (3.17), as well as the temperature evolution equation is as follows. All material properties and constitutive equations must be given for each intermediate state of the SC. Then assume that, at some initial conditions and prescribed boundary conditions, some SC occurs in some region V_n. In some way, we introduce incrementally the transformation strain and change the material properties (elastic moduli, heat capacity, thermal expansion coefficient and yield strength) from the initial to final values in a possible SC region. After solving the elastoplastic and thermal boundary-value problems for each step, we determine the variation in all fields, calculate the driving force $\bar{X}$ and resistance K^0 and at $\bar{X} - K^0 \geq 0$ determine the SC time t_s from equation (3.16) or equation (3.21). Then we vary the possible SC region and way of varying the transformation strain and properties from initial to final values in it and find such a SC region and way of varying the transformation strain and properties which minimize the transformation time.

The kinetic approach developed here allows us to receive qualitatively new results, in particular to introduce a kinetic concept of a thermodynamically admissible nucleus and to determine the actual geometric parameters of the new nucleus (see sections 3.3.1, 3.3.4 and 3.4.4).

3.2.8 Short history of the development of the continuum thermodynamic theory of SC in inelastic materials

To describe a PT in an elastic solid, the principle of minimum of Gibbs free energy is usually used. For inelastic materials, there was no corresponding principle, so a new approach had to be developed. Without any attempt to review all the related publications, we will limit ourselves to the main contributions to the continuum thermodynamic description of PTs in inelastic materials. We do not know any previous work on CRs in plastic materials; however, as shown in [6, 22], the formal continuum theory is the same for PTs and CRs.

3.2.8.1 Nucleation

The first results were related to the solution of some simple model problems. Lifshitz and Gulida [46] have considered the melting of a small spherical particle in an elastoplastic space. The appearance of the spherical nucleus in a sphere under applied external pressure was analysed in a paper by Roitburd and Temkin [47]. Bar'yachtar *et al* [48] using a Landau-type theory examined the appearance

of a spherical and plate-like nucleus in an infinite space without external forces. The ellipsoidal nucleus in an infinite space without external forces was considered by Kaganova and Roitburd [49]. In these papers the deformation theory of plasticity, which is thermodynamically equivalent to nonlinear elasticity, was used. In most of these papers the PT criterion and extremum principle for the definition of some unknown parameters are the same as for PTs in elastic materials, i.e. the Gibbs free energy of the whole system is minimized. It is known that, in contrast to elastic materials, such an extremum principle could not be proved for elastoplastic ones due to the necessity of considering the plastic dissipation and path-dependency.

An important conclusion was made in a paper by Roitburd and Temkin [47] that (in contrast to elastic material) the nucleation and interface propagation conditions in elastoplastic materials do not coincide. In this case the formulation of the problem of finding the equilibrium shape of a new phase inclusion in a paper by Kaganova and Roitburd [49] does not seem to us to be correct. They look to see which shape of inclusion corresponds to the minimum energy losses as it grows. As the new phase should appear first of all, the search for the shape of the new nucleus according to the extremum principles (3.12) (for time-independent kinetics) and (3.17) (for thermally activated kinetics) would be more appropriate.

Only in the paper by Roitburd and Temkin [47] is an alternative description of the appearance of a spherical nucleus used. It is assumed that some mechanical work (not energy !) should be less than the change in the chemical free energy which, in some particular cases, can be derived from recent considerations. Unfortunately this idea was not developed any further: the appearance of the ellipsoidal nucleus [49] is based on the principle of the minimum of the free energy. Numerous investigations of PTs in elastoplastic materials (Fischer *et al* [50], Marketz and Fischer [51–53]) are related to a comparison of the Gibbs free energy before and after the PT. Olson and Cohen [13, 15, 54] developed a dislocation model of martensite nucleation. The material and physical aspects of nucleation theory are reviewed by Olson and Roytburd [55]. Nucleation at some dislocation configurations and crack tip was studied by Boulbitch and Toledano [56] and Reid *et al* [57] using Landau–Ginzburg theory. Levitas [34, 58–60] suggested a nucleation condition in the form that a dissipation increment due to PTs only (excluding plastic and other types of dissipation) reaches its experimentally determined value (see equation (3.11)). Later [21, 61, 62], he developed a local description of PTs and justified this criterion. Using the postulate of realizability [21, 27, 28, 34], Levitas derived an extremum principle (3.10) for determining all unknown parameters of a nucleus [21, 34, 58–62]. For time-dependent kinetics, the postulate of realizability results in the principle of the minimum of the transformation time (3.17), see [22]. The relationship (3.13) between the dissipative threshold K and the yield stress σ_y was found in [21, 34].

3.2.8.2 Interface propagation

In the material science literature [15, 63] various contributions to the driving force for interface propagation were analysed and the growth of an ellipsoidal nucleus in a viscoplastic material was approximately modelled. The first model of martensitic plate growth in the plastic regime [15,63], despite a very approximate treatment of the stress–strain fields, revealed some very important features, in particular longitudinal growth arrest due to plastic accommodation. The first finite-element study of the appearance and thickening of a martensitic plate with fixed ends was performed by Marketz and Fischer in [51, 52]. In the physical literature, Roitburd and Temkin [47] solved the problem of the growth of a spherical inclusion in a spherical elastoplastic matrix; Kaganova and Roitburd [64] studied the same problem by allowing for defect heredity. As the driving force for the PT, the variation in the Gibbs energy plus the heat dissipated due to plastic straining in the whole body is adopted. This condition was not localized to the interface propagation condition; it was analysed in [21]. In the next paper by Kaganova and Roitburd [49] another approach for the interface equilibrium for elastoplastic ellipsoidal inclusion in elastic space was used. PTs in viscoelastic materials are considered by Arutyunyan and Drosdov [65]. However, a general equation for interface propagation was not formulated explicitly in these papers. In the paper by Kondaurov and Nikitin [66], all the balance equations for the points of a moving interface in a viscoplastic material, including the PT criterion, are obtained. However, the characteristic time of the PT is assumed to be much smaller than the characteristic time of viscous relaxation and the plastic strain increment is equal to zero during the PT. In this case, the PT conditions are the same as for elastic materials, which contradicts the very strong effect of plastic straining and plastic properties on PT. Under such an assumption, the dissipation due to plastic flow across the interface is absent and the driving force coincides with the Eshelby driving force [67], i.e. as for elastic materials.

Levitas [68] and, independently, Fischer *et al* [50] and Marketz and Fischer [51, 52] suggested using the Eshelby driving force for the interface propagation condition in elastoplastic materials. Levitas [21, 27, 28, 58–60] developed an approach in which the driving force for nucleation and interface propagation represents the dissipation increment due to PT only, i.e. excluding all other types of dissipation, in particular plastic dissipation. In [21, 61, 62] he justified this expression for the driving force using a local description of the PTs.

Two different approaches were used for different problem formulations: based on the Eshelby driving force in [69–72] and based on the dissipation increment due to PT only in [21, 23–25, 35]. It was demonstrated in [73] that a conceptual contradiction arises when the Eshelby driving force is applied for the description of interface propagation in plastic materials. Only an approach using a driving force based on the dissipation increment due to a PT does not exhibit this type of contradiction.

The interface propagation criterion and kinetic equation which combine the

advantage of a strict continuum thermodynamic derivation of the expression for the driving force with a physically based equation for the athermal and thermal parts of the interfacial friction obtained in [15, 26, 36] was suggested in [25]. It was applied to a martensite growth problem, see [25] and section 3.4.5.

3.2.8.3 Extremum principle

For inelastic materials, Patel and Cohen [74] suggested maximizing the mechanical work in order to choose the appropriate habit-plane (or invariant plane strain) variant. This, in fact, is equivalent to maximizing the Eshelby driving force (if interface propagation is considered), because invariant plane strain includes plastic shear in addition to transformation (Bain) strain and rigid-body rotation. Fischer *et al* [50], Marketz and Fischer [51, 52], Fischer and Reisner [71] and Cherkaoui *et al* [69, 70] also maximized the Eshelby driving force with respect to the proper habit-plane variant.

Ganghoffer *et al* [75] and Marketz and Fischer [53] maximize the work of stress along the transformation strain using local stress in the place of nucleation before the PT. Such an assumption generalizes the Patel and Cohen [74] extremum principle in the presence of internal stresses. At the same time, it is inconsistent in the limit case of elastic materials with the Gibbs energy Minimum principle, because stress variation during the PT is neglected. This leads to significant errors, because the stresses change very significantly during the PT (growth of transformation strain) and even change sign (see, e.g., [22, 34, 47] and section 3.3.4). Investigations of PTs in elastoplastic materials by Fischer *et al* [50] and Marketz and Fischer [51–53] are related to a comparison of the Gibbs free energy before and after PT. In Wen *et al* [76] some potential was suggested to be maximized. Typical for all these papers is that the PT conditions are not directly related to the second law of thermodynamics and dissipation due to the PT. That is why it was difficult to understand the physical sense of the proposed criteria and extremum principles and choose which one is correct and which is not.

Levitas [21,27,28,34] formulated a plausible assumption called the postulate of realizability, which results in the maximization of the difference $\bar{X} - K$ both for nucleation and interface propagation (see equation (3.12)). At constant K, this principle reduces to a maximization of $\bar{X}$ and to a principle of maximum actual transformation work with allowance for stress variation in the transforming region. The actual transformation work differs significantly from $\boldsymbol{T} : \boldsymbol{\varepsilon}_{\mathrm{t}}$ and can even have an opposite sign [35]. In [22] the more general extremum principle is derived from kinetic considerations (see equation (3.17)).

One of the positive points in applying the postulate of realizability, rather than guessing an extremum principle, is that the postulate of realizability can be used to derive some known and new extremum principles in various fields, like plasticity, irreversible thermodynamics, chemical reactions, ductile fracture, twinning, the problem of plastic spin and stability analysis [6, 21–25, 28–32].

The necessity for a global SC criterion and its specific expression (3.14), derived with the help of the postulate of realizability, was suggested by Levitas in [21, 27, 28]. This criterion has been applied to PT [23, 28, 31] and fracture [23] problems.

Note that our theory for SCs and PTs, which was outlined in this section has also found applications to fracture and twinning problems, as well as to generalized second-order and diffusive-displacive PTs [22, 23].

3.2.8.4 Semicoherent interface

Earlier [77–79] the possibility of semicoherent SC in elastic materials was estimated by comparing the energy of a coherent nucleus (displacements are continuous) and a semicoherent nucleus while taking into account the energy of the dislocations. A detailed dislocation model of a semicoherent nucleus was developed by Olson and Cohen in [15, 54]. On a larger scale, it is clear that the sliding along the interface is a dissipative process and comparison of energies is not sufficient. A non-coherent interface without friction was considered by Grinfeld [80] and Leo and Sekerka [81]. The dissipative concept in the theory of semicoherent SC in elastoplastic materials with little semicoherence and in the reference configuration was developed in [23, 27, 28, 34, 35]. An extension of this approach for arbitrary semicoherence and in an actual configuration is presented in [21]. Manipulations in the actual configuration allow us to find the contact points easily and to satisfy the traction continuity condition in them, which are difficult and sometimes impossible (at multiple intersections of many displacement discontinuity surfaces) in the reference configuration. A very sophisticated theory has been developed by Cermelli and Gurtin [82]. Examples of analytical and numerical solutions of problems for semicoherent interface and interface with fracture can be found in [23, 34, 35] and in sections 3.4.1 and 3.4.2.

3.2.8.5 Averaged description

An averaged description of PTs in terms of the volume fraction of martensite with small strain is presented by Levitas [59, 68, 83], Raniecki and Bruhns [84], Bhattacharya and Weng [85], Cherkaoui and Berveiller [69, 70] and with large strain in the book by Levitas [68] and the paper by Petryk [87]. An averaging procedure for semicoherent PT at finite strain is developed in [86]. A numerical study of martensite formation and averaging is presented in Leblond *et al* [88], Ganghoffer *et al* [75], Marketz and Fischer [51–53], Simonsson [89] and Levitas *et al* [35]. Strain-induced PTs are described by Olson and coauthors [14, 90] and Diani and Parks [91]. Current progress in the study of TRIP is presented in papers by Fischer *et al* [17, 72], Cherkaoui and Berveiller [69, 92], Olson [93] and two special issues of the International Journal of Plasticity [94, 95].

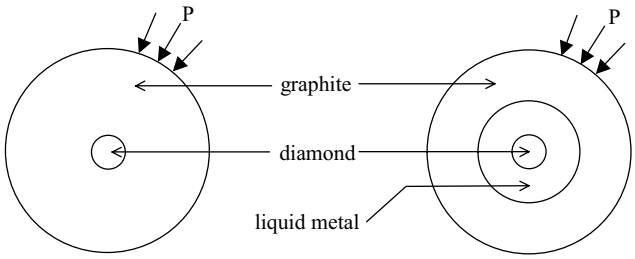

Figure 3.3. Appearance of a spherical nucleus in an elastoplastic sphere in a general case and for the graphite–diamond PT.

3.3 Review of applications of some analytical solutions

3.3.1 Spherical nucleus in an infinite elastoplastic sphere: phase transition graphite–diamond

Let us consider the PT in a spherical inclusion with radius r in an infinite elastic—perfectly plastic sphere under applied external pressure p (figure 3.3). Such a problem was considered from a thermodynamic point of view using different criteria in several papers [34, 47, 50], see the analysis in [34]. We will follow our paper [34], where this solution was applied, in particular, to the graphite to diamond PT and our paper [22], where the kinetic aspects were considered.

The elastic properties of the parent and new phases are the same, $\boldsymbol{\varepsilon}_{\mathrm{t}} = 1/3\varepsilon_0 \boldsymbol{I}\xi$, where ε_0 is the volumetric transformation strain and $\boldsymbol{I}$ is the unit tensor. Then the pressure $\tilde{p}$ in a nucleus is determined by the following formulas [47]: in the elastic regime

$$\tilde{p}_e = p - \frac{\varepsilon_0 \xi}{3C} \qquad |\xi| \le |\xi'| \qquad \xi' := \frac{2\sigma_y C}{\varepsilon_0} \tag{3.22}$$

in the plastic regime

$$\tilde{p}_p = p - \frac{2}{3}\sigma_y \left(\ln \frac{\varepsilon_0 \xi}{2\sigma_y C} + 1 \right) \qquad |\xi| > |\xi'|. \tag{3.23}$$

Here $C = 3(1-\nu)/2E$, E is Young's modulus, ν is Poisson's ratio, σ_y is the yield stress of the parent phase, $\xi'\varepsilon_0$ is the strain corresponding to the onset of plastic flow in the parent phase. Note that σ_y can be *positive* or *negative* and due to the condition $\varepsilon_0/2\sigma_y C > 0$ the signs of σ_y and ε_0 coincide. Pressure in the nucleus significantly reduces during the SC. In elastic regime, it reduces linearly and can even change sign. In the plastic regime, the pressure reduction is weaker. Calculation of the transformation work yields

$$\varphi = \int_{\boldsymbol{\varepsilon}_{\mathrm{t}1}}^{\boldsymbol{\varepsilon}_{\mathrm{t}2}} \boldsymbol{T} : \mathrm{d}\boldsymbol{\varepsilon}_{\mathrm{t}} = p\varepsilon_0 - \frac{\varepsilon_0^2}{6C} \tag{3.24}$$

at the elastic deformation and

$$\varphi = \int_{\boldsymbol{\varepsilon}_{t1}}^{\boldsymbol{\varepsilon}_{t2}} \boldsymbol{T} : \mathrm{d}\boldsymbol{\varepsilon}_t = \int_0^1 \tilde{p}\varepsilon_0 \,\mathrm{d}\xi = \int_0^{\xi'} \tilde{p}_e\varepsilon_0 \,\mathrm{d}\xi + \int_{\xi'}^1 \tilde{p}_p\varepsilon_0 \,\mathrm{d}\xi = p\varepsilon_0 - A_m \tag{3.25}$$

with

$$A_m := \frac{2}{3}\sigma_y\varepsilon_0\left(\frac{\sigma_y C}{\varepsilon_0} + \ln\frac{\varepsilon_0}{2\sigma_y C}\right) \tag{3.26}$$

at the elastoplastic deformation. It is evident that equation (3.24) can be obtained from equation (3.25) at $\sigma_y = \varepsilon_0/2C$, i.e. at $\xi' = 1$. Substituting φ into the PT criterion (3.18), we obtain the PT pressure in the elastic and elastoplastic regions, respectively,

$$p = \frac{\varepsilon_0}{6C} + \frac{1}{\varepsilon_0}(K + \Delta\psi) \tag{3.27}$$

$$p = \frac{2}{3}\sigma_y\left(\frac{\sigma_y C}{\varepsilon_0} + \ln\frac{\varepsilon_0}{2\sigma_y C}\right) + \frac{1}{\varepsilon_0}(K + \Delta\psi). \tag{3.28}$$

Because of the work of the internal stresses and K, the SC pressure can be much greater than the thermodynamically equilibrium pressure $p_e = \Delta\psi/\varepsilon_0$. Plastic accommodation reduces the work of the internal stresses and SC pressure.

Let us consider the graphite (G)–diamond (D) PT. The equilibrium pressure–temperature line calculated with chemical thermodynamics methods [96–98] is shown in figure 3.4; this means that the pressure and temperature variations, plastic straining and dissipation due to PT are neglected. The equilibrium line can be approximated by [96–98]

$$p_{eq} = 1.2575 + 0.0025\theta = a + b\theta \quad \text{(GPa)}. \tag{3.29}$$

In reality

- the solid–solid martensitic G–D PT proceeds at a pressure which is several times higher [96] (figure 3.4); and
- if a PT occurs in the presence of some liquid metals (e.g. Fe, Ni, Co, NiMn [98]), then the PT can proceed at the equilibrium pressure.

There are a number of physicochemical theories which try to explain these phenomena qualitatively assuming some special chemical reactions, catalytic properties of metals or their properties as solvent metals and so on [97, 98]. All of them may be correct but, first of all, the PT should be possible from the point of view of continuum thermodynamics. It will be shown that the thermodynamic continuum theory allows us to explain both the mentioned experimental results without any additional physical or chemical hypothesis.

Let us consider the appearance of a D spherical nucleus in an infinite G sphere under the prescribed external pressure p (figure 3.3(a)). To obtain a simple

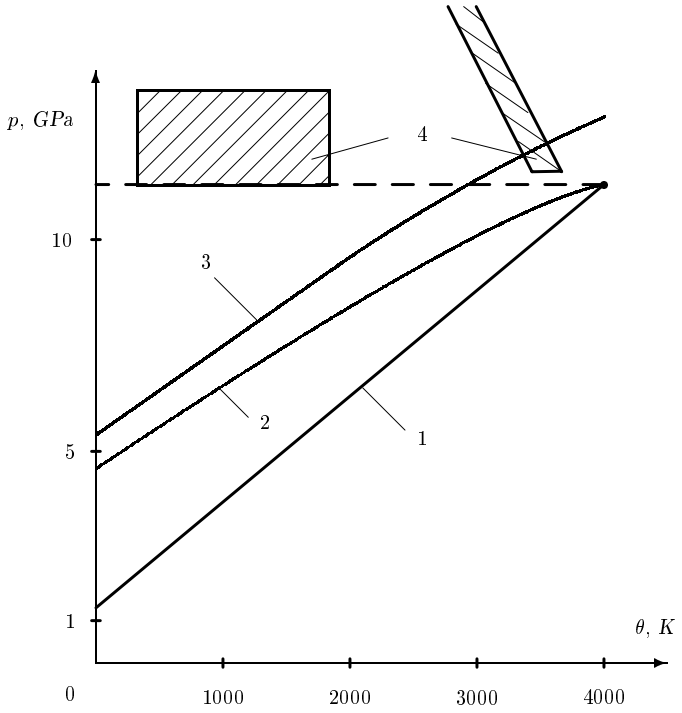

Figure 3.4. Phase transition G–D diagram: 1, equilibrium line; 2, calculated curve at $K = 0$ (isothermal); 3, calculated curve (adiabatic); 4, experiments ([96]).

analytical estimate, we will neglect many details, in particular finite strains. The variation in elastic moduli and thermal expansion will not be taken into account when defining the stress state and calculating the transformation work in the PT criterion. Consequently, equation (3.28) can be used. The variation in elastic moduli and thermal expansion will be taken into account in an implicit way. In the particular case $\sigma_y = K = 0$, the PT pressure in equation (3.28) should coincide with equilibrium pressure p_{eq}. We will use equation (3.29), which includes the variation of elastic moduli and thermal expansion, for p_{eq} and obtain

$$p = \frac{2}{3}\sigma_y \left(\frac{\sigma_y C}{\varepsilon_0} + \ln \frac{\varepsilon_0}{2\sigma_y C} \right) + \frac{K}{\varepsilon_0} + b(\theta - \theta_0) \qquad \theta_0 := -\frac{a}{b}. \tag{3.30}$$

Let us estimate the parameters in equation (3.30). The volumetric transformation strain $\varepsilon_0 = |1 - \frac{\rho_{\mathrm{d}}}{\rho_g}| = 0.5418$, where $\rho_{\mathrm{d}} = 3.5 \times 10^3$ kg m^{-3} and $\rho_g = 2.27 \times 10^3$ kg m^{-3} are the mass densities of D and G in the unloaded state. The compression modulus of G at $p = 10$ GPa is equal to $k = 75$ GPa [96]. At

$\nu = 0.3$, the constant

$$C = \frac{3(1-\nu)}{2E} = \frac{1-\nu}{2(1-2\nu)k} = 0.0117\ \text{GPa}^{-1}. \tag{3.31}$$

For the yield stress we adopt the linear temperature dependence [99]

$$\sigma_y(\theta) = \sigma_y(0)\left(1 - \frac{\theta}{\theta_\text{m}}\right) \tag{3.32}$$

where $\theta_\text{m} = 4000$ K is the melting temperature of both G and D (G–D–liquid triple point). We assume that at pressure $p = 10$ GPa, $\sigma_y(0) = 2$ GPa [100]. The result of the calculation of the PT pressure according to equation (3.30) at $K = 0$ is shown in figure 3.4, curve 2. The pressure increment due to mechanical work A_m/ε_0 at $\theta = 0$ K is 3.34 GPa and at $\theta = 2000$ K is 2.11 GPa. If we assume that the difference between the experimentally defined PT pressure (approximately $p_\text{ex} = 11.26$ GPa at arbitrary temperature) and pressure according to equation (3.30) at $K = 0$ is due to K, then the ratio K/A_m is maximum at $\theta = 0$ K and equals 1.97. At $\theta = 2000$ K it is 1.386 and at $\theta = 3000$ K it is 0.957. As these values are relatively small in comparison with $K/A_m = 9.445$ for steel [34], our assumption is plausible. It is interesting to note that the coefficient L in equation (3.13) varies from 3.35 at $\theta = 0$ K to 2.40 at $\theta = 3000$ K. This is a very narrow interval when we take into account the rather simplified character of our description.

We also took into account adiabatic heating due to PT heat and dissipation, using the model developed in [22]. This resulted in curve 3 in figure 3.4.

Consequently there are three main reasons why the experimental PT pressure significantly exceeds the pressure calculated using chemical thermodynamical methods:

- the pressure reduction in the course of the PT and corresponding decrease in transformation work;
- the dissipation due to PT; and
- the temperature increase during the transformation events.

Let us consider the appearance of the D nucleus in a liquid sphere which is located in a finite G sphere under the prescribed external pressure p (figure 3.3(*b*)). As an initial condition, assume that the pressure in liquid and the prescribed pressure are the same. The liquid acts in three ways.

(1) The melted metal in the given case transforms a martensitic PT into a diffusive PT [96–98], for which the dissipative threshold is zero.
(2) The maximum possible pressure variation in the transforming particle in the liquid is $\Delta p = K_\text{l}(v_\text{d} - v_\text{g})/v_\text{l}$, where v_g, v_d and v_l are the volume of the transforming particle before and after PT and the volume of liquid. The volume of liquid is usually comparable with the volume of the G sphere and

the pressure variation in an infinitesimal D nucleus is negligible, because $v_l \gg (v_g - v_d)$. The pressure variation is also negligible when the volume of the transforming particle is comparable with the volume of the liquid drop [34].

(3) The adiabatic process in the nucleus is replaced by an isothermal one.

Consequently there is no reason why the experimentally determined pressure needed for the appearance of a small D nucleus should exceed the pressure calculated using chemical thermodynamical methods. Thus, the thermodynamical continuum theory developed allows us to explain both the fundamental experimental results mentioned earlier without any additional physical or chemical hypothesis.

If we want to model the process of metal melting in G, then we should introduce the volumetric transformation expansion in the metal and vary the elastic properties. For constant elastic moduli, the volumetric transformation expansion results in pressure growth in the liquid. Consequently, the G–D PT can occur at an external pressure which is less than the equilibrium p_{eq} pressure. The same will occur when the compression modulus of the chosen liquid is higher than the compression modulus of the G at zero transformation expansion. It is known that the pressure in the reaction cell increases due to metal melting [101], i.e. the possibility of D synthesis under pressure which is less than equilibrium p_{eq} pressure can be real.

From this example we can derive three useful conclusions:

- It is possible to use a liquid or material with a small yield limit to decrease the pressure reduction in the course of PT.
- It is possible to replace martensitic PT by diffusive PT in order to remove the dissipative threshold in the PT criterion.
- The driving force for the PT can be increased by creating a pressure (stress) concentration in the transformation zone, for instance by using another PT with a corresponding transformation strain or material with higher elastic moduli.

Let us consider time-dependent kinetics. As X in the solution under consideration is independent of radius r, the kinetic equation (3.16) and transformation condition (3.15) read as

$$t_s = t_0 \exp\left(-\frac{(X - K^0 - E_a)\frac{4}{3}\pi r^3 - 4\Gamma\pi r^2}{R\theta_{ef}}\frac{N}{n}\right) \tag{3.33}$$

at

$$(X - K^0)\tfrac{4}{3}\pi r^3 - 4\Gamma\pi r^2 \geq 0. \tag{3.34}$$

Minimizing t_s with respect to r (according to principle (3.17)) we obtain the result that at $X - K^0 - E_a \leq 0$ the radius $r \to \min$, because the function under

consideration decreases monotonically with the growth of r. The minimum value of r can be found from SC condition $\bar{X} = K^0$, i.e.

$$(X - K^0)\tfrac{4}{3}\pi r_t^3 - \Gamma 4\pi r_t^2 = 0 \qquad \text{or} \qquad r_\mathrm{t} = \frac{3\Gamma}{(X - K^0)}. \tag{3.35}$$

Substitution of (3.35) in equation (3.33) results in

$$t_\mathrm{s} = t_0 \exp\left(\frac{E_\mathrm{a}}{R\theta_\mathrm{ef}}\frac{N}{n}\frac{4}{3}\pi r_t^3\right). \tag{3.36}$$

Let us analyse the results. If at a given boundary condition the SC condition (3.35) is satisfied, then a new nucleus with radius r_t appears during the shortest time determined by equation (3.36). We will call a nucleus with a radius r_t the *thermodynamically admissible nucleus*. It has nothing in common with the usual critical nucleus, which is determined by maximizing the Gibbs potential

$$G = -X\tfrac{4}{3}\pi r^3 + \Gamma 4\pi r^2 \tag{3.37}$$

with respect to r, i.e.

$$r_\mathrm{c} = \frac{2\Gamma}{X}. \tag{3.38}$$

It is evident that for a critical nucleus

$$\bar{X}_\mathrm{c} V_\mathrm{n} = -\frac{16}{3}\frac{\pi\Gamma^3}{(X)^2} < 0$$

i.e. its appearance is impossible from the point of view of the nucleation criterion and *contradicts the second law of thermodynamics*. The appearance of the critical nucleus requires energy fluctuations, which are not included in the thermodynamic theory. In contrast to the usual approach, we determine a thermodynamically admissible nucleus in terms of the kinetics: this is a nucleus with the minimum possible size which can appear from the point of view of the thermodynamics and appears during the shortest possible time. According to equation (3.35), X or $\bar{X}$ satisfy the 'static' SC condition $\bar{X} = K^0$ (as for rate-independent SC). Increase in X reduces the radius of the thermodynamically admissible nucleus, which leads to growth in the rate of transformation in equation (3.36). The critical nucleus will be considered in section 3.5.5.

Thermodynamically, a PT is possible at $X \geq K^0$, i.e. at pressure

$$p \geq \frac{\varepsilon_0}{6C} + \frac{1}{\varepsilon_0}(K^0 + \Delta\psi_0 - \Delta s_0(0.5(\theta_2 + \theta_1) - \theta_0)) \tag{3.39}$$

for an elastic material and at

$$p \geq \frac{2}{3}\sigma_y\left(\frac{\sigma_y C}{\varepsilon_0} + \ln\frac{\varepsilon_0}{2\sigma_y C}\right) + \frac{1}{\varepsilon_0}(K^0 + \Delta\psi_0 - \Delta s_0(0.5(\theta_2 + \theta_1) - \theta_0)) \tag{3.40}$$

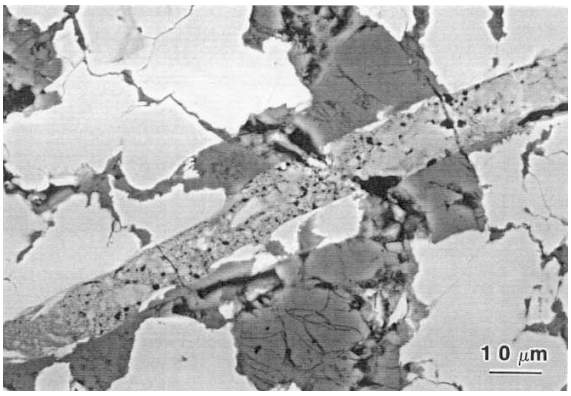

Figure 3.5. Shear localization and partial CR within a shear band in Ti–Si mixture [6].

in the elastoplastic regime. However, at small $X - K^0$, the radius of a thermodynamically admissible nucleus is large and the transformation time can significantly exceed the observation time. Only at relatively large $X - K^0$ and small r_t can a PT be observed during a reasonable time. As a kinetic PT criterion, we can assume that $t_s = t_{ob}$, where t_{ob} is the accepted observation time.

Application of the kinetic concept to a G–D PT will be considered elsewhere. A more detailed analysis of a G–D PT neglecting plasticity but taking into account the kinetic aspects is performed in our paper [102].

3.3.2 Strain-induced chemical reactions and phase transformations in shear band

Strain-induced chemical reactions were observed recently [103, 104] in experiments in the shear band in both Ti–Si and Nb–Si mixtures (see figure 3.5). The first attempt of continuum thermomechanical finite strain modelling of this phenomenon and an explanation of the possible reasons for the acceleration of the chemical reactions due to intense plastic shear is made in our papers [6, 22]. In particular, *the reaction-induced plasticity (RIP)* phenomenon, similar to transformation-induced plasticity (TRIP) for a PT, was revealed. The considerations in [6] were based on a simplified kinetic equation without correctly accounting for the actual transforming volume. In papers [22] our general kinetic approach outlined in section 3.2 was applied and a significant difference in the final results was demonstrated.

We assume that the transformation strain is a spherical tensor. Consider an infinite rigid-plastic half-space with prescribed normal σ_n and shear τ stresses on the whole surface (figure 3.6) under the plane strain condition. We assume the existence of a region with localized plastic shear deformation, i.e. shear band, along the whole surface. The material outside the shear band is rigid. It is assumed

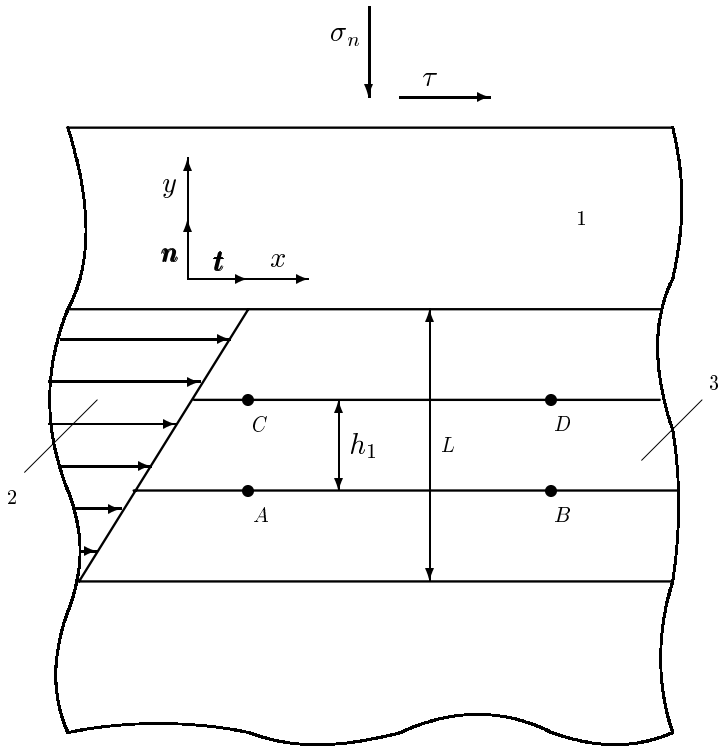

Figure 3.6. Schematic illustration of CRs in a shear band: 1, half space; 2, shear band with displacement; 3, layer with chemical reactions.

that a coherent SC occurs in the layer inside the shear band. For coherent SC the displacements are continuous across the interface. Adiabatic heating is taken into account. In figure 3.7, a transformed particle is shown after transformation strain which is purely volumetric. In order to satisfy the displacement continuity across the interface AB and independence of the solution of x, an additional plastic strain is needed (figure 3.7(b)). We assume that the total, transformation and plastic deformation gradients are homogeneous in a layer and that the stress field is homogeneous and time-independent.

It was found that the plastic shear γ due to RIP is related to the applied shear stress τ, yield stress σ_y and volumetric transformation strain ε_0 by the formula (see figure 3.8)

$$\gamma = 2|\varepsilon_0|\frac{\tau}{\sqrt{\sigma_y^2 - 4\tau^2}}. \tag{3.41}$$

It is easy to see that plastic flow occurs at arbitrary shear stress and that the

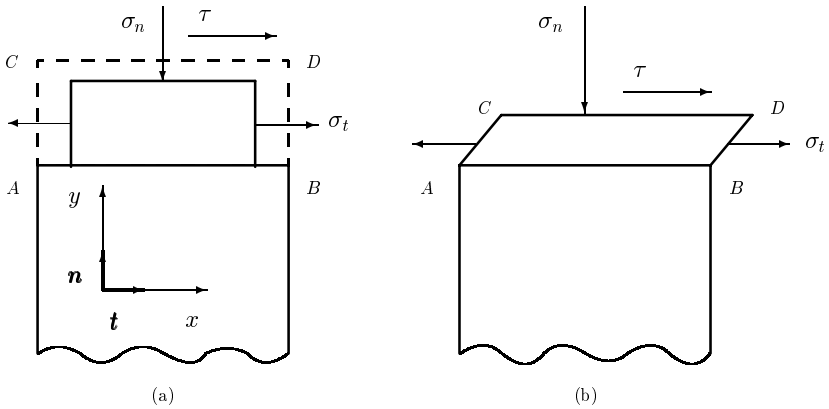

Figure 3.7. Diagram of a CR in a thin layer.

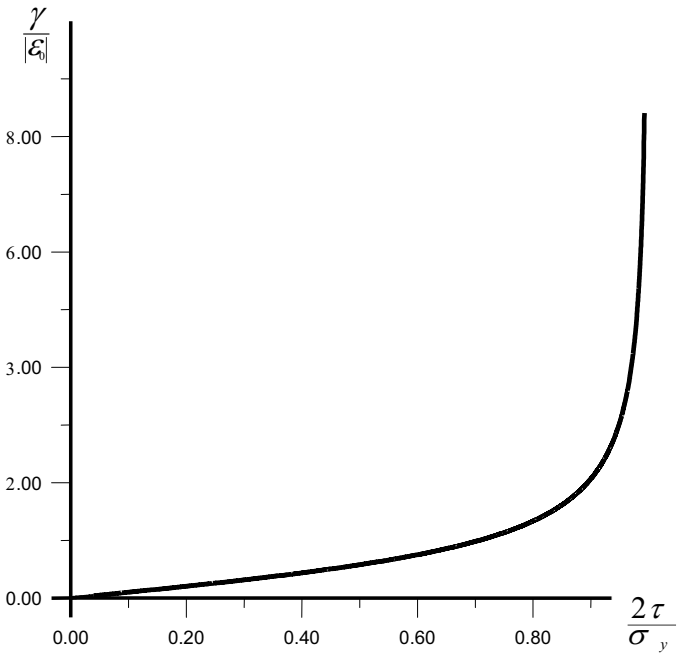

Figure 3.8. Relation between shear strain γ and shear stress τ for RIP.

external shear stress τ need not reach the yield shear stress. Plastic straining takes place due to variation in the volumetric transformation strain. When the shear stress tends toward the yield stress in shear (e.g. in a shear band), plastic shear tends to infinity, so very high plastic shear can be accumulated due to RIP.

Such an RIP can be very significant and leads to very intensive heating, more than 1500°. Similar results are obtained for TRIP for PT [26, 34].

TRIP and RIP can serve as a positive mechanochemical feedback (see section 3.5). Plastic straining and heating (if the driving force for SC grows with increasing temperature) due to TRIP and RIP accelerates PTs and CRs which lead to intensification of TRIP and RIP and, consequently, of the PT and CR, and so on.

RIP represents a new mechanism for the inelastic deformation of solids. We would like to mention that in [105] an extraordinary low-threshold stress to initiate CR in Ti–Si system is observed, which the authors relate to the ease of plastic deformations. However, neither of these materials has a low yield stress. The authors try to explain the intense plastic flow due to volume change at the PT in Ti and Si at a pressure of about 10 GPa.

The averaged pressure to initiate the CR is a few GPa; however, the authors assume that the local pressure may be sufficient for a PT. However, the volume change for CR $5\mathrm{Ti} + 3\mathrm{Si} \rightarrow \mathrm{Ti_5Si_3}$ is as high as -0.278 [105] and the RIP phenomenon is a good candidate to explain the ease of plastic flow and low-threshold stress to initiate CRs.

For the local driving force X, the temperature during and after the end of the CR as well as for the effective temperature is obtained [22]:

$$X = 0.5\left(2\sigma_{\mathrm{n}} - \sqrt{\sigma_y^2 - 4\tau^2}\right)\varepsilon_0 + 0.5\Delta s_0(\theta_1 + \theta_2) - \Delta U_0 \tag{3.42}$$

$$\theta = \theta_1 + \frac{A}{\nu}\xi \qquad \theta_2 := \theta(1) = \theta_1 + \frac{A}{\nu} \qquad \theta_{\mathrm{ef}} = 0.5(\theta_1 + \theta_2) \tag{3.43}$$

$$A := \varepsilon_0\left(\sigma_n + \frac{2\tau^2}{\sqrt{\sigma_y^2 - 4\tau^2}}\right) - \Delta U_0 \tag{3.44}$$

where ΔU_0 is the jump in the reference internal energy per unit volume in the reference configuration, h is the thickness of the layer in the reference configuration (before the chemical reaction), A is the heat source due to the reaction heat ΔU_0 and RIP. It is clear from equations (3.42)–(3.44) that at $\tau \rightarrow 0.5\sigma_y$ the heat source due to RIP tends to infinity and the temperature tends to the melting temperature.

Minimizing the reaction time with respect to h, i.e.

$$\frac{n}{N}R\theta_{\mathrm{ef}}\ln\frac{t_0}{t_{\mathrm{s}}} = \rho(X - K^0 - E_{\mathrm{a}})hlb - \gamma 2lb \rightarrow \max_h \tag{3.45}$$

where l and b are the length and width of the interface surface, we obtain $h \rightarrow \min$. It follows from the thermodynamic SC criterion that

$$h = \frac{2\gamma}{\rho(X - K^0)}. \tag{3.46}$$

Substituting equation (3.46) into kinetic equation (3.21) results in

$$t_s = t_0 \exp\left(\frac{E_a}{R\theta_{ef}} \frac{N}{n} \frac{2\gamma}{(X - K^0)} lb\right). \tag{3.47}$$

As the kinetic criterion of the initiation of the CR, it is assumed that the reaction time t_s is less than the deformation time t_d in the shear band.

The results obtained in (3.47) predict a strong effect by the driving force and an increase in the effective temperature due to RIP on a decrease in transformation time. The driving force increases due to shear stress by two macroscopic mechanisms (see equations (3.42)–(3.44)): reduction in the term $\sqrt{\sigma_y^2 - 4\tau^2}$ related to fulfilment of the plasticity condition; and an increase in the reaction end temperature θ_2 (at $\Delta s_0 > 0$). Analysis of equation (3.47) shows a very strong dependence of the transformation time on $X - K^0$ at small $X - K^0$ with a sharp transition to weak dependence between these parameters at large $X - K^0$. The condition $t_s = t_d$ determines the driving force X necessary to initiate the reaction: the smaller the activation and surface energy are, the smaller the driving force necessary for nucleation is and the sharper the transition from a high driving force sensitivity to a low one. At relatively high $X - K^0$ the transformation time is insensitive to the effective temperature and activation energy, i.e. equation (3.47) describes the transition to athermal kinetics.

It is expected that the RIP phenomenon may play an important role in solid–gas CRs in explosives, e.g. in HMX or nano-composite explosives. Due to high gas pressure in voids, RIP may be even more pronounced than for solid–solid CRs. One of the important problems which has to be solved is to find the condition for shear-band formation for different types of PT and CR (for solid–solid and solid–gas PTs and CRs, with a weaker or stronger product and with different thermomechanical properties for the reactant and product). For some cases, it may happen that a CR triggers strain localization rather than *vice versa*.

Let us consider the following possible scenario. In the microscopic region with the local shear stress of magnitude of the yield stress (due to external stresses and internal stresses caused by some defects), and at higher temperature, the CR can start fluctuationally, e.g. a few gas bubbles appear. High gas pressure will lead to RIP and heating due to RIP and reaction heat. This will lead to material softening, strain localization, more intensive heating in a larger region and a CR there. We plan to find at which initial temperature and shear stress such a situation is possible.

The problem of a PT in a thin layer in a rigid-plastic half-space is solved in [21, 34] at small strain and in [26] at large strains. Such a problem models the PT as a result of friction in the neighbourhood of the contact surface, under impact loading, at moving interface or in a shear band. The non-trivial consequence of accounting for geometrical nonlinearities (even at small strains) is a definite *transformation path*, i.e. sequences of volumetric and shear transformation strain variation during the PT.

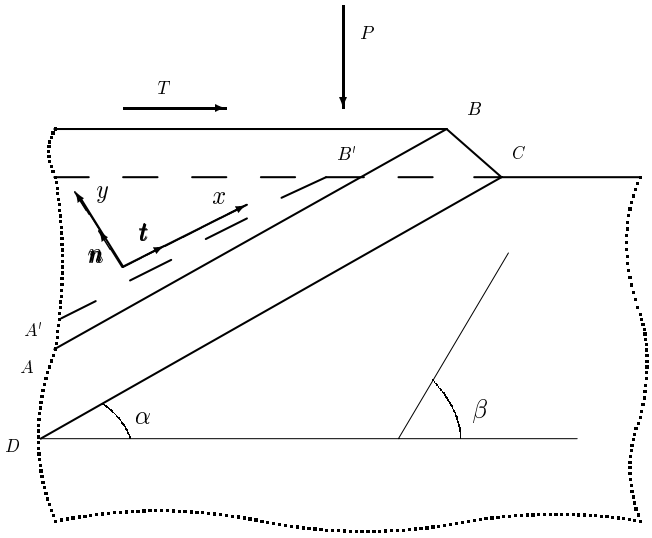

Figure 3.9. Coherent PT in thin layer ABCD.

3.3.3 PT in a thin inclined layer under homogeneously distributed normal and shear stresses

The problem of a PT in a thin layer (shear band) in a rigid-plastic half-space under the action of homogeneously distributed normal and shear stresses (figure 3.9) is solved in [34]. The solution demonstrates how the combination of the PT criterion and the yield condition for the parent phase can explain various aspects of the material's behaviour:

- If a new phase has a smaller yield stress than the parent one, then the shear stress promotes a PT.
- If a new phase has a yield stress $\sigma_{y2} \geq 2\sigma_{y1}$, the shear stresses practically do *not affect* the PT condition.
- Shear stresses can render the PT *impossible*, if due to the necessity of fulfilling the yield condition for a parent phase a PT criterion is violated.

The solutions illustrate the fundamental difference in PT conditions for strongly non-homogeneous pressure distributions in the problem of PT of materials under compression and shear in rotational Bridgman or diamond anvils (see [34] and section 3.5) and for homogeneously distributed stresses. In particular, under homogeneous fields additional shearing promotes significantly the appearance of soft materials and weakly affects the appearance of strong materials. For a non-homogeneous pressure distribution, additional shearing promotes the appearance of strong materials and suppresses the weak phases. Consequently

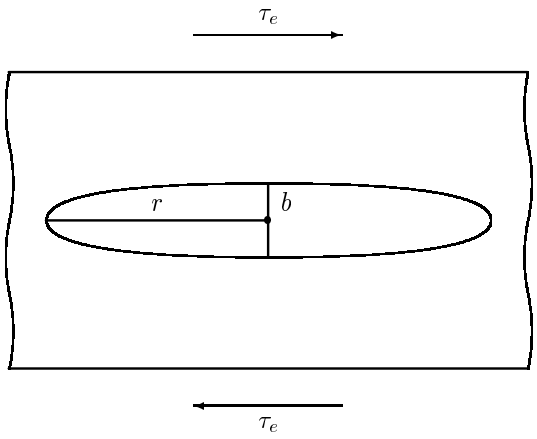

Figure 3.10. Appearance of ellipsoidal nucleus.

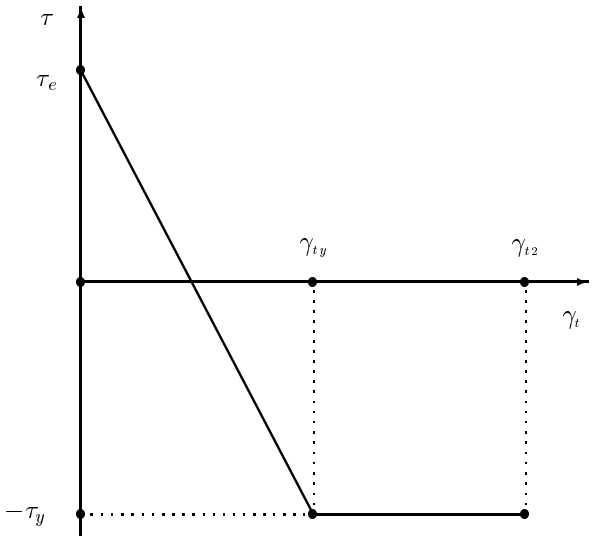

Figure 3.11. Stress variation in the nucleus in the course of transformation strain growth.

each experimental situation should be simulated carefully before any conclusion is made.

3.3.4 Phase transition in ellipsoidal inclusion

Let us consider a PT in a thin (penny-shape) ellipsoidal inclusion of radius r and semi-thickness b, $r \gg b$, inside an infinite space under the action of remote shear

stress τ_e (figure 3.10). The space is elastic, the inclusion is elastoplastic [22]. All fields are homogeneous in V_n. The transformation strain contains the shear component $0.5\gamma_t$ only. Adapting the Eshelby solution [106] we obtain for the shear stress in the inclusion (figure 3.11)

$$\tau = \tau_e - \eta\gamma_t\frac{b}{r} \qquad \text{at } \gamma_t < \gamma_{ty} \qquad \eta := \frac{\mu\pi(2-\nu)}{4(1-\nu)}$$
$$\tau = -\tau_y \qquad \text{at } \gamma_{ty} \le \gamma_t \le \gamma_{t2} \qquad \gamma_{ty} := \frac{\tau_e + \tau_y}{\eta}\frac{r}{b} \tag{3.48}$$

where μ is the shear modulus and ν Poisson's ratio. During the growth of γ_t the shear stress decreases, changes sign and reaches the yield stress τ_y in the opposite direction to the external stress. Here γ_{ty} is the value of γ_t at which plastic flow starts. Calculating the transformation work

$$\int_0^{\gamma_{t2}} \tau \, \mathrm{d}\gamma_t = -\tau_y\gamma_{t2} + 0.5(\tau_e + \tau_y)^2\eta^{-1}\frac{r}{b}.$$

From the thermodynamic PT criterion $(X - K^0)V_n - \gamma S_n \ge 0$ or

$$\left(A + B\frac{r}{b}\right)\frac{4}{3}\pi r^2 b - \Gamma 2\pi r^2 \ge 0 \tag{3.49}$$
$$A := -\tau_y\gamma_{t2} - \Delta\psi - K^0 \qquad B := 0.5(\tau_e + \tau_y)^2\eta^{-1} \tag{3.50}$$

follows the relation between r and b

$$2Ab \ge 3\Gamma - 2Br. \tag{3.51}$$

Maximizing the transformation rate with respect to r and b, i.e.

$$\left(M + B\frac{r}{b}\right)\frac{4}{3}\pi r^2 b - \Gamma 2\pi r^2 \to \max \qquad M := A - E_a \tag{3.52}$$

we obtain the actual r and b. For example, if $M + B(r/b) < 0$ and $A > 0$, then $r \to \min, b \to \min$ and the principle of the minimum of transforming mass under constraint (3.49) or (3.51) (with the sign $=$) results in

$$r = \frac{\Gamma}{B} \qquad b = \frac{\Gamma}{2A} \qquad V_n = \frac{2\pi}{3}\frac{\Gamma^3}{AB^2}. \tag{3.53}$$

Let $A < 0$, then b in equation (3.53) is less than zero. In this case condition $b \to \min$ is satisfied at $b = a$, where a is the lattice parameter in the b direction. The corresponding r can be found from the thermodynamic criterion

$$r = \frac{3\Gamma - 2Aa}{2B} \qquad \frac{r}{b} = \frac{3\Gamma - 2Aa}{2Ba} \le \frac{\eta\gamma_{t2}}{\tau_e + \tau_y}. \tag{3.54}$$

The inequality (which follows from $\gamma_{ty} \le \gamma_{t2}$) determines a lower bound for A.

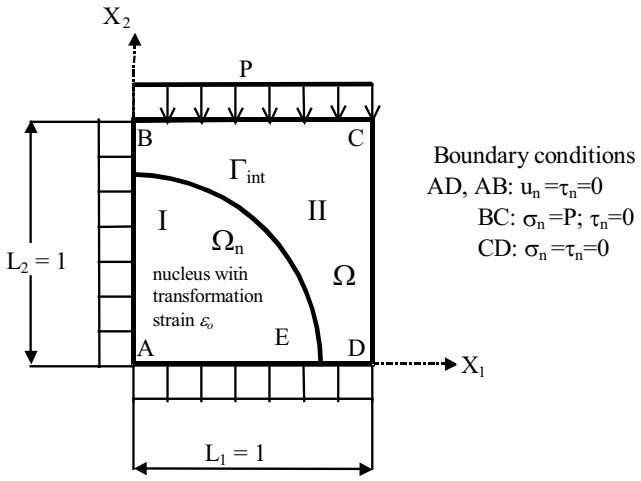

Figure 3.12. A quarter of a cross section of a spherical transforming inclusion within a cylindrical matrix.

3.4 Review of application of some numerical solutions

Algorithms for finite-element solutions at finite strains are presented in [23, 24]. Various numerical solutions can be found in [23–25, 31, 35].

3.4.1 Interaction between PT, plasticity, semicoherence and fracture—mutual support

Let us consider a unit cell consisting of a spherical inclusion within a cylindrical matrix (figure 3.12) [24, 35]. Assume that at the given temperature and external axial stress the spherical region undergoes a SC with purely dilatational transformation strain ε_0. The relationships between transformation work φ and ε_0 are presented in figure 3.13 for a coherent and semicoherent interface with different values of friction and for interface with fracture. A larger value for the transformation work gives a larger driving force for the SC. The smallest φ holds for a coherent interface. Semicoherence at small friction and fracture increases the driving force significantly.

This example exhibits the mutual support between the various micromechanisms of inelasticity. Let the external stress be too low to initiate plasticity, sliding and fracture without a PT. PT without plasticity, sliding or fracture also cannot occur, because the driving force is too small. Consequently, each of these processes cannot proceed separately. When at least two processes occur simultaneously, they help each other through the field of internal stresses and both are possible.

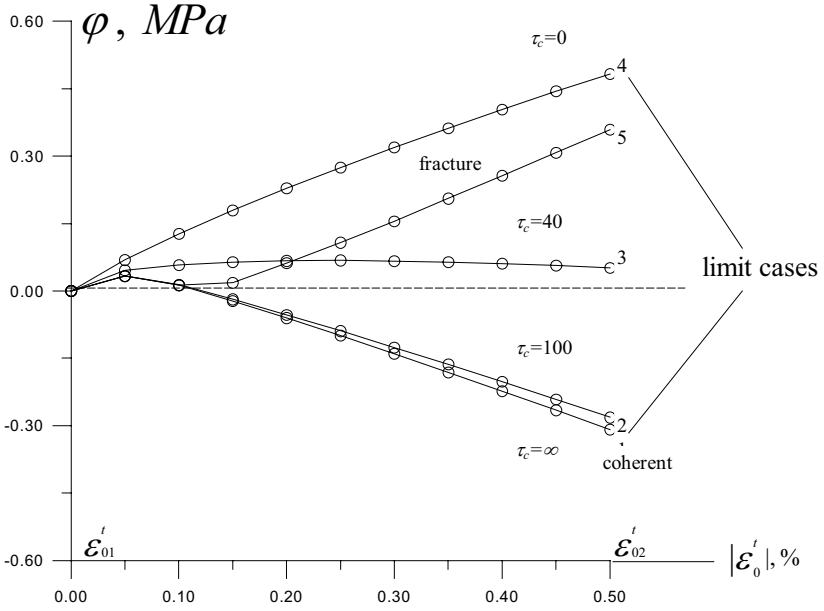

Figure 3.13. Relationships between the transformation work φ and transformation volumetric strain ε_0 at $P = 150$ MPa: 1, coherent interface; 2–4, semicoherent interface with maximum critical shear stresses $\tau_c = 100$, 40, 0 MPa, respectively; 5, with fracture on the interface, maximum normal stress $\sigma_c = 50$ MPa.

3.4.2 Interface propagation

The cases of moving coherent and semicoherent interfaces in a cylindrical sample under fixed axial stress are studied in [24, 35], see figure 3.14. Interface propagation is modelled by layer-by-layer PTs. The results are discussed in the following. A coherent interface in an elastic material at $K =$ constant is unstable, i.e. if a PT occurs in the first layer, then with the same temperature and external stresses, a PT should occur in all the remaining layers, because the transformation work φ grows (figure 3.15). To describe the stable phase equilibrium we should assume a heterogeneous distribution of K or growing K with an increasing volume fraction c of the new phase. Figure 3.16 shows the isobands of the radial displacement distribution for a semicoherent interface in the elastic matrix. After the PT is finished in the layer, the displacement discontinuities at the layer interface become fixed. The semicoherence stimulates significantly the PT condition in the first layer (φ increases). The PT condition in the second layer for a semicoherent interface is worse (i.e. the driving force is smaller) than for the coherent interface but a little bit better than for the first layer

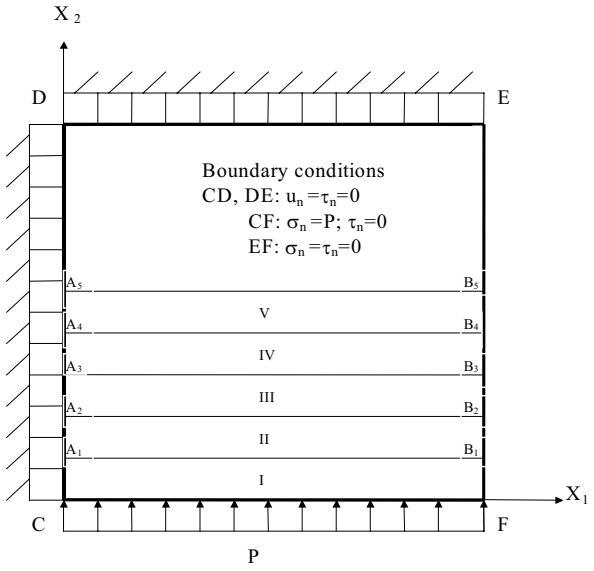

Figure 3.14. Moving coherent and semicoherent interfaces in a cylindrical sample under fixed axial stress. A_1B_1, A_2B_2, A_3B_3, A_4B_4 and A_5B_5 are the positions of the interface at different process time instants (I, II, III, IV, V are the regions where the PT occurs after corresponding displacement of the interface). X_2 is the axis of rotation.

of an incoherent interface. That is why at $K =$ constant or for a slightly growing $K(c)$ a semicoherent PT in the second layer can immediately occur after a PT in the first layer with the same external conditions. The value φ for semicoherent PT in the third layer is smaller than in the first and second layers and much smaller than in the third layer for a coherent PT (figure 3.15). If $K(c)$ is large enough to stop the coherent interface motion with fixed external parameters after a PT in layers 2–4 ($\varphi \simeq 0$ MPa), then it is necessary to change the external parameters very significantly in order to shift the semicoherent interface ($\varphi \simeq -12$ MPa).

With such a change in the external parameters, a PT can occur in other parts of the sample which leads to the formation of a discrete microstructure. To study which microstructure is formed, each layer was considered as a possible PT region. The actual PT region is chosen according to the extremum principle (3.12). The results are presented in [24]. The computation results explain the known experimental facts that a semicoherent interface has a low mobility or cannot move at all. The reason for the decreasing value of φ for a semicoherent interface is the change in internal stresses.

Plastic deformation of the matrix acts in the same way as semicoherence: it promotes the nucleation condition, a PT occurs in the second layer immediately

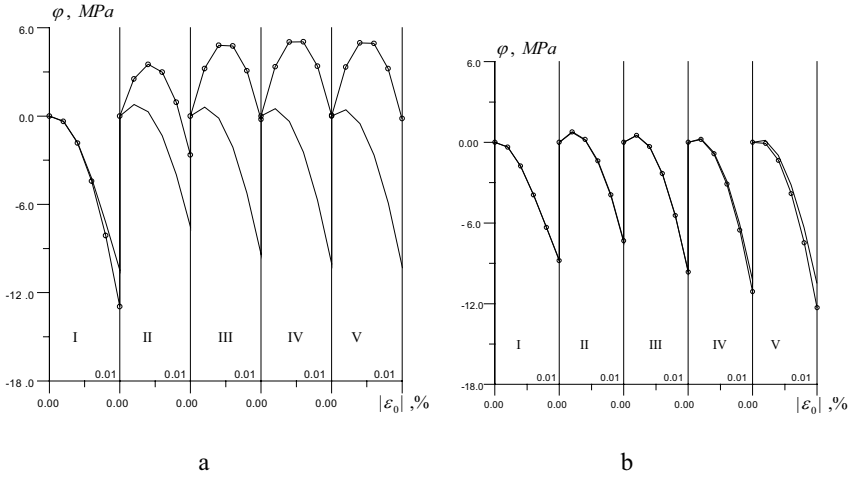

Figure 3.15. Variation of transformation work φ for the ith layer in the course of a PT in the ith layer for moving coherent (a) and semicoherent (b) interfaces, i = I, II, III, IV, V: ○, for an elastic matrix; ——, for an elastoplastic matrix.

after the PT in the first layer with the same external condition. For a PT in layers 3–5, it is necessary to change the external conditions in order to enforce a PT, i.e. due to plasticity it is possible to get stable interface motion.

For an elastic material with a coherent interface, continuous interface propagation is favourable. Semicoherence and plasticity considerably change the distribution of the stress–strain state during the PT and can lead to the formation of a discrete microstructure, especially with small yield stress or friction at the interface. One other reason is related to strain hardening and (due to equation (3.13)) to increasing the threshold K. As plastic deformations are concentrated near the interface and decay with growing distance from the interface, K decays when moving away from the interface. This promotes the formation of a discrete structure and determines the natural spacing. Displacement discontinuities (dislocations) remaining after interface propagation (figure 3.16(f)) represent a memory of a semicoherent PT.

3.4.3 Strain-induced nucleation at a shear-band intersection: competition between PT and plasticity

It is known from experiments [12,13] such as the electron microscopy observation in figure 3.17 [14] that

- shear-band intersections are the major nucleation sites;
- growth beyond the intersection region is generally very restricted;
- transformation occurs during the intersection events; and
- transformation does not occur at every shear-band intersection.

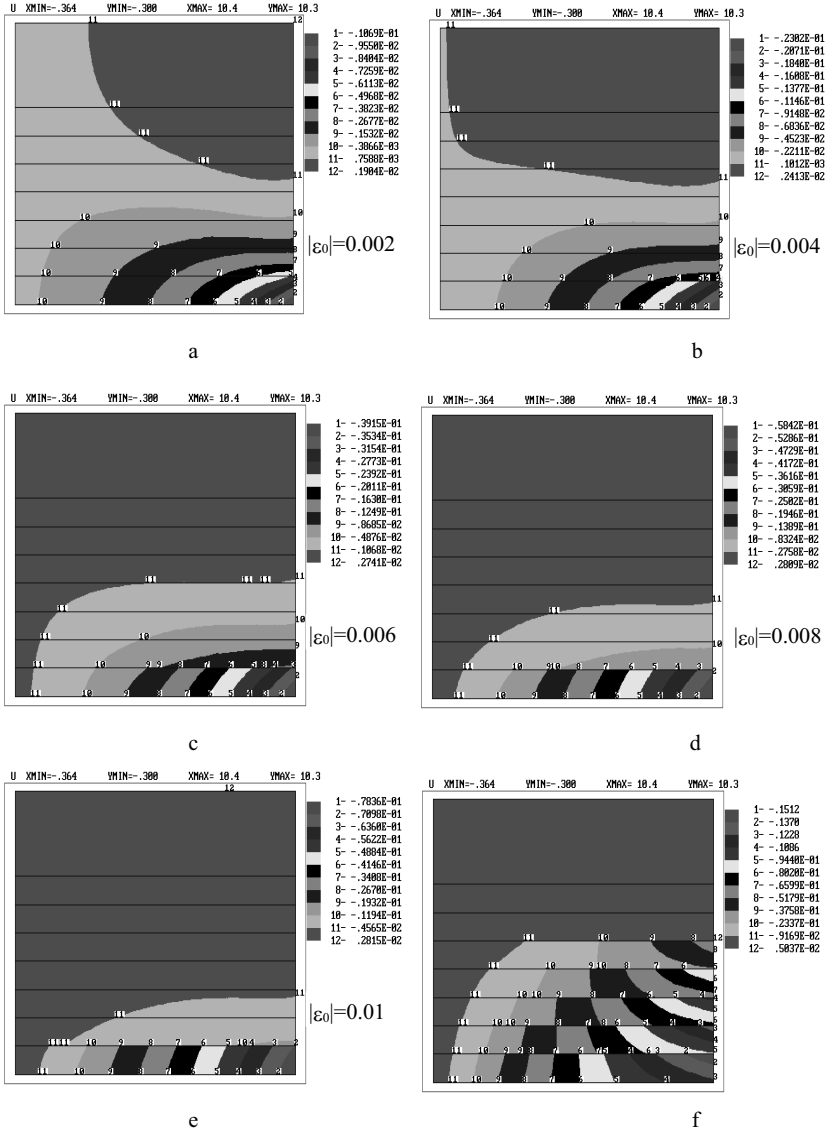

Figure 3.16. Isobands of radial displacement distribution (cm) for semicoherent interface for different values of transformation strain in course of a PT within the first layer (*a*)–(*e*) and after the interface reached the middle of a sample (*f*).

The mechanical formulation and solution of a model problem of nucleation at shear bands at a fixed homogeneous temperature and $K^0 =$ constant are described in [31].

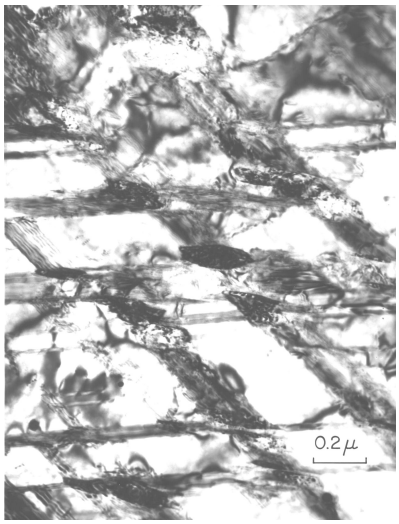

Figure 3.17. Bright field transmission electron micrograph showing a martensitic particle (dark) formed at shear-band intersections in cold-worked 301 stainless steel (from [14]).

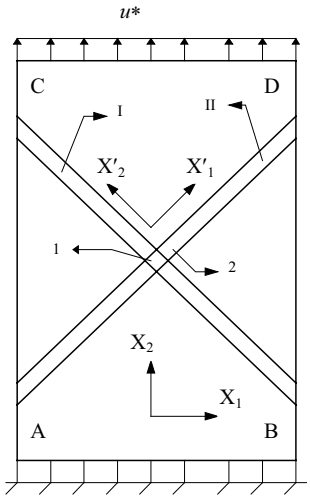

Figure 3.18. Cross section of a sample with martensitic particle (1 or 2) at a two shear-band (I and II) intersection.

First we consider the problem of nucleation at a shear-band intersection under a prescribed normal displacement (figure 3.18). Shear bands are introduced in advance (figure 3.18), the material is assumed to deform elastoplastically within the shear bands and elastically outside the shear bands. The transformation strain is introduced at the intersection of the shear bands proportionally to

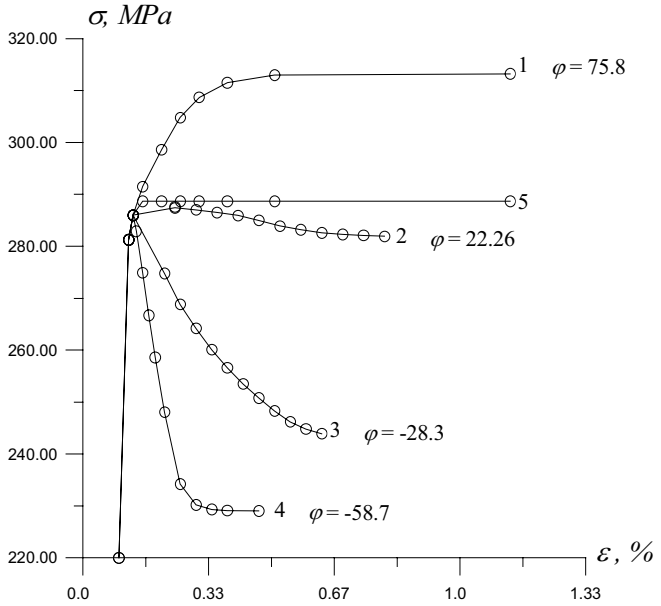

Figure 3.19. Relationships between macroscopic axial stress σ and strain ε (at different values ε after the PT is completed) during appearance of martensite at shear band intersection (region 1): 1, transformation work $\varphi = 75.8$ MPa; 2, $\varphi = 22.26$ MPa; 3, $\varphi = -28.3$ MPa; 4, $\varphi = -58.7$ MPa; 5, without PT.

the growing prescribed vertical displacement u^* for various values of maximal displacement $u^*_{\max}$. In figure 3.19, the relationship between the external axial stresses P and normal displacement u at boundary CD and the corresponding values of the transformation work φ are given. Curve 5 corresponds to deformation without a PT. If we know the temperature, then from PT criterion (3.18) we can find the corresponding value of the transformation work φ and choose (in figure 3.19) at which prescribed displacement the PT can occur. At the same time solution 5 without a PT is always possible, because it satisfies all the continuum thermodynamical equations. According to stability criterion (3.14), when the P–u curve for the solution with a PT (curve 1 in figure 3.19) exceeds the P–u curve for the solution without a PT, a PT will not occur, despite the fact that the local PT criterion can be satisfied. In the opposite case (curves 2–4 in figure 3.19) the deformation process with a PT is more stable.

It has been demonstrated that for strain-induced transformation at shear-band intersections the transformation work is maximal in comparison with other possible locations, i.e. a shear-band intersection is, in fact, the most favourable nucleation place. Further growth of the nucleus beyond the

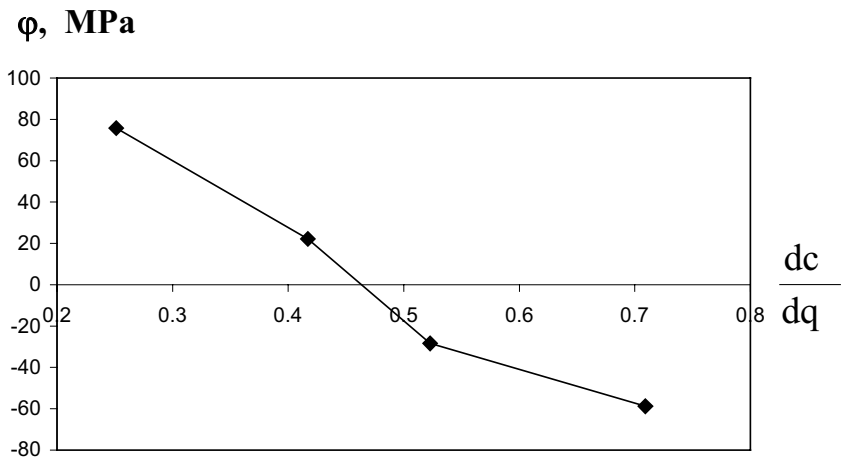

Figure 3.20. Transformation work φ *versus* $\mathrm{d}c/\mathrm{d}\varepsilon_{\mathrm{p}}$ for strain-induced nucleation at a shear-band intersection (FE calculations in [31]).

intersection is inhibited, because the transformation work decreases significantly and transformation at other shear-band intersections is favoured. The higher transformation work also explains why a PT is favoured during the intersection event rather than after intersection and cooling at fixed stress. The transformation work depends strongly on the number of active shear-band intersections at the prescribed macroscopic strain increment. This favours sequential transformation at multiple intersections, even when the intersections are completely equivalent. At a given temperature, the necessary transformation work is determined from the PT criterion and the number of active intersections is obtained using the numerical solution.

One of the results which can be extracted from this investigation is that the transformation work depends significantly on the ratio $\Delta c/\Delta\varepsilon_{\mathrm{p}} \simeq \mathrm{d}c/\mathrm{d}\varepsilon_{\mathrm{p}}$, where Δc is a small increment in the volume fraction of the strain-induced new phase and $\Delta\varepsilon_{\mathrm{p}}$ is the prescribed small, uniaxial averaged plastic strain increment. For macroscopically uniaxial straining, $\varepsilon_{\mathrm{p}} = q$, where q is the accumulated plastic strain (Odqvist parameter). Namely, the transformation work decreases linearly with the growth of $\mathrm{d}c/\mathrm{d}\varepsilon_{\mathrm{p}}$, see figure 3.20. We will use this result in section 3.5.5.

Hence, all four experimental observations enumerated here can, at least qualitatively, be described in the framework of continuum thermomechanics without detailed physical mechanisms. Of course, this does not diminish the role of concrete micromechanisms in the interaction between PT and plasticity. In particular, stress concentration due to discrete dislocations and due to the difficulty in transmitting slip in a shear band across another shear band can further increase the driving force for PT. An important point is that there are purely macroscopic (mechanism-independent) reasons for these phenomena, and that

each microscopic mechanism has to be checked from the point of view of the continuum thermodynamics.

Calculations also demonstrate a large difference between the PT conditions for displacement- and stress-controlled boundary conditions. For given fixed external stresses, martensite growth increases the macroscopic axial strain and the transformation work, favouring growth beyond the intersection region, in contrast to the restricted growth predicted under displacement control. The maximum transformation work corresponds to the case when the whole band transforms into the martensitic state without plastic straining and is equal to the total work of the applied stress. Consequently, in stress-controlled experiments, shear-band intersection is not the best place for nucleation. A plate-like nucleus is more favourable. These results are in line with experiments. The effect of adiabatic heating was analysed in [24].

Stability analysis was also performed for another problem of PT in a spherical particle inside a cylindrical matrix [24]. These examples illustrate the competition between two different mechanisms of inelastic deformation, namely dislocation plasticity, described by flow theory, and deformation of crystal lattice due to a PT. The tool suggested—the extremum principle for determination of the stable deformation process—can be applied to describe the competition between other micromechanisms of inelastic straining, e.g. twinning, damage and so on. Note that in the case of softening behaviour at the PT, the stability analysis is also important for a PT in elastic materials [28].

3.4.4 Appearance of a martensitic plate in an elastoplastic material

Let us consider the appearance of a small temperature-induced martensitic plate in an elastoplastic material for the case of a plane strain state [23,24], see figure 3.21. The inverse problem is solved, i.e. the position and size of the transforming region is specified *a priori* and then the condition for a PT is determined. To evaluate the condition of martensitic plate formation with different ratios of its width and length, calculations were made for five cases of the appearance of a nucleus in regions I, I and II, I–III, I–IV and I–V, respectively. The following elastoplastic properties of steel were used in the calculations: Young's modulus $E = 2 \times 10^5$ MPa, Poisson's ratio $\nu = 0.3$, the yield stress $\sigma_y = 2.5 \times 10^2$ MPa for an austenitic matrix and $\sigma_y = 8 \times 10^2$ MPa for a martensitic nucleus. The boundary of the sample is free from stresses which corresponds to experiments for a temperature-induced PT. For our calculations the transformation strain $\boldsymbol{\varepsilon}_t$ is subdivided into 60 increments. The final value of $\boldsymbol{\varepsilon}_t$ has the following components in the Cartesian coordinate system X_1X_2 (figure 3.21)

$$(\varepsilon_t)_{12} = 0.1 \qquad (\varepsilon_t)_{22} = 0.026 \tag{3.55}$$

the other components are zero. Solving the elastoplastic problem with an incrementally enlarged transformation strain, the stresses and value of the transformation work φ were determined.

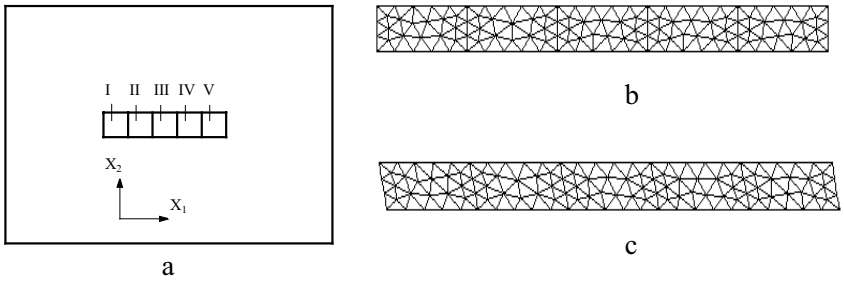

Figure 3.21. (*a*) Plane strain problem with stress-free boundary and thermally induced PT in regions I–V; FE meshes of regions I–V before (*b*) and after (*c*) the PT with simultaneous PTs in regions I–V.

According to the numerical results, the small martensitic plate deforms practically elastically with the exception of small regions near the short sides, figure 3.22. In the parent phase, the plastic strains are concentrated around the transformed plate, figure 3.22. The relation between the transformation work and ratio of width to length of the nucleus, $x = l/h$, is obtained and approximated by a parabolic function:

$$\varphi = \bar{A} + Bx + Cx^2 \qquad \bar{A} = -72.11\ \text{MPa}$$
$$B = 6.40\ \text{MPa} \qquad C = -0.29\ \text{MPa}. \tag{3.56}$$

Application of the principle of minimum transformation time

$$(A_1 + Bx + Cx^2)lh - 2\Gamma(l + h) \to \max_{x,l} \tag{3.57}$$

where $A_1 := \bar{A} - K^0 - \Delta\psi - E_a$, results in two algebraic equations

$$A_1 + 2Bx + 3Cx^2 = \frac{2\Gamma}{h} \qquad A_1 x - Cx^3 = \frac{2\Gamma}{h} \tag{3.58}$$

which are equivalent to a cubic equation with respect to x. Analysis shows that this equation has a thermodynamically admissible solution for a very high driving force and small activation energy only. Applying the principle of minimum of transforming volume together with the thermodynamic criterion

$$(A + Bx + Cx^2)l = 2\Gamma(1 + x) \qquad A := \bar{A} - K^0 - \Delta\psi \tag{3.59}$$

we obtained

$$V_n = lh = \frac{l^2}{x} = 4\Gamma^2 \frac{(1 + x)^2}{x(A + Bx + Cx^2)^2} \to \min_{x,l}$$

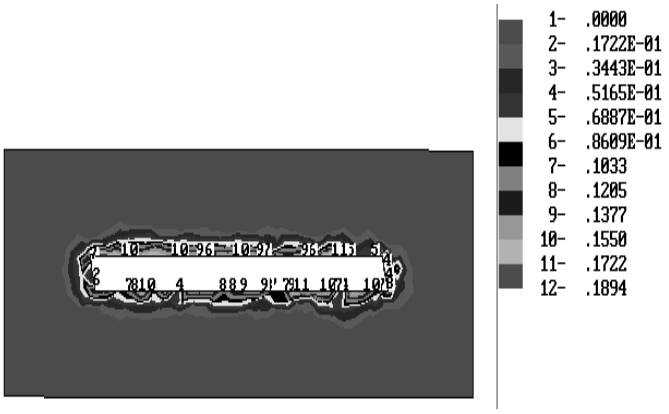

a

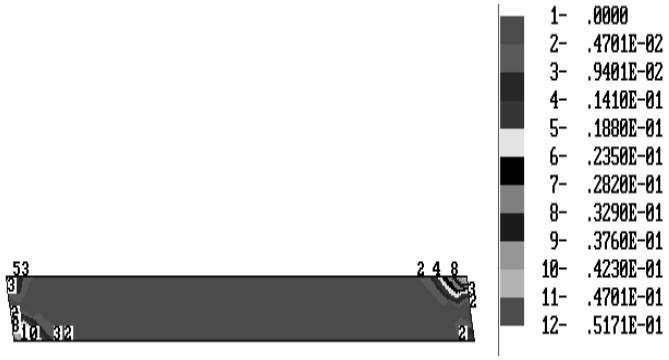

b

Figure 3.22. Isobands of accumulated plastic strain q in a matrix near the martensitic plate (*a*) and in the martensitic plate (*b*) after the PT.

and explicit expressions for the ratio of width to length of the nucleus and its length. In particular, at $x \gg 1$ we get

$$x = -\frac{B + \sqrt{B^2 + 12AC}}{6C} \qquad l = \frac{2\Gamma(1+x)}{(A + Bx + Cx^2)}. \tag{3.60}$$

The higher the driving force is, the smaller the nucleus is and, hence, the shorter transformation time. For example, at $A = 0$ we get $x = 7.36$, $l = 0.533\Gamma$ and at $A = -30$, we obtain $x = 10.61$, $l = 4.40\Gamma$.

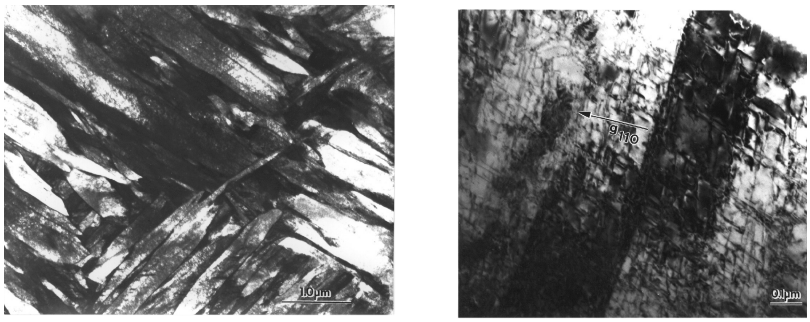

a) b)

Figure 3.23. (*a*) Bright field transmission electron micrograph of a lath martensite microstructure in Ferrium C69 steel oil quenched from 1100 °C (courtesy of Dr Gautam Ghosh). (*b*) Higher magnification view showing the dislocation substructure associated with plastic accommodation during martensitic growth (courtesy of Dr Gautam Ghosh).

3.4.5 Growth of a martensitic plate inside the austenitic matrix

Martensitic PTs in steels is characterized by a combination of a 2–5% volumetric transformation strain and a 20% transformation shear. The appearance of such high eigen strains in martensitic regions is known to be accompanied by plastic deformation (accommodation) in the austenite and martensite [15, 63, 107, 108] phases. Figure 3.23 shows a typical lath martensitic microstructure in a quenched alloy steel (commercial Ferrium C69 steel Fe–28Co–3Ni–5Cr–2.5Mo–0.17C marketed by QuesTek Innovations) with a high transformation temperature. The higher magnification view in figure 3.23(*b*) shows the dislocation substructure within the laths associated with plastic accommodation during growth. This plastic deformation changes the stress field, driving force and kinetics of martensitic transformation. It has been proposed that plastic accommodation causes the technologically important plate/lath morphological transition in steels [15, 63].

Plate martensite grows radially until it is stopped by a strong inhomogeneity, such as a grain boundary or another martensite plate. Lath martensite is arrested inside the grain without any such inhomogeneity. The problem is to find a mechanism for the growth arrest, which will identify material parameters controlling the plate/lath morphological transition and microstructure. Another problem is to explain why dislocations and, consequently, the plastic strain are concentrated in a martensite rather than in an austenite despite the yield stress of martensite being three times that of austenite. A further question is the exact relation between thermally activated kinetics at the interface level and athermal kinetics at the macrolevel.

The problems of the appearance and growth of a temperature-induced rectangular martensitic unit in an austenitic matrix in both bulk and near-free-surface environments were formulated, solved and analysed in [24, 25]. The interface velocity as a function of temperature and interface position is calculated. The following conclusions were made in [25].

1. Very non-trivial and heterogeneous stress–strain fields in the austenite and martensite and their non-monotonic variation during the transformation process are found, see, in particular, figures 3.24 and 3.25. The plastic shear strain in some points can reach 60% in the direction of the transformation shear and, after an elastic stage, change sign and vary by 40%. The edge profile of the moving interface varies in a non-trivial way as well (figure 3.24): the normal transformation shear profile is followed by a wave-like profile with a reverse shear near the corners and, finally, a practically undeformed vertical line. The jump in plastic shear strain across the interface reaches 90%. These results demonstrate the necessity of a finite strain treatment accounting for the jump in plastic strain across the interface in the expression for the driving force. Allowance for the Bauschienger effect, kinematic hardening and crystal plasticity would be desirable in future improved models.
2. The solution obtained explains why plastic deformation is concentrated in martensite rather than in austenite, despite the yield stress of martensite being much larger than that of austenite. At the initial stage, intense plastic deformations are generated near the interface from the austenite side, which then are inherited by growing martensite. At further stages, internal stresses cause additional plastic flow in martensite. Plastic flow in austenite is very limited (see figure 3.25(c)) because of a relatively small shape change in the contour of the martensitic unit (see figure 3.24(c)). Such a complex strain variation makes a very important contribution to the driving force for and athermal resistance to interface motion.
3. After the appearance of the martensitic particle, the transformation work decreases from -50.35 to -100.79 MPa during lengthening by 10%. The athermal interfacial dislocation forest hardening increases during such a growth from zero to 30.22 MPa which is one order of magnitude higher than the interfacial friction due to solute hardening. Both these changes lead to growth arrest and, consequently, to lath martensite instead of plate martensite. At the same time, rather high matrix internal shear stresses can promote autocatalytic nucleation of martensitic variants with the same or opposite transformation shear.
4. For elastic growth, martensite can be stopped only by a grain boundary or by another martensitic plate. The growth arrest inside the grain and transition from plate to lath martensite obtained in our calculations is due to the moving interface interacting with a TRIP strain. The smaller the yield stress of austenite is, the larger the plastic strain is, resulting in a stronger

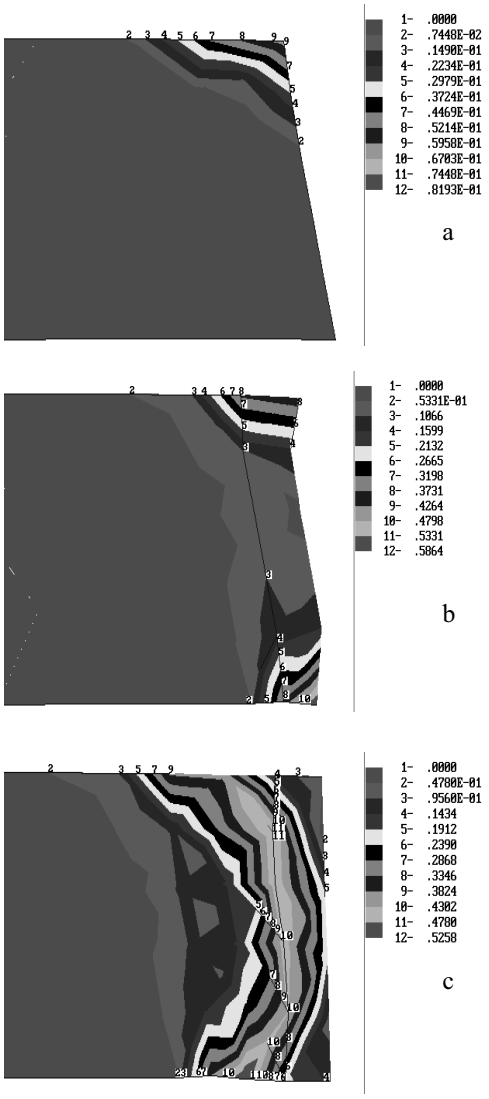

Figure 3.24. Isobands of the accumulated plastic strains in the right-hand part of the martensitic plate after nucleation (*a*) and two different interface advances (*b*) and (*c*). The new transformed regions in (*b*) and (*c*) are separated by a thin line.

tendency to growth arrest. Lath martensite is thus observed for steels with relatively high martensitic temperature, because the yield stress decreases with increasing temperature. Consequently, by controlling the yield stress

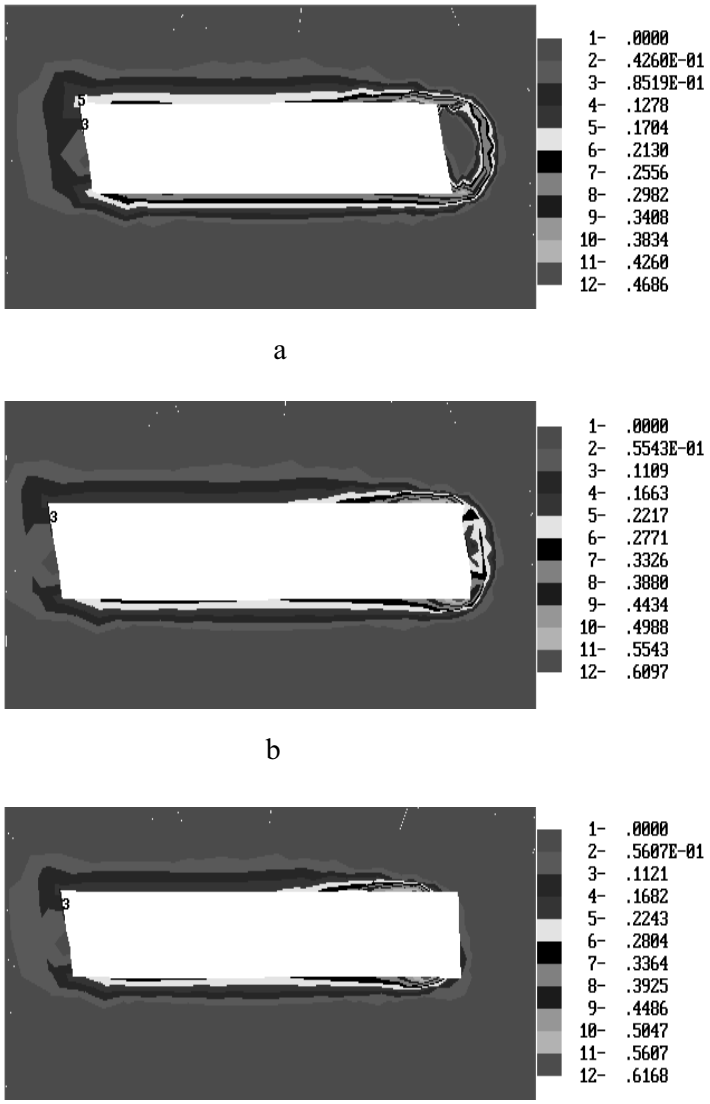

Figure 3.25. Isobands of the accumulated plastic strains in austenite near transformation regions after transformation in regions corresponding to those in figure 3.24.

of austenite (e.g. by proper alloying) one can control the microstructure and properties of steels.

5. A free surface does not significantly affect the driving force until its distance

from the moving interface falls below 0.75 of the thickness of martensitic region. Then the transformation work increases while the accumulated plastic strain q and associated dislocation forest hardening decreases sharply. If the interface is not arrested at this point, it then accelerates to the free surface. The edge interface profile goes through a wave-like form similar to the martensitic region in a bulk material but the final form corresponds to a transformation shear slightly compensated by plastic accommodation, forming an asymmetric 'tent-shaped' relief.

6. For time-independent nucleation, the transition from thermally activated kinetics at the interface level to athermal kinetics at the macrolevel is related to the fact that, independently of interface velocity, growth is terminated after some interface advance due to violation of the kinetic interface propagation criterion. For growth near the free surface, cessation is due to reaching the free surface.

In future research, rate and scale effects should be included to capture the path-dependent behaviour in nucleation and growth better. This may be based on a combination of dislocation-based viscoplasticity and gradient plasticity.

3.4.6 Modelling of the technological process in diamond synthesis

The industrial synthesis of D is a very complicated non-stationary and inhomogeneous process. One of the types of high-pressure apparatus for diamond synthesis is shown in figure 3.26 [109, 110]. The symmetry of the high-pressure apparatus about the vertical axis OA and horizontal plane OB makes it possible for us to limit the study to one quarter of its axial section.

The reaction mixture consists of G and metal and, after the PT G–D, of D as well. A container made of rock (pyrophillite, lithographic limestone) plays the role of deformable gasket. The heater is a mixture of G and rock. A cemented carbide die is press-fitted in a block of steel rings. Two compound plates reduce the axial stresses acting on the plate of the press. Such a system is compressed by the press to a pressure in a reaction mixture 4.5–5.5 GPa. The reaction mixture is heated to the diamond synthesis temperature (1600–2000 K) by passing a low-voltage current through the mixture. Then the metal is melted and G is dissolved into a metal. If the pressure exceeds the equilibrium value (3.29) for the G–D system, then carbon is crystallized in the form of D.

It is known that good quality D can only be obtained near the equilibrium line (3.29) [97, 98]. It follows from known experiments [111] and our simulation [110, 112–115] that the temperature and pressure are distributed extremely inhomogeneously. The question arises: how is it possible to obtain good quality D in some experiments under such inhomogeneous conditions? To answer this question we will use the results of our numerical modelling of D synthesis [34, 110, 112–116].

First of all, the compression of the system by the press is modelled [112, 115]. Large elastoplastic deformation of the container, reaction mixture and heater,

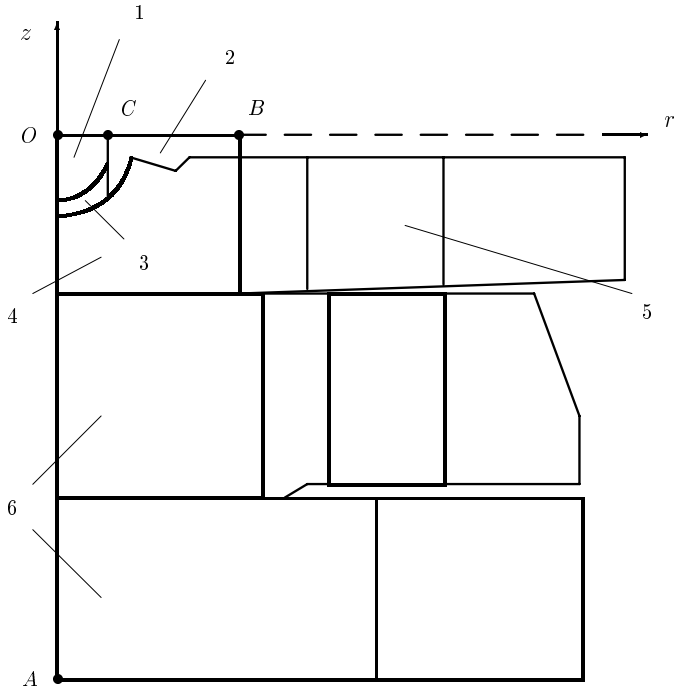

Figure 3.26. High-pressure apparatus for diamond synthesis: 1, reaction mixture; 2, container; 3, heater; 4, die; 5, block of rings; 6, compound plates.

the pressure dependence of the mechanical properties and contact sliding on the boundary between the die and container are taken into account. The theory of large elastoplastic deformation of materials under high pressure developed in [40] was used. Then electrical heating, stress redistribution, metal melting and the G–D PT were studied.

The thermostress state of the reaction mixture in a high-pressure apparatus changes during electric heating which results in a pressure increase. At the same time the G–D PT occurs starting from some instant of heating corresponding to attaining the technological parameters for diamond synthesis. This, in turn, affects the distribution of the electric, temperature and stress fields in the high-pressure apparatus. Therefore, there is interdependence between the processes of electrical and heat conduction, thermoplasticity and PT, i.e. the electric potential field depends on the temperature, pressure and D fraction fields; the temperature field depends on the electric potential, pressure and D fraction distributions fields; the stress fields depend on the temperature and D fraction and the D fraction field depends on the pressure and temperature distributions in the reaction zone. Besides this, there are physical and geometrical nonlinearities caused

by the temperature dependence of the thermophysical properties, the pressure dependence of the elastic and plastic properties and by the occurrence of large elastic and plastic strains.

A corresponding finite-element model has been developed to describe the processes running in a high-pressure apparatus during diamond synthesis with allowance for the enumerated features.

The complete system of equations comprises equations from plastic flow theory with allowance for finite strains, the equation of electrical conduction, the equation of non-stationary heat conduction, the kinetic equation for the rate of the D crystal growth, and the equations for carbon phase equilibrium (3.29) and metal solvent melting [110, 113–115]. The reaction zone is considered to be a mechanical mixture of G, a metal solvent and D, the efficient properties of which are determined from the components properties and mass fraction. The PT is taken into account through the changes in the properties, the mass fraction of D and the compressive volumetric transformation strain. The rate of D mass fraction change in the region of its possible synthesis (when the metal is melted and D is stable) is determined by the topochemical Avraamy–Yerofeyev equation. The time dependence of the temperature, pressure and volume fraction of D at two points in the reaction mixture is shown in figure 3.27. First, D crystals appear in the centre of the mixture. Then, with a D fraction increase and a decrease in the reaction mixture specific volume, a monotone pressure drop is observed. At $t = 51$ s, D growth in the high-pressure apparatus centre ceases. This corresponds to a pressure drop below the equilibrium pressure for the G–D system.

At the same time D synthesis occurs in the neighbourhood of the central point and the pressure decreases there as well. As the force averaged over the line OC in the horizontal section of the high-pressure apparatus remains practically constant, the pressure at point O increases.

The point O at the instant of time $t = 55$ s returns to the D stability region, D concentration growth is restarted, the pressure drops again and so on.

Consequently, pressure self-regulation is revealed which consists of pressure oscillation near the G–D equilibrium line. D crystals grow near the equilibrium line due to this effect, which explains why it is possible to produce high-quality D under very inhomogeneous pressure and temperature fields.

3.5 High-pressure mechanochemistry: conceptual multiscale theory and interpretation of experiments

3.5.1 Introduction

The most fundamental results in strain-induced SCs under high pressure were obtained in rotating Bridgman or diamond anvils (figure 3.28). After compression of the materials in Bridgman or diamond anvils, a very high pressure is produced in the centre of the specimen which leads to a number of PTs and CRs. It is known from numerous experiments that the addition of plastic shear, due to the

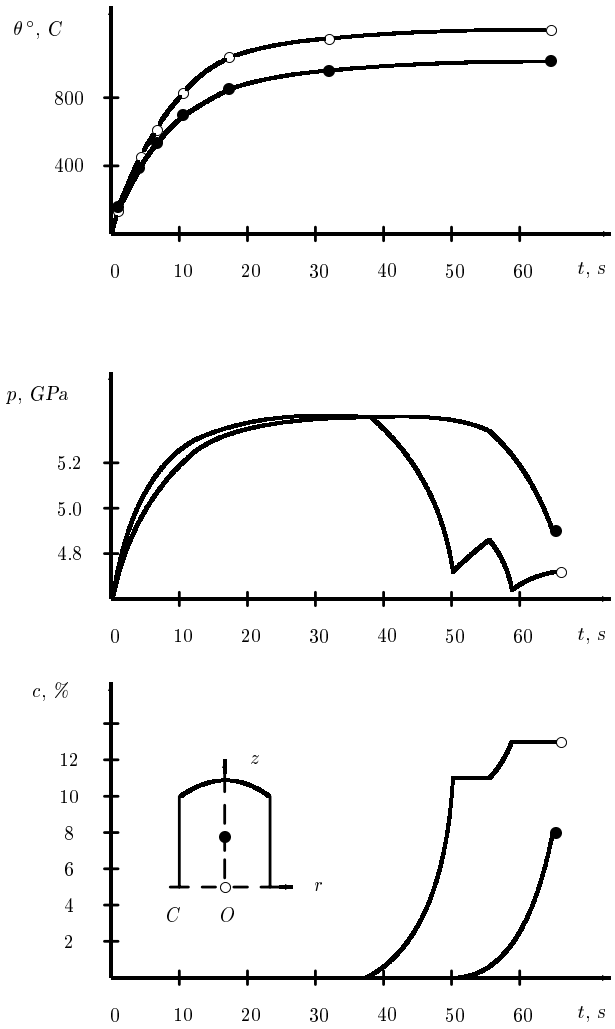

Figure 3.27. Time dependence of temperature θ, pressure p and diamond volume fraction at two points in the reaction mixture [109].

rotation of an anvil, leads to findings that have both fundamental and applied importance. In particular, it leads to the following results: (a) to a significant (by a factor of three to five) reduction in SC pressure and pressure hysteresis, (b) to the appearance of new phases, which cannot be obtained without additional shear, (c) to the substitution of a reversible PT by an irreversible PT and (d) to strain-controlled kinetics. These experimental results are discussed in details in section 3.5.2.

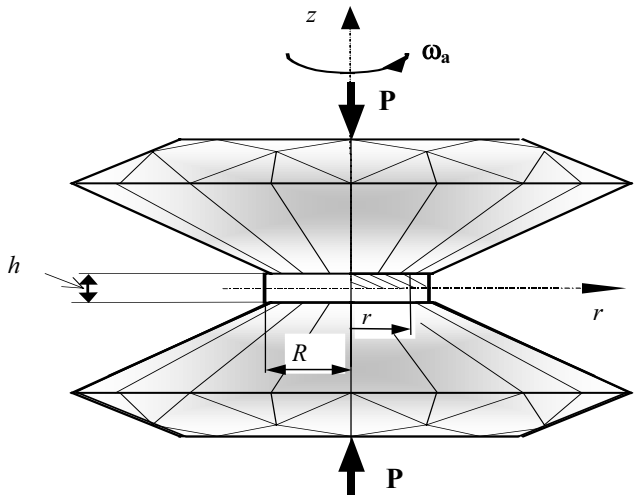

Figure 3.28. A diagram of compression and shear of materials in a rotational diamond anvil cell. The material is compressed by an axial force, P, followed by the rotation of one of the anvils with an angular velocity, ω_a.

Due to these experimental results, plastic strain is considered to be a factor which produces new physical mechanisms for CRs and PTs. There is, for example, a quantum mechanical theory based on the assumption that large plastic shears produce a so-called atom–ion state, which allows qualitative discussion about material behaviour under such conditions [117]. Gilman [118–121] suggests that *elastic* shear strain can accelerate CRs by lowering the HOMO (highest occupied bonding molecular orbital)—LUMO (lowest unoccupied anti-bonding molecular orbital) energy gap. He claims that this mechanism explains why ultra-fast CRs in a detonation front can occur athermally, and propagate supersonically [119, 120]. The specific examples which he discussed are lead azide, ammonium ions and nitrate ions. Gilman also mentioned that shear-induced reactions have been largely ignored in the explosives literature.

It is not clear, however, how to make the effect of *elastic* shear strains consistent with the previously described experiments on rotating Bridgman anvils. SCs do not occur without *plastic* shear despite the fact that friction shear stress and, consequently, elastic shear of the same magnitude are present at compression without or after anvil rotation.

Possible mechanisms for the effect of plastic deformation on the reactivity of solids are explained by qualitative models 'ROLLER' [122] and 'CONMAH' [123], see also [124]. For shock-induced CRs in a titanium–silicon mixture, Thadhani *et al* [105] emphasized that 'the initiation of chemical reactions in shock compression of powders is controlled by solid-state mechanochemical processes

and cannot be qualitatively or quantitatively described by thermochemical models'. They analysed qualitatively the importance of mechanochemical concepts, local stresses, viscoplastic flow and fracture for understanding of solid-state reactivity.

Two possible mechanisms explaining the effect of plastic shear on CRs are assumed in [125]. According to the first mechanism, a stressed chemical bond is chemically activated and reacts with other molecules under collision due to plastic flow of substances. The second mechanism is related to the transfer of high elastic bond energy into an oscillatory energy of molecules and, consequently, their high reactivity.

However, there has been no theory describing thermodynamic and kinetic coupling between plasticity and SC and any one of the previously described experimental effects. In [34], some doubts were formulated about a fundamental role of plastic shear. In fact, with the compression of materials in Bridgman or diamond non-rotating anvils, the mean value of plastic strain reaches 1000%. Additional plastic shear strains exceed several thousand per cent (see our finite-element calculation [126]) near the surfaces of the anvils due to contact friction and have the same character as shear strain in rotating Bridgman anvils. Why do none of the physical mechanisms for the effect of plastic strains on PTs and CRs manifest themselves at such large plastic shear strain but appear with the rotation of an anvil, giving an additional 10–100% plastic strain only? The fact that, without PTs, the pressure distribution is independent of the rotation of the anvil and the prehistory of deformation [127] confirms that strain hardening is saturated and plastic properties do not change any more. Also, PT starts at the centre or close to the centre of the disc where shear stress and strain are absent.

In our paper [34], the first macroscopic continuum theory, which gave a new and completely unexpected look on some of these phenomena, were developed. It dealt with the regularities of macroscopic plastic flow in thin cylindrical disc under compression and shear in rigid anvils with and without SC. Despite significant oversimplification, the theory explains, semiquantitatively, phenomena enumerated under items 1, 3, 7 and 9 in section 3.5.2 and allowed us to make some predictions how to obtain similar effect even without rotation of the anvil. One of the noteworthy confirmations of our approach is that of obtaining an irreversible PT from rhombohedral to superhard cubic phase of BN at a low pressure of 5.6 GPa and at room temperature, instead of 55 GPa under hydrostatic conditions [128, 129], see section 3.5.9.

A more quantitative analysis, however, shows that a macroscopic approach in some cases is not sufficient for the explanation of these phenomena even at the order of magnitude accuracy. It can be shown that the magnitude of the decrease in PT pressure predicted by theory [34] is much smaller than that observed experimentally. The theory [34] gives an upper bound for strain-controlled kinetics which cannot be reached in most cases.

We will show here that further development of the macroscopic theory will allow us to describe quantitatively some important mechanism-independent

features of shear-induced SCs. However, it is insufficient for the description of mechanism-dependent phenomena. We also develop approximate nanoscale and microscale approaches and analyse numerous phenomena of strain-induced PTs and CRs. They are based on a general theory of SC in plastic materials, which we developed in [21, 22, 34], see section 3.2. We believe that our models will be applicable for various materials and loadings. This belief is supported by results described in item 14 of section 3.5.2.

In this section, we develop a multiscale continuum thermodynamic theory which explains the key phenomena occurring during strain-induced SCs under high pressure and allows us to develop a new characterization of PTs and CRs under plastic deformation, as well as methods to control PTs and CRs (see [130]).

At the nanoscale, the main reason for these phenomena is related to the generation of new defects during plastic flow, which produce a strong stress concentration and serve as new nucleation sites. We developed a model for nucleation at the tip of dislocation pile-up. It is demonstrated that shear stress can lead to the substitution of thermally activated nucleation with barrierless nucleation and significantly reduce SC pressure for direct SC, as well as increase SC pressure for reverse SC.

At the microscale, a new strain-controlled kinetic equation is developed which takes into account the possibility of direct and reverse SC and the difference in plastic strain in each phase because of the different yield stress of the phases. It is shown that there is a number of reasons why plastic strain promotes the appearance of hard phases more than weak phases. The conditions for zero-pressure hysteresis were also demonstrated.

At the macroscale, the mechanics of plastic flow and SC in rotating diamond anvils is described. Changes in the PT and CR conditions due to the rotation of the anvil are related to the possibility of additional axial displacement, which compensates for a volume decrease, increases pressure and plastic strain. It is also found that the rotation of an anvil can lead to new phases, which were not obtained without anvil rotation.

The solutions predict the unique potential of the rotating anvil method to produce high-strength metastable phases.

To avoid unnecessary complications, we will use a small strain formulation. Finite strain theory and some analytical and numerical solutions can be found in [21, 23–26]. Our experience shows that allowing for finite strain does not change conceptual conclusions, which are the main goal of this work.

3.5.2 Experimental phenomena

Research into PTs and CRs in rotational Bridgman anvils was initiated by Bridgman [131] who reported that he could cause a number of chemical reactions, in particular, to cross-link polymers, decompose compounds and drive substitutional reactions, see also [132, 133]. Enikolopyan *et al* [134–136] and Zharov [125, 137, 138] extended Bridgman's work to various inorganic and

organic compounds and to the polymerization of various organic monomers. Decomposition of more than 30 oxides were studied by Vereschagin *et al* [139]. Blank *et al* developed the rotational diamond anvil cell (RDAC) and obtained a number of very interesting results, see [140–154]. The mechanical aspects of material behaviour in RDAC were analysed in [127]. Recently, experimental research using RDAC was initiated in the USA [155, 156].

Here we enumerate and systematize some experimental phenomena, which occur during the compression and shear of various materials in RDAC. These phenomena are important for the analysis of the effect of plastic strain on high-pressure SCs.

1. *Rotation of one anvil significantly reduces the PT pressure* for some materials. For example, for PT B1 $\rightarrow$ B2 in KCl, the pressure at the diffuse interface between these phases decreases from 2.4–3.0 GPa to 1.8 GPa due to rotation [146]; see also our data [157]. The PT from cubic to orthorhombic phase in PbTe (0.50 volume fraction of orthorhombic phase) was produced at 4.6 GPa under the rotation angle $\varphi = 40^\circ$ but was not observed at 6.6 GPa without shear. Without shear, the volume fraction of the orthorhombic phase varied from 0.15 to 0.2 in a pressure range of 9.6–12.3 GPa [153]. For the PT from diamond-cubic structure I to bcc structure III, the PT pressure is reduced in Ge from 9 GPa without shear to 3 GPa at rotation angle 1000° and from 11 to 2.5 GPa for similar PT in Si [144, 151]. The pressure drops from 12.3 to 5.7 GPa for the PT from structure III to metal tetragonal (II) phase in Si; and from 9.3 to 4.2 GPa for the PT from semiconductor structure III to the metal tetragonal (II) phase in Ge [144, 151]. The PT semiconductor–metal in InTe starts at pressure 2.2 GPa without shear and can be detected at 0.4 GPa at 1000° of rotation of the anvil [142].

   The rotation of one anvil significantly reduces the threshold pressure for the beginning of some CRs. For example, the pressure of tens of GPa does not cause a transformation (opening of aromatic circles) of aromatic hydrocarbons; however, under the rotation of an anvil at pressure 8–10 GPa, transformations accompanied by the rupture of aromatic circles are observed in benzene, pyridine and thiophene [125, 138].

   It has been shown in [158] that benzene and thiophene can polymerize under a pressure no lower than 20 GPa for benzene and 16 GPa for thiophene, respectively. Under shear, polymerization occurs at 8.5 GPa for benzene and 5 GPa thiophene [159, 160].

   At the same time, it was found in [161] that for some PT (PbO_2I $\leftrightarrow$ PbO_2II, calcite $\leftrightarrow$ aragonite, quartz $\leftrightarrow$ coesit) additional shear does not change the PT pressure at any temperature; however, it significantly accelerates the PT kinetics. The equilibrium pressure–temperature line is the same but under the shear stress, the reaction starts at a temperature lower by 100–300 K. The volume fraction *versus* time plot shows that at the beginning, the transformation rate is comparable with and without

shear. However, for a longer time, kinetics with shear is much faster and saturation occurs at different fractions. These results contradict all previously mentioned experiments.

Note that even under the compression without the rotation of an anvil, plastic deformation significantly reduces the PT pressure. For example, an irreversible PT from γ-Al_2O_3 to a new phase was recently reported under a quasi-hydrostatic pressure over 50 GPa and a non-hydrostatic pressure above 35 GPa [162]. We also mention the results on shock loading of InSb single crystal [163]: due to shear stresses, the PT occurs at a pressure of 0.95 GPa which is much lower than the static value of 2.5 GPa.

2. *Small 'steps' (regions with almost constant pressure) are found at the very heterogeneous pressure distribution* (figure 3.29) [127, 145, 146, 151]. These steps correspond to two-phase regions (diffuse interfaces) in which PTs occur. It is suggested that the pressure value at these steps should be used as the pressure characterizing the PT under consideration [146, 151]. However, there is no theory supporting this hypothesis. Moreover, it follows from the simplified equilibrium equation [40, 164] that the pressure gradient is proportional to the yield stress in shear (see equation (3.87)); consequently, the yield stress in the two-phase region is zero during the PT. This contradicts numerous stress–strain curves for TRIP steels measured in the process of strain-induced PT [12].
3. *Rotation of an anvil reduces pressure hysteresis*, i.e. the difference Δp between the start pressure of direct and reverse PTs. For the PT semiconductor $\leftrightarrow$ metal in InSb, $\Delta p = 1.0$ GPa under shear instead of 1.75 GPa under hydrostatic conditions [143]. The other definition of pressure hysteresis is the difference in pressure at the steps in pressure distribution (diffuse interface between phases) at direct and reverse PT. For the B1 $\rightarrow$ B2 PT in KCl after the rotation of an anvil by 15°, the pressure at the interface was 1.8 ± 0.1 GPa at direct and reverse PT (i.e. there is no hysteresis); without rotation, the pressure at the plateau was 2.4–3.0 GPa at the direct and 1.2–1.4 GPa at the reverse PT [146]. From this, it was claimed that the pressure at the interface under compression and shear can be interpreted as an equilibrium pressure which can be used for the pressure–temperature phase diagram. As we will show later, this is not true.
4. *Direct PT pressure under shear is lower than equilibrium pressure.* For some PT (e.g. semiconductor $\rightarrow$ metal in InSb, InTe, Ge (I $\rightarrow$ II) and Si (I $\rightarrow$ II) [142–144]), direct PT pressure under shear is lower than equilibrium pressure. It is also lower than the reverse PT pressure under hydrostatic conditions. This means that plastic shear not only reduces hysteresis but lowers equilibrium pressure as well. This complicates the interpretation of pressure measured at the diffuse interface as an equilibrium pressure because it depends on shear.
5. *Rotation of an anvil leads to new phases (materials) which were not produced without rotation*. As examples we can mention the rhombohedral

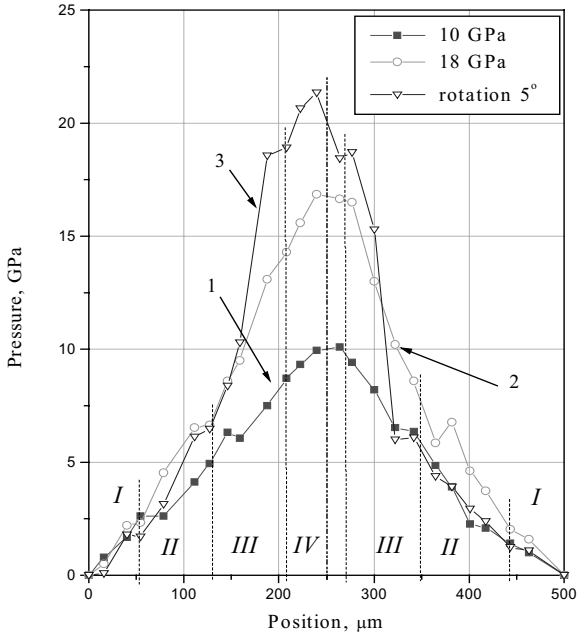

Figure 3.29. Radial pressure profiles in a fullerene sample before (2) and after (3) a shear strain [127].

phase of GeTe [165], Cu I–VIII′ phase [145], phase *V* of fullerene C_{60} [127, 152, 157]. Phase V of fullerene, which was obtained in [152] and confirmed in [127, 157] at a pressure of 18 GPa and superimposed shear at room temperature (see figure 3.29), is harder than diamond. After this discovery, several phases of fullerine were obtained without shear, e.g. at pressure 9.5 GPa and temperature 700–900 K and at pressure 13 GPa and temperature 900–1830 K [149]. As examples of new CRs we can mention the macromolecular products of methylmethakrylate and maleic anhydride, which were not obtained without shear deformation [125, 138]. Other examples are: the addition of NH_3 at the –C=C– bond (aminoacid synthesis), synthesis of amides from ammonium salts of saturated acids, esterification reaction, polymerization of solid vinyl monomers, and peroxide decay and synthesis of peptides from amino acids [137]. Under shear, γ-BN interacts with water at pressure 1–1.5 GPa; without shear, it does not interact even at 27 GPa [140].

6. *In some cases, shear deformation substitutes a reversible PT with an irreversible PT*. As a specific example, the reversible graphite → lonsdaleite (hexagonal diamond) transition has been observed at a pressure of 16–30 GPa at room temperature; the irreversible graphite → lonsdaleite transition has been obtained at pressures of 17 and 19 GPa under shear

at room temperature [150]. Consequently, the rotation of an anvil allows production of phases which are metastable at normal pressure and *can be used in engineering applications*.

These results indicate that shear deformation increases pressure hysteresis, which contradicts the results in item 3.

7. *The volume fraction of the new phase is an increasing function of the rotation angle and consequently of the plastic shear strain. When the rotation stops, PT stops as well* (see [142] for PT semiconductor → metal in InTe, [166] for a PT from cubic to orthorhombic in BaF_2 and references on similar relations for PTs in titanium and zirconium). Therefore, a pressure–temperature–shear phase diagram is suggested [144, 151] and strain-controlled kinetics is considered. Thus, plastic shear is considered the new fundamental thermodynamic parameter.

   A similar regularity takes place for various CRs (see [125, 138] for the polymerization of acrylamide, methacrylamide, maleic anhydride, and trioxan). The CR occurs during the deformation events rather than afterwards.

8. *The rate of solid-state CR increases by a factor of* 10^2–10^5 *with shear strain compared with liquid-phase reaction*, e.g. for some polymerization reactions in acrylamide, styrene and butadiene [125, 138]. The rate of reaction is weakly or almost independent of pressure and temperature [125]. According to estimates analysed in [125, 138], *heating due to plastic flow is not significant and cannot be responsible for such high reaction rates*. An assumption about the existence of hot spots where the material is melted cannot explain high rates of CR as well [125, 138].

9. *Pressure growth in the transferring region.* Sometimes, under shear at a fixed compressive force, the pressure grows in the transforming region despite the volume decrease due to PT [127, 145, 146, 148, 151–153, 157]. This is the so-called 'pressure self-multiplication effect' (figure 3.29). Similarly, pressure decreases in the transforming region during the reverse PT with shear under constant force, despite the volume increase. These effects were revealed in [146] for the B1 → B2 PT in KCl: the pressure in the centre of the disc has been increased (decreased) on 50–70% after shear due to direct (reverse) PT; see also [127, 157]. For PT in PbTe from a NaCl (cubic)-type structure to a GeS (orthorhombic)-type structure, as well as from GeS to CsCl (cubic)-type structure, the pressure grows from 4.6 to 6.6 GPa and from 9.6 to 12 GPa, respectively [153]. The pressure growth is remarkable in fullerene during the IV → V PT: from 21 to 32 GPa, from 23 to 38 GPa [152] and from 18 to 21.5 GPa [127, 157] (figure 3.29).

   At the same time, at the diffuse interface, the pressure reduces from 9 to 7 GPa for the PT from the semiconductor bcc (III) to the metal tetragonal (II) phase in Ge under shear [144, 151]. Pressure decreases in the centre of disc from 34 to 24 GPa on the appearance of a new Cu I–VIII′ phase under shear at constant load [145].

The pressure self-multiplication effect under a fixed applied load is also observed without the rotation of an anvil. The PT B1 $\rightarrow$ B2 in KCl causes a 30% increase in pressure during heating from 300 up to 600 K with an initial pressure of 6 GPa at the centre [147]. During the PT from rhombohedral to cubic BN caused by rotational plastic instability, pressure grows from 5.6 GPa to an extremely high estimated value of 60–76 GPa [128].

These results represent a violation of the Le Shatelie principle.

10. *The rate constant for CR in organic compounds in the presence of indifferent compounds (non-reacting matrix) depends linearly on the yield stress of the matrix* [137, 167]. A matrix with a high yield stress increases the reactivity and *the deformation in such a matrix produces chemical transformations of even those compounds which otherwise did not enter the reactions.* The pressure required to initiate reactions can be significantly lower. For example, use of adamantan as a matrix reduces the threshold pressure for polymerization of succinic acid dinitrile from 10 to 3 GPa; for polymerization of naphtaline from 4 to 2 GPa; for the decomposition of $Mo(CO)_6$ from 7 to 3.5 GPa; for the decomposition of $W(CO)_6$ from 5 to 2.5 GPa [137]. A matrix with the yield strength lower than that for reagents slows down the reaction.
11. *Increase in rotation rate reduces PT pressure.* For the semiconductor–metal in InSb, an *increase in rotation rate* from 5×10^{-3} to 5×10^{-1} grad s^{-1} at the rotation angle $\varphi = 10^{\circ}$ *reduces PT pressure* from 1.9 to 1.4 GPa [143]. A decrease in the PT pressure with an increase in the deformation rate is observed for the B1 $\rightarrow$ B2 PT in KCL and RbCl in an extrusion test. For example, an increase in the deformation rate by a factor of 6.15 for RbCl leads to a decrease in the PT pressure from 0.75 to 0.62 GPa at strain of 0.1 [38]. The rate of rotation of an anvil does not affect the volume fraction of the polymer produced [125, 138]. However, the reduction in the rate of anvil rotation suppresses decomposition of some oxides [139].
12. *Plastic straining changes the transformation path*. For example, it causes the I $\rightarrow$ II PT instead of I $\rightarrow$ II$'$ $\rightarrow$ II for the semiconductor–metal PT in InTe [142]. Some phases (e.g. semiconducting III phases in germanium and silicon) appear at pressure release and at shear at a constant pressure but were not observed at a pressure increase without rotation [144, 151].
13. *Pressure hysteresis for PT after preliminary plastic deformation is proportional to the material hardness and consequently the yield stress* [21, 34, 37–39].
14. *Regardless of the method used for creating the high pressure and shear deformation conditions (rotating anvils, shock wave, extrusion, extrusion through an annual gap with simultaneous rotation of dorn), the same reactions occur which do not occur at the usual compression* up to a pressure of 8 GPa [137]. Examples mentioned in [137] are the addition of NH_3 at the –C=C– bond (aminoacid synthesis), synthesis of amides from ammonium salts of saturated acids, esterification reaction, polymerization of solid vinyl

monomers, and peroxide decay and synthesis of peptides from amino acids.

15. *Without a PT, the pressure distribution is practically independent of rotation*, e.g. for NaCl [127, 146]. We obtained stronger results for NaCl and X18H10T hardened steel [127]. Without a PT, the pressure distribution is practically independent of the complex deformation history, including the unloading and rotation of the anvil. As it will be discussed in section 3.5.8 (see also [34, 40]), this means that the strain hardening is saturated and the plastic properties have reached their steady state.

Summarizing these experimental results, one can conclude that additional rotation of an anvil and consequently, plastic shear leads to a significant reduction in SC pressure, in some cases lower than equilibrium pressure and even lower than pressure of reverse SC at hydrostatic conditions (however, for some materials, additional shear does not change the SC pressure but it significantly accelerates SC kinetics); to reduction in pressure hysteresis; to the appearance of new phases, which were not obtained without additional shear; to the substitution of reversible SC by an irreversible one, which allows one to use these phases in engineering applications; to change the SC path; sometimes to the pressure growth in transforming zone at constant force during direct SC (despite the volume decrease), as well as to the pressure decrease in the transforming zone at constant force during reverse SC (despite the volume increase). Moreover, the volume fraction of the new phase is an increasing function of the plastic shear strain, i.e. strain-controlled rather than time-controlled kinetics is considered; an increase in rotation rate reduces SC pressure.

There is a number of problems which we would like to address in this section.

1. What are the main reasons for these effects and some of the contradictions?
2. Is it possible to define the equilibrium pressure in experiment using RDAC technique?
3. How to characterize and describe high-pressure SC under non-hydrostatic conditions and plastic straining? Is the pressure–temperature–shear diagram informative?

The goals of this section are:

(a) to develop a first conceptual three-scale theory which explains, in a first approximation, these phenomena;
(b) to apply this theory for the interpretation of measurements of the SC pressure and the characterization of strain-induced SCs under high pressure;
(c) to summarize possible methods to control the SCs; and
(d) to outline new coupled theoretical, experimental and modelling problems based on the new understanding gained from the developed theory.

Ultimately, it is necessary to develop a theory which will allow computational modelling of strain-induced SCs and comparison of SCs in various high-pressure apparatuses and various loading processes.

Consideration at the nano- and micro-scale will be done for crystalline solids. Macroscopic treatment can be applied, probably for any material. For convenience, compressive stress (pressure) and strains will be considered as positive.

3.5.3 Net driving force for structural changes in inelastic material

Recently, a new general continuum thermodynamic and kinetic theory for SCs in elastoplastic materials was developed [21, 22, 34], see section 3.2. We will only use the equations necessary for our study. In the simplest case, when the temperature is fixed and homogeneous in a transforming volume and elastic properties of phases are the same, the net thermodynamic driving force for SC in the region V_n bounded by surface Σ is as follows [21, 22]:

$$F := (\bar{X} - K)V_n = \int_{V_n} \int_0^{\boldsymbol{\varepsilon}_{t2}} \boldsymbol{T} : \mathrm{d}\boldsymbol{\varepsilon}_t \, \mathrm{d}V_n - (\Delta\psi(\theta) + K)V_n - \int_\Sigma \Gamma \, \mathrm{d}\Sigma. \quad (3.61)$$

Here $\bar{X}$ is the driving force for SC, which represents the total calculated dissipation increment due to SC only (i.e. excluding all other types of dissipation, e.g. plastic dissipation) during the entire transformation process, averaged over the transforming region; K is the athermal dissipation due to SC related mostly to interface friction; $\boldsymbol{T}$ is the stress tensor; $\Delta\psi$ is the jump in the thermal part of the Helmholtz free energy per unit volume; θ is the temperature; Γ is the surface energy per unit area. The key point of equation (3.61) is that it takes into account the whole history of stress variation during the transformation process, which depends, in particular, on the interaction of the transforming region with the surrounding material. This may explain why the PT pressures obtained not only in different high-pressure apparatuses but also in the same apparatus under different conditions (e.g. geometry and properties of a gasket) differ significantly. Another important point is that the driving force (3.61) takes into account the stress tensor rather than the pressure only. For elastic materials, the expression for XV_n coincides with the change in Gibbs free energy of the whole system [21], i.e. as in a standard approach.

3.5.4 Nanoscale study

It is well-studied that strain-induced nucleation, e.g. in TRIP steels at normal pressure, occurs at new defects generated during plastic flow. However, we are not aware of any experimental or theoretical work for materials compressed and sheared in diamond anvils which (a) determines the nucleating defects, (b) describes theoretically its effect on nucleation and (c) tries to describe phenomena from section 3.5.2.

In this section, we consider one possible mechanism of intensification of SCs by the stress concentration created by the dislocation pile-up. Dislocation pile-up is the strongest defect used to model slip transfer from grain to grain [168],

temperature induced martensitic PT [55] and deformation twinning [168]. Our model has some distinctions and will allow us to explain some of the phenomena described in section 3.5.2 and find controlling parameters. For an explanation of the reduction of SC pressure by a factor of 3–5, the strongest defect is required like pile-up consisting of ∼20 dislocations (see below). If the dislocation pile-up would not be able to explain such an effect, none of the other defects could help and new physics would be required. However, we do not exclude that for some materials with the weaker effect of shear stress on SC pressure, other defects (grain and subgrain boundaries, twins and stacking faults) may be more important. For these defects, some points in the approach of this paper can be applied as well. Note that under high pressure, even brittle materials can undergo large plastic deformations, so our model is applicable for them as well. We hope that this first conceptual approach in the field will lead to future systematic experimental and theoretical studies

Assume that plastic flow occurs by activation of Frank–Read or Köehler sources and the motion of the generated edge dislocations to a barrier (e.g. grain, twin or subgrain boundary). A dislocation pile-up of length l assists in nucleating the second-phase region. A nucleus will be considered as a pill-box with sizes $2L \times 2c \times b$, with $n = c/L \ll 1$ (figure 3.30), inclined under angle ϕ in the pile-up direction. Plane stress and small strain formulations will be used. Transformation strain $\boldsymbol{\varepsilon}_{\mathrm{t}}$ in the nucleus is an invariant plane strain consisting of shears, 0.5γ, along the sides L and c (due to the symmetry of $\boldsymbol{\varepsilon}_{\mathrm{t}}$) and normal strain, ε, along side c. Allowing the other components of transformation strain to be trivial does not change the main conclusions. External stresses have normal, σ_1 and σ_2, and shear, τ, components, where τ is the resolved shear stress for dislocation motion, i.e. the yield stress in shear.

To estimate the driving force, one has to calculate the transformation work which after all these assumptions can be written as

$$A_{\mathrm{t}} = \int_{V_{\mathrm{n}}} \int_0^{\boldsymbol{\varepsilon}_{\mathrm{t}}} \boldsymbol{T} : \mathrm{d}\tilde{\boldsymbol{\varepsilon}}_{\mathrm{t}} \, , \mathrm{d}V_{\mathrm{n}} \qquad \boldsymbol{T} = \boldsymbol{\sigma} + \boldsymbol{\sigma}_{\mathrm{es}} + \boldsymbol{\sigma}_{\mathrm{d}} \tag{3.62}$$

where $\boldsymbol{\sigma}$, $\boldsymbol{\sigma}_{\mathrm{es}}$ and $\boldsymbol{\sigma}_{\mathrm{d}}$ are the contributions to the total stress $\boldsymbol{T}$ from the external stress, internal stresses due to transformation strain (Eshelby inclusion stress) and dislocation pile-up, respectively. Since stresses $\boldsymbol{\sigma}$ and $\boldsymbol{\sigma}_{\mathrm{d}}$ are independent of $\boldsymbol{\varepsilon}_{\mathrm{t}}$, integration over the $\boldsymbol{\varepsilon}_{\mathrm{t}}$ is trivial. For the external stress, the Mohr transformation is used. The work of $\boldsymbol{\sigma}_{\mathrm{es}}$ is estimated for an ellipsoidal cylinder of infinite length with semi-axes L and c. We have [106]

$$\begin{aligned} \sigma_{\mathrm{es}} &= -\frac{\mu}{1-\nu} n\tilde{\varepsilon} \qquad \tau_{\mathrm{es}} = -\frac{\mu}{1-\nu} n\tilde{\gamma} \\ \int_{V_{\mathrm{n}}} \int_0^{\boldsymbol{\varepsilon}_{\mathrm{t}}} \boldsymbol{\sigma}_{\mathrm{es}} : \mathrm{d}\tilde{\boldsymbol{\varepsilon}}_{\mathrm{t}} \, \mathrm{d}V_{\mathrm{n}} &= \pi Lcb \left(\int_0^{\varepsilon} \sigma_{\mathrm{es}} \, \mathrm{d}\tilde{\varepsilon} + \int_0^{\gamma} \tau_{\mathrm{es}} \, \mathrm{d}\tilde{\gamma} \right) \\ &= -4bn^2 L^2 s(\varepsilon^2 + \gamma^2) \end{aligned} \tag{3.63}$$

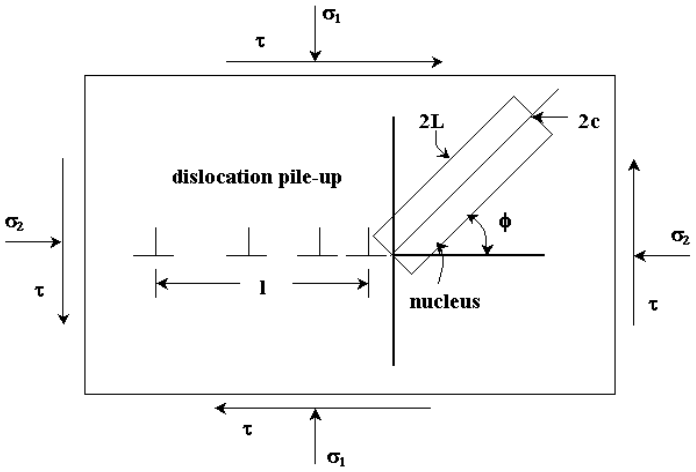

Figure 3.30. The nucleation scheme at the tip of dislocation pile-up.

where $s = \mu\pi/8(1-\nu)$ and μ and ν are the shear modulus and Poisson ratio, respectively.

The stress field of the pile-up will be approximated by the stress field of the superdislocation [168]:

$$\sigma = \frac{l\tau}{2}\frac{\sin\phi}{r} \qquad \tau_l = \frac{l\tau}{2}\frac{\cos\phi}{r} \tag{3.64}$$

where r is the current radius of the points of the nucleus, τ_l and σ are the shear and normal stresses along sides L and c. This will give us the lower bound since, for small distances, the stress for the pile-up varies as $r^{-1/2}$; however, the analytical expression is too complex for close-form integration. Note that stresses

$$l\tau = \mu N|\boldsymbol{b}|/(\pi(1-\nu)) \tag{3.65}$$

are proportional to the number N of dislocations in a pile-up (and approximately to plastic strain), i.e. they can be extremely high [168]. Here $\boldsymbol{b}$ is the Burgers vector. We can estimate the corresponding transformation work:

$$\begin{aligned}\int_{V_n}\int_0^{\boldsymbol{\varepsilon}_t} \boldsymbol{\sigma}_d : \mathrm{d}\boldsymbol{\varepsilon}_t\,\mathrm{d}V_n &= \frac{l\tau}{2}(2cb)\int_c^{2L}(\varepsilon\sin\phi+\gamma\cos\phi)\frac{\mathrm{d}r}{r}\\ &= l\tau bLn\ln\frac{2}{n}(\varepsilon\sin\phi+\gamma\cos\phi)\end{aligned} \tag{3.66}$$

where the cut-off radius for the dislocation is taken as c, which underestimates the transformation work. Finally one obtains

$$F = \left(\left(\frac{\sigma_1+\sigma_2}{2}+\frac{\sigma_1-\sigma_2}{2}\cos 2\phi+\tau\sin 2\phi\right)\varepsilon\right.$$

$$+\left(\frac{\sigma_2-\sigma_1}{2}\sin 2\phi+\tau\cos 2\phi\right)\gamma\Bigg)4bnL^2$$
$$-(\Delta\psi+K)4bnL^2-4bn^2L^2s(\varepsilon^2+\gamma^2)$$
$$+l\tau bLn\ln\frac{2}{n}(\varepsilon\sin\phi+\gamma\cos\phi)-4\Gamma L(b+bn+2nL). \quad (3.67)$$

According to the postulate of realizability [21, 22, 34], the net driving force has to be maximized with respect to ϕ and n which is impossible to do analytically. We first maximize it with respect to ϕ for the case when the contribution from the pile-up is much stronger than from the external stresses, i.e. by varying ϕ in the pile-up term only. Then one obtains, from equation (3.67),

$$\tan\phi=\frac{\varepsilon}{\gamma}\qquad F=AL^2+BL\qquad B=l\tau bn\ln\frac{2}{n}\sqrt{(\varepsilon^2+\gamma^2)}-4\Gamma b$$
$$A=(\sigma_2\varepsilon+\tau\gamma)4bn-(\Delta\psi+K)4bn-4bn^2s(\varepsilon^2+\gamma^2)-8\Gamma n. \quad (3.68)$$

This also gives us the lower bound for F. Despite the result that F is independent of σ_1, because of the macroscopic von Mises yield condition $(\sigma_1-\sigma_2)^2+3\tau^2=3\tau_y^2$ (τ_y is the yield stress in shear) and the closeness of τ to τ_y, σ_1 and σ_2 are also close. If $B<0$, which is the case for the weak or no dislocation pile-up and low τ, nucleation requires thermal fluctuations (see section 3.5.4.2). We start with the case $B>0$.

3.5.4.1 Barrierless nucleation

If $B>0$, which is true for the strong dislocation pile-up and large τ, even for $A<0$ for relatively small L, one has $F>0$. This shows that barrierless nucleation occurs independently of the magnitude of A and pressure. However, the equilibrium value of $L_e=-B/A$, determined from the condition $F=0$, depends on A. We can maximize B with respect to n; however, the obtained value $n=2/e=0.74$ does not satisfy condition $n\ll 1$ which was used in the previous derivations. We assume $n=0.1$ as the maximum reasonable value satisfying this condition. Then the criterion for barrierless nucleation, $B>0$, is

$$l\tau>13.35\frac{\Gamma}{\sqrt{(\varepsilon^2+\gamma^2)}}. \quad (3.69)$$

If we take $\Gamma=0.1$ N m^{-1} (typical value for semicoherent interface for steels), $\varepsilon=0.1$ and $\gamma=0.2$, then $l\tau>5.97$ N m^{-1}. This condition can be easily satisfied for reasonable values of τ and l, e.g. $\tau=0.1$ GPa, $l=60$ nm or $l=1$ μm and $\tau=6$ MPa. For a coherent nucleus for ferrous and non-ferrous alloys, $\Gamma=0.01$ N m^{-1} which makes barrierless nucleation even easier.

Alternatively, we can estimate the number of dislocations N necessary for barrierless nucleation by combining equations (3.65) and (3.69)

$$N>13.35\frac{\Gamma(\pi(1-\nu))}{\mu|\boldsymbol{b}|\sqrt{(\varepsilon^2+\gamma^2)}}.$$

If, in addition to the above parameters, we chose $|\boldsymbol{b}| = 3 \times 10^{-10}$ m and $\nu = 0.3$, then $N > 1$ corresponds to $\mu \geq 43.76$ GPa; N dislocations will lead to barrierless nucleation for $\mu \geq 43.76/N$ GPa. For example, for steel $\mu = 80$ GPa, only one dislocation is sufficient for barrierless nucleation. Consequently, thermally activated regime is important for materials with relatively low elastic moduli, small transformation strains, and small Burgers vector.

Let us define the effect of shear stress on SC pressure for a detectable size of nucleus at $\sigma_1 = \sigma_2 = p$. From condition $L = -B/A$, one derives

$$p = \frac{\Gamma}{\varepsilon}\left(\frac{2}{b} + \frac{1}{nL}\right) + \frac{\Delta\psi + K + ns(\varepsilon^2 + \gamma^2)}{\varepsilon} - \tau\left(\frac{\gamma}{\varepsilon} + \frac{1}{4}\sqrt{1 + \left(\frac{\gamma}{\varepsilon}\right)^2}\frac{l}{L}\ln\frac{2}{n}\right). \tag{3.70}$$

The larger b is, the larger will be the driving force for nucleation and the smaller the SC pressure will be. One has to choose the maximum possible b, which is the length of dislocation in the b-direction. The main parameter which determines a reduction in the SC pressure due to shear stresses is l/L. The characteristic size of the strain-induced unit in steel is 100 nm [13, 14, 31], so $L = 50$ nm. Parameter l depends significantly on microstructure and is limited, approximately, by a quarter of the grain size. If we take $l = 1$ to 10 μm, then $l/L = 20$–200. In this case, the effect of macroscopic shear stress is negligible in comparison with the effect of dislocation pile-up and the SC pressure can be reduced significantly.

We estimate this effect for the following values of material parameters: $\Delta\psi = 1$ GPa, $K = 0.5$ GPa, $\varepsilon = 0.1$, $\gamma = 0.2$, $\mu = 80$ GPa, $\nu = 0.3$, $\Gamma = 0.1$ N m^{-1}, $n = 0.1$, $b = 10^{-6}$ m. Then

$$p = 17.24 + 10^{-8}/L - (2 + 1.675l/L)\tau\,(\text{GPa}). \tag{3.71}$$

The dependence $p(\tau)$ for $l = 10^{-6}$ m and various L is shown in figure 3.31. Because the term $10^{-8}/L$ is negligible for the L of interest, the relationship in figure 3.31 can be considered as function of l/L. The larger nucleus is, the smaller the effect of the pile-up and shear stresses will be. For an infinite nucleus, which corresponds to $A = 0$, we have $p = 17.24 - 2\tau$. For $2L = 50$ nm and $l = 10^3$ nm, equation (3.70) simplifies to

$$p = 17.64 - 68.99\tau\,(\text{GPa}). \tag{3.72}$$

For a minimal value $\tau = 5.97 \times 10^{-3}$ GPa, determined from the condition $B = 0$, one has $p = 17.23$ GPa. For $\tau = 0.2$ GPa, $p = 3.84$ GPa, i.e. a reduction in SC pressure by a factor of three to five and higher can be justified using this model. For $\tau = 0.256$ GPa, $p = 0$, which is essentially lower than the SC equilibrium pressure, $p_e = 10$ GPa and even the reverse SC pressure of 2.6 GPa under hydrostatic conditions.

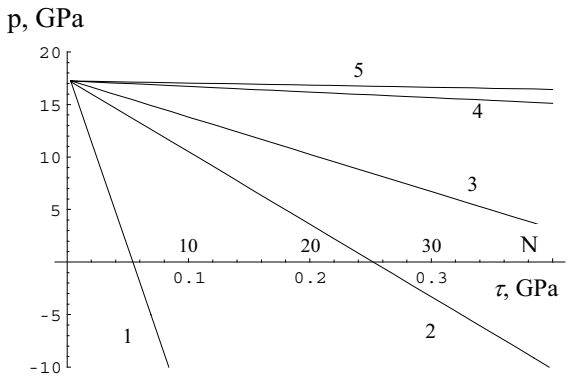

Figure 3.31. Dependence of SC pressure on shear stress and number of dislocations N for athermal nucleation at a dislocation pile-up for the pile-up length $l = 10^{-6}$ m and various nucleus length $2L$: 1, 10^{-8} m; 2, 10^{-7} m; 3, 5×10^{-7} m; 4, 10^{-6} m; 5, ∞.

Using equation (3.65), we can estimate the effect of a number of dislocations in a pile-up on SC pressure. Neglecting the third term in equation (3.71), for the above parameters one obtains

$$p = 17.64 - 1.828 \times 10^{-8} N/L \text{ (GPa)}$$

where L is in m. For $L = 25 \times 10^{-9}$ m, one has $p = 17.64$–$0.731N$ (GPa). Consequently, 25 dislocations in a pile-up can reduce the SC pressure to zero. For $L = 10^{-7}$ m, 100 dislocations are necessary, which is also not an exotic number. For data in figure 3.31, we obtain $\tau\,(\text{GPa}) = 0.0109N$, which allows us to express a SC pressure p versus N.

Barrierless nucleation, which does not require thermal fluctuations, explains the strain-controlled rather than time-controlled kinetics. Indeed, the prescribed strain increment generates dislocation pile-ups with barrierless, i.e. very fast nucleation and growth of the new phase up to the length L_{eq}. For the observation time of 1 s, this looks like instantaneous SC. As straining stops, no new defects and nuclei appear and the growth of existing nuclei is thermodynamically impossible.

Pure hydrostatic pressure in homogeneous systems does not cause plastic flow and the appearance of strong stress concentrators, which explains the unique role of shear stress and strains on SC. Even for $\gamma = 0$ (e.g. for isostructural, electronic PTs in Ce and its alloys), i.e. when τ does not contribute to transformation work, equations (3.70)–(3.72) exhibit a significant effect of τ on p because of the pressure concentration at the tip of the pile-up (see equation (3.64)).

One of the conditions of applicability of this model is that the dislocation pile-up does not activate alternative mechanisms of stress relaxation like

dislocation slip, twinning or fracture. This limits maximum τ by τ_r necessary for the activation of alternative relaxation mechanisms, as well as l. Stress τ_r is not smaller than the macroscopic yield stress in shear, which was taken into account in the range of τ in the above estimates. Pressure strongly suppresses fracture and moderately increases the critical stress for dislocation slip. That is why mechanochemical effects are more pronounced under high pressure. If only SC and dislocation slip compete, then any increase in strain rate has to promote the SC, similar to competition between slip and twinning [169]. For slip, higher shear stress is necessary for a higher strain rate, which increases τ in equations (3.70)–(3.72). Indeed, some experiments show a significant reduction in PT and CR pressure under increased strain rate [38, 139, 143]. Because length l is limited by the grain size, which significantly reduces during large plastic deformation, one way to intensify SC is related to the increase in grain size and l. This can be done by annealing and re-crystallization after compression of the disc at pressures slightly lower than the smallest pressure for strain-induced SC. However, a reduction in grain size has to suppress strain-induced SC, which is the case for explosives [5]. As the yield stress in shear τ is limited, there exists a lowest possible pressure, $p_\varepsilon^{\mathrm{d}}$, below which strain-induced SC is impossible. An increase in the yield stress (by increasing strain and strain-rate) leads to a decrease in $p_\varepsilon^{\mathrm{d}}$ which is observed experimentally [38, 139, 143, 144]. Here and later, the subscripts d and r designate direct and reverse SC.

Effect of shear stresses is especially strong for SC with large γ/ε, e.g. with small volumetric strain and large shear or uniaxial transformation strain. For example, for martensitic PT in $NiTi$ SMA alloy, $\gamma = 0.13$ and $\varepsilon = 0.0034$, $\gamma/\varepsilon = 38$ which produces the strong effect of shear stress even without pile-up, and magnifies the influence of the pile-up by factor γ/ε.

It is necessary to note that a dislocation pile-up generates both compressive (for positive ϕ) and tensile (for negative ϕ) pressure of the same magnitude. Consequently, it simultaneously promotes both direct and reverse SC in different regions. The same equations with tensile ε can be applied for the description of reverse SC. We will take these results into account at the microscale.

3.5.4.2 Thermally activated nucleation

If $B < 0$, which is the case for the weak or no dislocation pile-up and low τ, then SC is possible for $A > 0$ only. Because $F < 0$ for $L < -B/A$, nucleation requires thermal fluctuations. There is a critical length $L_c = -B/(2A)$ which is determined by the minimization of F (similar to the maximization of the Gibbs potential) and will be used to find an activation energy Q. Let us designate $\bar{B} = B/(4b)$, $A = ab - 8\Gamma n$ with $a = (p\varepsilon + \tau\gamma - \Delta\psi - K)4n - n^2 4s(\varepsilon^2 + \gamma^2) > 0$. Substituting critical nucleus length $L_c = -B/(2A)$ in the equation for $Q = -F$, one obtains an expression for the activation energy

$$Q = \frac{4\bar{B}^2 b^2}{ab - 8\Gamma n}. \tag{3.73}$$

Minimizing Q with respect to b, one obtains

$$b = \frac{16\Gamma n}{a} \qquad A = 8\Gamma n \qquad Q = 128\frac{\Gamma n \bar{B}^2}{a^2}. \tag{3.74}$$

For an observable nucleation rate, it is usually assumed $Q = 40k\theta$, where $k = 1.38 \times 10^{-23}$ N m K^{-1} is the Boltzmann constant. Solving this equation for p, one obtains

$$p = \frac{\Delta\psi + K + ns(\varepsilon^2 + \gamma^2)}{\varepsilon} + \frac{\Gamma}{\varepsilon}\sqrt{\frac{\Gamma}{5k\theta n}} - \tau\left(\frac{\gamma}{\varepsilon} + 0.25l\sqrt{\frac{\Gamma}{5k\theta n}\left(1 + \left(\frac{\gamma}{\varepsilon}\right)^2\right)n \ln\frac{2}{n}}\right). \tag{3.75}$$

Substituting the same numbers as before (except $\mu = 20$ GPa in order to have $N > 2$), one obtains the relationship $p(\tau)$ for various temperatures, see figure 3.32. Using equation (3.65), we obtain $\tau(\text{GPa}) = 0.0136N$ and can estimate effect of a number of dislocations in a pile-up on SC pressure. All plots intersect at the point corresponding to $B = 0$ and barrierless nucleation, therefore it is senseless to continue them for a larger τ. The smaller temperature is, the stronger effect of shear stress is. If the term with γ/ε is negligible, SC pressure depends on the combination τl. For $\theta = 300$ K, one obtains

$$p = 22.5 - 1165\tau(\text{GPa}). \tag{3.76}$$

The effect of shear stresses is much more pronounced for a thermally activated regime than for barrierless nucleation. However, because shear stress is limited by the condition $B \leq 0$, the minimal pressure for thermally activated nucleation is 15.71 GPa.

For a thermally activated regime, i.e. for relatively weak defects, one has to take into account pre-existing defects, because they can produce a comparable stress concentration. For example, they can be generated by preliminary thermomechanical treatment and are locked after unloading [168]. Using equation (3.65), one can estimate internal shear stress τ_i in the absence of external stresses, which are caused by a dislocation pile-up of length l consisting of N dislocations. Then equation (3.64) is valid with τ_i substituted for τ and equation (3.75) can be transformed to

$$p = f(\theta) + \frac{\Gamma}{\varepsilon}\sqrt{\frac{\Gamma}{5k\theta n}} - 0.25\tau_\text{i} l\sqrt{\frac{\Gamma}{5k\theta n}\left(1 + \left(\frac{\gamma}{\varepsilon}\right)^2\right)n \ln\frac{2}{n}}. \tag{3.77}$$

The first term in equation (3.75) is designated as $f(\theta)$, where $p = f(\theta)$ represents the equation of the SC line for an infinitely long waiting time in the absence of external and internal shear stresses and defects. If K and Eshelby energy is negligible, $f(\theta)$ represents an equilibrium line between phases. Since the term

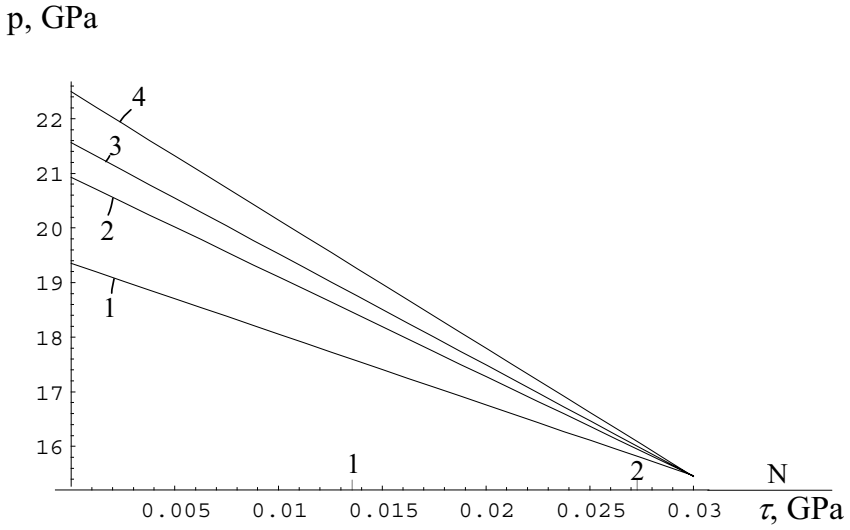

Figure 3.32. Dependence of SC pressure on shear stress and number of dislocations N for thermally activated nucleation at a dislocation pile-up for the pile-up length $l = 2\times10^{-7}$ m and various temperatures θ: 1, 1000 K; 2, 500 K; 3, 400 K; 4, 300 K.

$\tau\gamma/\varepsilon$ in equation (3.75) is negligible, the effect of both external and internal shear stresses can be expressed in terms of the number of dislocations in the pile-up (see equation (3.65)). Let us consider the case when $\tau = \tau_{\rm i}$, then equations (3.75) and (3.77) give practically the same result. In figure 3.33, the relationships $p(\theta)$ are plotted for the equilibrium PT line $p = f(\theta) = 10 + \theta/100$ and for the lines described by equation (3.77) (or equation (3.75)) for several values of $\tau_{\rm i}\, l = \tau\, l$. Deviation from the equilibrium line is a kinetic effect which decreases with temperature growth. Let, e.g., $\tau_{\rm i} l = 5.2 \times 10^{-9}$ GPa m with no external stresses. Above some temperature, say $\theta \simeq 500$ K, deviation of equation (3.77) from the equilibrium line is within the experimental error and the experimental kinetic curve can be used to determine the 'equilibrium' phase diagram. By applying an external stress, we practically do not change the internal stress due to pile-up $\tau_{\rm i}$, because an external stress is much lower than the stress due to the pile-up. However, an external stress produces new dislocation pile-ups. The difference between pre-existing defects and defects with the same N nucleated during plastic flow is outlined in the following. After exhausting all pre-existing defects, the kinetics of pressure-induced PT is saturated. For strain-induced nucleation, many more defects can be generated and more product phases can appear. This was observed in experiments [161] for PbO_2I $\rightarrow$ PbO_2II PT: the kinetics with shear is almost the same as without shear at the beginning of the PT and much more intensive for a larger time. Note that external shear stress at $\theta > 500$ K does not change the 'equilibrium' phase diagram (because it is negligible in comparison

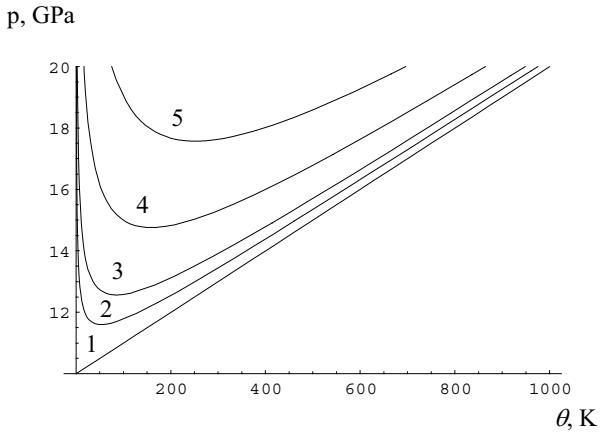

Figure 3.33. SC pressure *versus* temperature for thermally activated nucleation at a dislocation pile-up for several values of $\tau_i l = \tau l$, expressed in 10^{-9} GPa m: 1, the equilibrium PT line; 2, 5.6; 3, 5.2; 4, 4.0; 5, 2.0.

with the stress due to pile-ups), as is observed in experiments [161]. If $\tau l > \tau_i l$, e.g. $\tau l = 5.6 \times 10^{-9}$ GPa m, then external shear again does not change 'phase equilibrium' conditions but reduces the temperature at which the PT occurs at 'phase equilibrium' conditions, as it occurs in experiments [161].

Consequently, the experimental results [161] mentioned in item 1 of section 3.5.2, which contradict all other results in that item, can be explained by considering the thermally activated regime and taking into account the pre-existing defects of potency comparable with strain-induced defects. We can take into account the pre-existing defects for barrierless regime; however, they probably are much weaker than the strain-induced ones.

A similar consideration can be done for a pile-up of screw dislocations. However, they are less effective because they do not produce normal stresses and the shear stress is smaller by factor of $1/(1 - \nu)$ than for edge dislocations. Because pile-ups of different lengths are generated during plastic flow, a statistical consideration is necessary in more detailed models.

Note that Gilman's mechanism [118–120] may be real in the region of high stress concentration and, consequently, large elastic shear. At the macroscale, elastic shear is limited by the yielding and does not exceed $\tau_y/(2\mu) = 10^{-3}$–10^{-2}.

3.5.5 Microscale treatment

3.5.5.1 Thermodynamically consistent strain-controlled kinetic equation

Let us make the following simplifications. We decompose the stress, $\boldsymbol{T}$, into a sum of the macroscopic part $\boldsymbol{T}_m$, which is homogeneous in a representative volume $V \gg V_\mathrm{n}$, and the microscopic contribution, $\tilde{\boldsymbol{T}}$, which fluctuates inside the volumes V and V_n. As $V \gg V_\mathrm{n}$, the variation of the macroscopic stress, $\boldsymbol{T}_m$, is negligible during a small SC increment. The maximum macroscopic shear stress, τ, is limited by the macroscopic yield stress, which is smaller by a factor of $2R/h = 10$–100 than the pressure in the centre of the disc (R and h are the radius of the anvil and the current thickness of the disc sample respectively), see section 3.5.6. It will be neglected. For CR, plastic flow produces a fragmentation and mixing of components similar to liquid phase CR [138], so mixing will not be considered as a limiting factor. Strain-induced CR occurs at the places of stress concentration as well CR [138]. Because of the relatively large size of the transforming region, the surface energy is neglected as well. Then thermodynamic SC criterion, i.e. the condition that the net driving force F reaches zero [21, 22], can be written as

$$X := p\varepsilon_0 + \frac{1}{V_\mathrm{n}} \int_{V_\mathrm{n}} \int_0^{\boldsymbol{\varepsilon}_{\mathrm{t}2}} \tilde{\boldsymbol{T}} : \mathrm{d}\boldsymbol{\varepsilon}_\mathrm{t}\, \mathrm{d}V_\mathrm{n} - \Delta\psi(\theta) = K \tag{3.78}$$

where $p = 1/3\boldsymbol{I} : \boldsymbol{T}$ is the macroscopic hydrostatic pressure and ε_0 is the volumetric transformation strain. To calculate the integral in equation (3.78), the specific mechanism of strain-induced nucleation has to be known and then the corresponding boundary-value problem has to be solved numerically. For example, the nucleation at the shear-band intersection in TRIP steel was investigated in our paper [31] using the PT criterion equation (3.78) and a finite-element solution of the corresponding problem. One of the results which can be extracted from this investigation is that the transformation work depends significantly on the ratio $\Delta c/\Delta\varepsilon_\mathrm{p} \simeq \mathrm{d}c/\mathrm{d}\varepsilon_\mathrm{p}$, where Δc is a small increment of the volume fraction of a strain-induced new phase and $\Delta\varepsilon_\mathrm{p}$ is the prescribed small, uniaxial averaged plastic strain increment. Namely, the transformation work decreases (almost linearly in [31]) with the growth of $\mathrm{d}c/\mathrm{d}\varepsilon_\mathrm{p}$, see figure 3.20. Qualitatively, this has to be the case for any mechanism of nucleation at strain-induced defects, e.g. at the slip band and dislocation pile-up, considered earlier. However, to find the explicit relations, additional statistical assumptions and bulky numerics are required.

To approximately take into account, in an averaged over V microscopic SC criterion, the contribution of nano- and microscopic mechanisms of strain-induced nucleation, we substitute the integral with its approximate estimate

$$X_\mathrm{d} := p\varepsilon_0 - \Delta\psi + \Delta X_\mathrm{d} \left(1 - \frac{a}{(1-c)^\zeta} \left(\frac{\mathrm{d}c}{\mathrm{d}q_1}\right)^\chi\right) = K_\mathrm{d}. \tag{3.79}$$

Here q_1 is the accumulated plastic strain (Odqvist parameter) in the phase 1, $\dot{q} = (2/3\boldsymbol{d}_\mathrm{p} : \boldsymbol{d}_\mathrm{p})^{0.5}$, $\boldsymbol{d}_\mathrm{p}$ is the plastic strain rate, ΔX_d is the maximal microscopic contribution to the transformation work (at infinitesimal $\mathrm{d}c/\mathrm{d}q_1$), and a, χ and ζ are parameters. The factor $(1-c)^\zeta$ takes into account that SC $1 \to 2$ occurs in phase 1 only. Let us define the SC equilibrium pressure p_e by the condition $p_\mathrm{e}\varepsilon_0 - \Delta\psi = 0$, the pressure p_h^d under which SC can occur under hydrostatic condition without a strain-induced contribution by the equation $p_\mathrm{h}^\mathrm{d}\varepsilon_0 - \Delta\psi = K_\mathrm{d}$ (the energy of internal stresses is neglected for simplicity) and the minimal pressure p_ε^d under which SC can start (i.e. $c \simeq 0$) with infinitesimal rate (i.e. $\mathrm{d}c/\mathrm{d}q_1 \simeq 0$) by equation $p_\varepsilon^\mathrm{d}\varepsilon_0 - \Delta\psi + \Delta X_\mathrm{d} = K_\mathrm{d}$. Then $\Delta X_\mathrm{d} = (p_\mathrm{h}^\mathrm{d} - p_\varepsilon^\mathrm{d})\varepsilon_0$. Solving equation (3.79) for $\mathrm{d}c/\mathrm{d}q_1$, one obtains a thermodynamically consistent strain-controlled kinetic equation

$$\left(\frac{\mathrm{d}c}{\mathrm{d}q_1}\right)^\chi = \frac{(1-c)^\zeta}{a}\frac{p - p_\varepsilon^\mathrm{d}}{p_\mathrm{h}^\mathrm{d} - p_\varepsilon^\mathrm{d}}. \tag{3.80}$$

If the right-hand side of equation (3.80) is less than zero, we will take it as zero.

Simultaneously, strain-induced $2 \to 1$ SC will occur in phase 2. It can be described by similar equations:

$$X_\mathrm{r} := p\varepsilon_0 - \Delta\psi - \Delta X_\mathrm{r}\left(1 - \frac{b}{c^k}\left(\frac{\mathrm{d}c_1}{\mathrm{d}q_2}\right)^m\right) = -K_\mathrm{r} < 0 \tag{3.81}$$

$$\left(\frac{\mathrm{d}c_1}{\mathrm{d}q_2}\right)^m = \frac{c^k}{b}\frac{p_\varepsilon^\mathrm{r} - p}{p_\varepsilon^\mathrm{r} - p_\mathrm{h}^\mathrm{r}} \tag{3.82}$$

where $c_1 = 1 - c$ ($c_2 = c$), $\Delta X_\mathrm{r} = (p_\varepsilon^\mathrm{r} - p_\mathrm{h}^\mathrm{r})\varepsilon_0 > 0$ is the maximal microscopic contribution to transformation work (at infinitesimal $\mathrm{d}c_1/\mathrm{d}q_2$) at reverse SC, k, b and m are the parameters; pressure p_h^r under which the reverse SC can occur under hydrostatic condition without a strain-induced contribution is defined by the equation $p_\mathrm{h}^\mathrm{r}\varepsilon_0 - \Delta\psi = -K_\mathrm{r}$, and the maximal pressure p_ε^r under which the reverse SC can start (i.e. $c \simeq 1$) with infinitesimal rate (i.e. $\mathrm{d}c_1/\mathrm{d}q_2 \simeq 0$) is defined by equation $p_\varepsilon^\mathrm{r}\varepsilon_0 - \Delta\psi - \Delta X_\mathrm{r} = -K_\mathrm{r}$. To define the Odqvist parameter for each phase, we assume

$$\frac{q_1}{q_2} = \left(\frac{\sigma_{y2}}{\sigma_{y1}}\right)^w \qquad \text{and} \qquad q = c_1 q_1 + c_2 q_2$$

where from

$$q_1 = q\frac{\sigma_{y2}^w}{c\sigma_{y1}^w + (1-c)\sigma_{y2}^w} \qquad q_2 = q\frac{\sigma_{y1}^w}{c\sigma_{y1}^w + (1-c)\sigma_{y2}^w} \tag{3.83}$$

where q is the Odqvist parameter of the two-phase mixture and σ_{yi} is the yield stress of ith phase. According to equation (3.83), the stronger the phase is, the smaller fraction of the equivalent strain is concentrated in it; for $\sigma_{y1} = \sigma_{y2}$ one

has $q_1 = q_2 = q$. As for $\sigma_{y2} = (4 - 10)\sigma_{y1}$, q_2 is negligible, we estimate parameter $w = (2 - 5)$. Adding algebraically rates of direct and reverse SC and taking into account equation (3.83), one obtains the final kinetic equation

$$\frac{\mathrm{d}c}{\mathrm{d}q} = \frac{\sigma_{y2}^w}{c\sigma_{y1}^w + (1-c)\sigma_{y2}^w}\left(\frac{(1-c)^\zeta}{a}\right)^{1/\chi}\left(\frac{p - p_\varepsilon^\mathrm{d}}{p_\mathrm{h}^\mathrm{d} - p_\varepsilon^\mathrm{d}}\right)^{1/\chi} - \frac{\sigma_{y1}^w}{c\sigma_{y1}^w + (1-c)\sigma_{y2}^w}\left(\frac{c^k}{b}\right)^{1/m}\left(\frac{p_\varepsilon^\mathrm{r} - p}{p_\varepsilon^\mathrm{r} - p_\mathrm{h}^\mathrm{r}}\right)^{1/m}. \tag{3.84}$$

For the case $k/m = \zeta/\chi = g$, an analytical stationary solution of equation (3.84) can be found:

$$c_s = \frac{1}{1 + M(1-\tilde{p})^{1/k}/\tilde{p}^{1/\zeta}} \qquad \tilde{p} := \frac{p - p_\varepsilon^\mathrm{d}}{p_\varepsilon^\mathrm{r} - p_\varepsilon^\mathrm{d}}$$
$$M := \left(\frac{\sigma_{y1}}{\sigma_{y2}}\right)^{w/g}\frac{a^{1/\zeta}}{b^{1/k}}\frac{(p_\mathrm{h}^\mathrm{d} - p_\varepsilon^\mathrm{d})^{1/\zeta}}{(p_\varepsilon^\mathrm{r} - p_\mathrm{h}^\mathrm{r})^{1/k}}(p_\varepsilon^\mathrm{r} - p_\varepsilon^\mathrm{d})^{(1/k - 1/\zeta)}. \tag{3.85}$$

It follows from equation (3.85) that for $p \to p_\varepsilon^\mathrm{d}$ (and for $p \le p_\varepsilon^\mathrm{d}$, i.e. when direct SC is impossible), one has $c_s = 0$. For $p \to p_\varepsilon^\mathrm{r}$ (and for $p \ge p_\varepsilon^\mathrm{r}$, i.e. when reverse SC is impossible), one obtains $c_s = 1$. Between these two pressures, c_s varies from 0 to 1 and the shape of $c_s(p)$ curve depends on material parameters, see figure 3.34. In particular, if $M = 1$ (e.g. for equal material parameters of both phases) and $\zeta = k = 1$, then $c_s = \tilde{p}$. If $M \to 0$ (e.g. if the second phase is much stronger and/or $b^{1/k}/a^{1/\zeta} \to 0$, i.e. the kinetics of the reverse PT is suppressed, and/or $(p_\mathrm{h}^\mathrm{d} - p_\varepsilon^\mathrm{d})^{1/\zeta}/(p_\varepsilon^\mathrm{r} - p_\mathrm{h}^\mathrm{r})^{1/k} \to 0$), then $c_s \to 1$. In the opposite case, $M \to \infty$, $c_s \to 0$.

If $c < c_s$, then direct SC will occur for straining under constant pressure $p_\varepsilon^\mathrm{r} > p > p_\varepsilon^\mathrm{d}$. In the opposite case, the reverse PT will take place. A number of conclusions can be made from our analysis.

1. SC is promoted by plastic deformation at a pressure above p_ε^d only. Large plastic strain below p_ε^d suppresses SC because of strain hardening and growth of K_d. This explains a seeming contradiction formulated in [34], namely why large plastic deformation during the compression of materials does not cause SC, while relatively small shear strain at relatively high pressure promotes SC significantly.

2. If direct and reverse SC occur in the same pressure range (i.e. $p_\varepsilon^\mathrm{d} \simeq p_\mathrm{h}^\mathrm{r}$ and $p_\mathrm{h}^\mathrm{d} \simeq p_\varepsilon^\mathrm{r}$) and with comparable kinetics, then even if the pressure for the initiation of a SC can be reduced significantly because of strain-induced nucleation, only a small amount of product phase can be produced at a small pressure around p_ε^d. A significant amount of product phase can be obtained under the pressure around p_h^d, i.e. as for pressure-induced SC.

A significant amount of a high-pressure phase or complete SC can be induced by a large strain at low pressure if kinetics of reverse SC is suppressed only, i.e. for a small M (figure 3.34). One of the conditions for a small M, $(\sigma_{y2}/\sigma_{y1})^{w/g} \gg 1$,

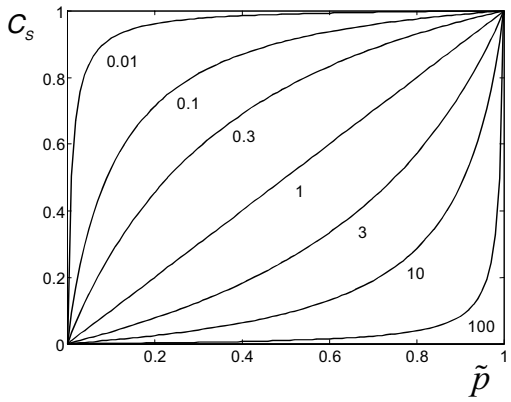

Figure 3.34. Relation between the stationary value of the volume fraction of the second phase and dimensionless pressure. The numbers near the curves designate the values of M.

shows that large plastic strains promote the appearance of hard phases more than weak phases. When this condition is fulfilled, then plastic flow localizes inside of phase 1 causing $1 \rightarrow 2$ SC, while small plastic strain in phase 2 causes a small advance of a reverse SC. For example, if strain-induced diamond or cubic BN appears in graphite or hexagonal BN (which have negligible yield strength in comparison with diamond and cubic BN), they cannot be deformed plastically inside the first phase and cannot be transformed back even at atmospheric pressure and room temperature.

Note that a diamond-to-graphite PT was recently reported in [170] under the indentation of diamond by a diamond indenter. The high pressure suppresses this PT which was explained qualitatively in [170] by the non-hydrostatic stress state. Estimates, however, show that the macroscopic shear stress, which is limited by the yield stress, cannot cause PT. High pressure (despite the fact that it reduces the macroscopic driving force) allows plastic deformation without fracture. Strain-induced PTs can occur under high macroscopic pressure, because the local pressure, due to new defects, will be much smaller or could even reach the tensile for $\phi < 0$. Alternatively, plastic deformation, under high pressure, induces defects, which cause PTs during unloading, i.e. during an increase in the macroscopic driving force. In particular, a PT from phase II to III in Ge and Si occurs during indentation under unloading [171].

3. Let us consider the case with $p_\varepsilon^{\mathrm{d}} \neq p_{\mathrm{h}}^{\mathrm{r}}$ and $p_{\mathrm{h}}^{\mathrm{d}} \neq p_\varepsilon^{\mathrm{r}}$. At $p_\varepsilon^{\mathrm{d}} > p_{\mathrm{h}}^{\mathrm{r}}$, direct SC starts at a pressure which is larger than the reverse PT pressure at hydrostatic conditions, which is the case for most known PTs. However, it is possible according to our estimates in section 3.5.4 that $p_\varepsilon^{\mathrm{d}} < p_{\mathrm{h}}^{\mathrm{r}}$, i.e. the direct PT starts at a pressure which is less than the reverse PT pressure at hydrostatic conditions. Such an unusual situation was observed for semiconductor $\rightarrow$ metal PT in InSb, InTe, Ge (I $\rightarrow$ II) and Si (I $\rightarrow$ II) [142–144]. This result was

interpreted as a significant reduction in the equilibrium PT pressure because of plastic shear. However, as previously discussed, $p_\varepsilon^{\mathrm{d}}$ can be lower than the equilibrium PT pressure, i.e. the previous experimental results do not imply a change in equilibrium pressure. If it is defined in the general case of unequal elastic moduli by the equation $p_{\mathrm{e}}\varepsilon_0 - \Delta\bar{\psi} = 0$, then a relatively small change in the equilibrium pressure is possible because of the change of elastic moduli and of the stored energy of internal stresses due to a plastic deformation. Here $\bar{\psi}$ is the Helmholtz free energy. The change in the elastic moduli of metals due to plastic deformation does not exceed 10–20% and the ratio of stored energy to plastic work is 5–20% and decreases with the growth of plastic work. There is no available data on the plastic strain dependence of the jump in elastic moduli and stored energy. However, the equilibrium pressure does not appear in any equation for the strain-induced SC and, consequently, cannot be determined from strain-induced experiment.

For $p_\varepsilon^{\mathrm{d}} > p_\varepsilon^{\mathrm{r}}$, a reverse PT does not occur for $p > p_\varepsilon^{\mathrm{d}}$ and a complete PT is possible. In this case the second term in the right-hand side of equation (3.84) disappears and $c_s = 1$. For example, graphite can be transformed (via amorphous carbon) to diamond at room temperature, $p =$ 19–25 GPa and shear strain of 0.2 [141]. However, a reverse PT is practically impossible under such pressure because of the small plastic deformation which a diamond can experience.

4. Zero pressure hysteresis was observed at pressure $p = 1.8$ GPa for the B1 $\leftrightarrow$ B2 PT in KCl [146] and it was assumed that this is an equilibrium pressure which can be used for plotting pressure-temperature phase diagrams. However, if the system is in a stationary state under any pressure p with $c = c_s$, then any infinitesimal pressure increase (decrease) followed by plastic straining will cause a $1 \to 2$ ($2 \to 1$) SC, i.e. pressure hysteresis is zero. Again, the equilibrium pressure cannot be determined from a strain-induced experiment.

Material parameters in equation (3.84) can be found in the following way. For small c, equation (3.84) can be simplified to

$$\frac{\mathrm{d}c}{\mathrm{d}q} = \frac{1}{a^{1/\chi}}\left(\frac{p - p_\varepsilon^{\mathrm{d}}}{p_{\mathrm{h}}^{\mathrm{d}} - p_\varepsilon^{\mathrm{d}}}\right)^{1/\chi}. \tag{3.86}$$

Pressure $p_{\mathrm{h}}^{\mathrm{d}}$ can be found from an experiment on SC under hydrostatic conditions. If we experimentally determine the pressure, when the first detectable amount c_{d} of phase 2 appears, as a function of strain q, then $p_\varepsilon^{\mathrm{d}}$ is determined as the PT pressure at a very large (infinite) q, and the parameters a and χ can be determined by fitting an experimental curve and the curve obtained from equation (3.86).

To estimate the order of magnitude of parameter a, we can assume that at $p = p_{\mathrm{h}}^{\mathrm{d}}$, the rate

$$\frac{\mathrm{d}c}{dq} = \frac{1}{a^{1/\chi}} = \frac{1}{\varepsilon_0}$$

where from $a = \varepsilon_0^{\chi}$ (equation (3.121) was used with $\mathrm{d}q = -\mathrm{d}h/h$).

Repeating the same procedure for the $2 \rightarrow 1$ PT starting with the pure phase 2, we can determine $p^{\mathrm{r}}_{\varepsilon}$, $p^{\mathrm{r}}_{\mathrm{h}}$, b and m. By determining the relation $c_s(p)$ experimentally and comparing it with equation (3.85), one can determine parameters M, ζ and k and, consequently, g and $(\sigma_{y1}/\sigma_{y2})^w$. The yield stresses, σ_{y1} and σ_{y2}, can be determined using the standard uniaxial compression test or hardness test of low and high (if metastable) pressure phases which were preliminary deformed to a very large strain to reach the limit hardening state. This state can be found from the observation that the hardness or yield stress stop varying with strain growth. An alternative way of determining σ_{y1} and σ_{y2}, which does not require the metastability of the high-pressure phase at room pressure, is developed in [40]. It is related to measuring the pressure distribution in each phase and the thickness of the specimen compressed in diamond anvils and to use a simplified equilibrium equation. After finding σ_{y1} and σ_{y2}, one can determine w.

3.5.5.2 Possible microscopic ways of controlling SCs

One aim of controlling strain-induced SCs, leading to high-pressure phases metastable at ambient pressure, is to decrease K_{d} and $p^{\mathrm{d}}_{\varepsilon}$ for a direct SC and to increase K_{r} and reduce $p^{\mathrm{r}}_{\varepsilon}$ (or at least $p^{\mathrm{r}}_{\mathrm{h}}$) below atmospheric pressure.

According to the equation $K = L\sigma_y\varepsilon_0$, annealing at a pressure slightly below $p^{\mathrm{d}}_{\varepsilon}$ will reduce the yield stress σ_y, K_{d} and $p^{\mathrm{d}}_{\varepsilon}$. Consequently, heating under pressure or after intermediate unloading can be used to further decrease pressure for the initiation of stress- and strain-induced SCs. Moreover, heavy plastic strain producing a high dislocation density may inhibit the appearance of new strong stress concentrations like dislocation pile-ups. Annealing can increase the probability of generating strong stress concentrations. Grain growth decreases σ_y (according to the Petch–Hall relationship) and increases the maximal length of dislocation pile-up. This is in line with our nanoscale analysis.

A reduction in $p^{\mathrm{r}}_{\mathrm{h}}$ and $p^{\mathrm{r}}_{\varepsilon}$ can be achieved by a large plastic deformation of the high-pressure phase at a pressure slightly above $p^{\mathrm{r}}_{\varepsilon}$ (to avoid strain-induced reverse SC). Another point is to find an unloading path, which minimizes or avoids plastic straining during unloading. Then one has to reduce $p^{\mathrm{r}}_{\mathrm{h}}$ below atmospheric pressure (rather than to worry about $p^{\mathrm{r}}_{\varepsilon}$ as well). For example, plastic deformation of the high-pressure phase II of Ge and Si by a rotation by 10° reduced the PT pressure to the semiconducting phase III from 4.3 to 2.3 GPa for Ge and from 4.7 to 2.7 GPa for Si [144]. One possible way to reduce plastic strain during unloading is to make unloading as fast as possible (quenching from a high-pressure state). Then, there will not be time for plastic strain to accumulate.

Our analysis also explains the contradictory statement in section 3.5.2 that plastic straining reduces pressure hysteresis (item 3) and substitutes reversible PT with irreversible ones (item 6), i.e. increases the hysteresis. Hysteresis reduces when both direct and reverse SCs are strain-induced. Hysteresis increases when, after large plastic strain, the reverse SC is not strain-induced (i.e. is pressure-induced).

Alternative phases. If alternative phases 2 and 3 can appear as a result of SC from phase 1, then the kinetic equation for the volume fraction of each phase has to take into account strain-induced direct and reverse SC of each phase into the other phases. Let the yield stress and elastic moduli of phase 2 (which we designate as 'w', weak) be significantly smaller than those of phase 3 ('s', strong). Note that for a stronger phase, the maximal energy of internal stresses, σ_{es}, and $K = L\sigma_y\varepsilon_0$ are larger than for a weaker phase (assuming the same L). That is why even if $p_e^{1\to w} > p_e^{1\to s}$, it may happen that $p_h^{1\to w} < p_h^{1\to s}$. Then the stronger phase cannot be obtained under hydrostatic loading. Let us discuss some reasons why plastic straining has to promote SC to a stronger phase to a greater extent than to a softer phase.

1. Stress concentration, due to new defects and, consequently, ΔX, is greater in a stronger phase.
2. If a stronger phase appears, the deformation is more concentrated in the parent phase and $\sigma_{ys}/\sigma_{y1} > \sigma_{yw}/\sigma_{y1}$ in kinetic equations. If both the strong and weak phases appear, again the deformation is more concentrated in the weaker phase which may cause SC w $\to$ s.
3. As shown in [34] (see also section 3.5.4), the pressure gradient in the central transforming region is proportional to the yield stress. Consequently, pressure grows faster with the appearance of the stronger phase, which, in turn, promotes the SC.

In addition, the active plastic deformation leads to the relaxation of the energy of internal stresses, σ_{es}, which is more significant for the stronger phase.

As supporting examples, we can consider PTs in Ge and Si, for which a strong, semiconducting phase I can be transformed to a strong, semiconducting phase III or a weak, metallic phase II [144]. Despite the fact that $p_e^{1\to w} > p_e^{1\to s}$ for these materials, the $1 \to$ w PT occurs under hydrostatic conditions, but the $1 \to$ s PT does not. The rotation of the anvil leads to the PT from phase I to III instead of to the weaker phase II [144]. It follows from the continuity of the curves for PT pressure *versus* q for both PTs that some critical plastic strain is necessary for changing from PT $1 \to$ w to PT $1 \to$ s.

Consequently, the method based on the compression of materials with the rotation of an anvil is especially important for the search for and production of high strength materials.

Reasons 2 and 3 also explain the results reported in [137, 138] and summarized in item 10 of section 3.5.2. A matrix with a yield stress higher (lower) than that for reagents significantly promotes (suppresses) the CRs, because the plastic strain is concentrated in the reacting material (matrix). Moreover, the pressure gradient and pressure in the central part of the disc is higher (lower) for the stronger (softer) matrix at the same applied load, see [34] and section 3.5.6, and the comparison in [137,138] was performed at the same total force. Similarly, we can conclude that adding stronger particles to the material under study will facilitate SC and could cause SCs which were not obtained otherwise, e.g.

metallic hydrogen [172–174]. Adding weaker particles will suppress SC which is important, e.g., for explosives.

Note that if $p_e^{l\to w} > p_e^{l\to s}$, the pressure for obtaining the stronger phase during the rotation of the anvil has to be limited to avoid strain-induced PT s $\to$ w. This is the case for PT in Ge and Si [144]. If $p_e^{l\to w} < p_e^{l\to s}$, there is no limitation on pressure.

These results will be qualitatively the same for any reasonable kinetic equation, because they are based on experimental and theoretical facts that direct and reverse strain-induced SC can occur simultaneously, that limiting pressures p_ε^d and p_ε^r exist and that strain in the weaker phase is larger than in the stronger phase.

3.5.6 Macroscopic plastic flow and structural changes

To analyse the actual tests in RDAC, to be able to extract correct experimental information from them, to improve these tests and to explain some phenomena enumerated in section 3.5.2, one needs to have a solution for the macroscopic plastic flow in a specimen. Let us consider the problem of the compression of a thin cylindrical disc of current thickness h by an applied axial force P; at some thickness h_0, one anvil starts to rotate with angular velocity ω_a and rotates by angle φ_a under $P =$ constant (figure 3.28). The axisymmetric problem formulation is adopted. The angular velocity of the deformed material ω differs from ω_a because of relative sliding. By putting the coordinate system $r\theta z$ in the moving gravity centre of the disc, we will consider the rotation with velocity $\omega/2$ at $z = h/2$ and with $-\omega/2$ at $z = -h/2$. This will allow us to use a symmetry condition in the calculation of the power of shear stress $\boldsymbol{\tau}$ at both contact surfaces. We assume that the plastic deformations are large enough and the model of isotropic perfectly plastic material is applicable [40]. Some steps in the solution of this problem without SC are known [34, 164]. They are based on the assumption that the disc material does not twist, i.e. there is complete sliding between the anvil and disc in the circumferential direction. Experimentalists believes that the material twists together with anvils and data that it is true in some cases exist [148, 154]. We will find the complete solution of this problem including the determination of rotation of the material, and generalize it to the case with SC. We will neglect the elastic deformations of the anvils and deformed disc, the pressure non-homogeneity in the z-direction and use the simplified equilibrium equation, well known in the metal forming theory [40, 164, 175]

$$\frac{\partial p}{\partial r} = -\frac{2\tau_r}{h} \tag{3.87}$$

as well as the continuity condition

$$\frac{\dot{h}}{h} + \frac{\partial V_r}{\partial r} + \frac{V_r}{r} = -\varepsilon_0 \dot{c}(r). \tag{3.88}$$

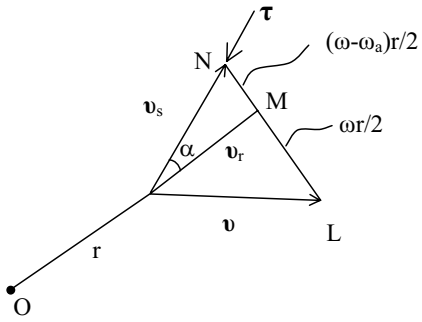

Figure 3.35. Relative position of the material velocity $\boldsymbol{v}$ and velocity of relative sliding along the contact surface $\boldsymbol{v}_s$; $MN = (\omega - \omega_a)r/2$, $ML = \omega r/2$.

Here r is the spatial radial coordinate, V_r is the radial velocity, τ_r is the radial component of the shear frictional stress $\boldsymbol{\tau}$ on the boundary S between the anvils and a disc. The boundary conditions are: $p = \sigma_0 + \sigma_y$ at the external radius of the anvil $r = R$, where σ_0 is the pressure at $r = R$ due to the external support of the material being outside the working region of the anvils $r > R$; and $V_r = 0$ at $r = 0$. The shear frictional stresses $\boldsymbol{\tau}$ are directed oppositely to the velocity $\boldsymbol{v}_s = \{V_r; (\omega - \omega_a)r/2\}$ of the relative sliding of a compressed material on the boundary S, where V_r and $(\omega - \omega_a)r/2$ are the radial and circumferential components of $\boldsymbol{v}_s$ (figure 3.35). For a thin disc, the magnitude of $\boldsymbol{\tau}$ usually reaches its possible maximum value equal to the yield stress in shear $\tau_y = \sigma_y/\sqrt{3}$ (the von Mises yield condition is used), i.e.

$$\boldsymbol{\tau} = \frac{\boldsymbol{v}_s}{|\boldsymbol{v}_s|}\frac{\sigma_y}{\sqrt{3}}.$$

In the case without rotation of the anvil $\tau_r = \sigma_y/\sqrt{3}$ and equation (3.87) yields (figure 3.36(*a*))

$$\frac{\partial p}{\partial r} = -\frac{2}{\sqrt{3}}\frac{\sigma_y}{h} \qquad p = \sigma_0 + \sigma_y\left(1 + \frac{2}{\sqrt{3}}\frac{R-r}{h}\right). \tag{3.89}$$

The applied load is determined by the integration of $p(r)$ over S:

$$P = \pi R^2\left(\sigma_0 + \sigma_y\left(1 + \frac{2}{\sqrt{3}}\frac{R}{3h}\right)\right). \tag{3.90}$$

3.5.6.1 Solution for the case without structural changes

Let us first consider the case without SC, i.e. $\dot{c} = 0$. The kinematics of the problem which satisfy equation (3.88) can be described by the following

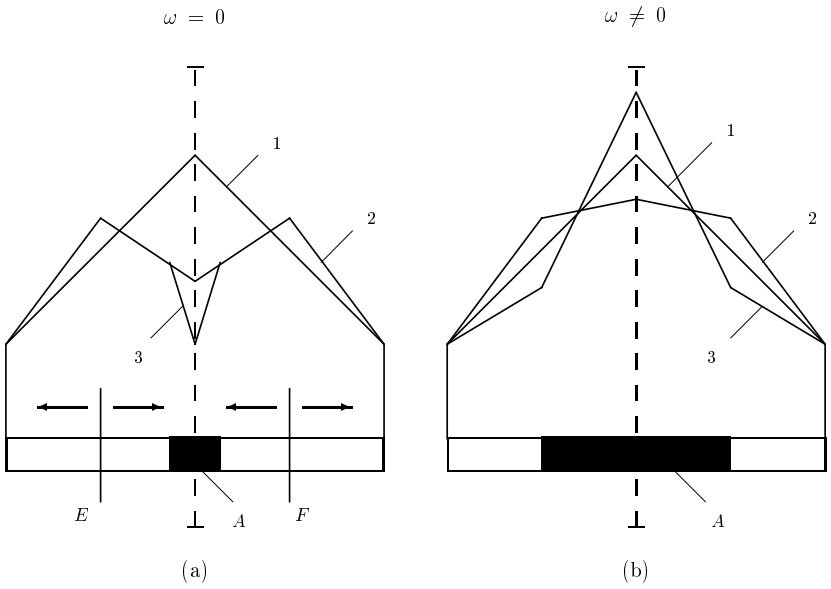

Figure 3.36. Pressure distribution (*a*) without anvil rotation (1, before SC; 2, after SC at $\sigma_{y1} = \sigma_{y2}$; 3, after SC at $\sigma_{y1} < \sigma_{y2}$) and (*b*) with anvil rotation (1, $\sigma_{y1} = \sigma_{y2}$; 2, $\sigma_{y1} > \sigma_{y2}$; 3, $\sigma_{y1} < \sigma_{y2}$).

equations:

$$V_z = \frac{\dot{h}z}{h} \qquad V_\mathrm{r} = -\frac{\dot{h}r}{2h} \qquad V_\theta = \frac{\omega r z}{h} \tag{3.91}$$

$$e_z := -\frac{\partial V_z}{\partial z} = -\frac{\dot{h}}{h} \qquad e_r := -\frac{\partial V_\mathrm{r}}{\partial r} = \frac{\dot{h}}{2h}$$

$$e_\theta := -\frac{V_\mathrm{r}}{r} = \frac{\dot{h}}{2h} = e_r \qquad \hat{\gamma} := \frac{\partial V_\theta}{\partial z} = \frac{\omega r}{h}. \tag{3.92}$$

Here e_z, e_r and e_θ are normal and the $\hat{\gamma}$ are the shear components of the deformation rate tensor. Note that we have changed the sign in the definition of the normal components of the deformation rate tensor in order to make the compressive strains positive. The sliding velocity vector $\boldsymbol{v}_\mathrm{s}$ and shear stress

$$\boldsymbol{\tau} = \frac{\boldsymbol{v}_\mathrm{s}}{|\boldsymbol{v}_\mathrm{s}|}\frac{\sigma_y}{\sqrt{3}}$$

are inclined at an angle α to the radius (figure 3.35) with

$$\cos\alpha = \frac{|V_\mathrm{r}|}{\sqrt{V_r^2 + ((\omega - \omega_\mathrm{a})r/2)^2}} = \frac{1}{\sqrt{1 + ((\omega - \omega_\mathrm{a})h/\dot{h})^2}} \tag{3.93}$$

and, consequently,

$$\tau_{\mathrm{r}} = \sigma_y \cos\alpha/\sqrt{3}. \tag{3.94}$$

Integration of equation (3.87), taking into account equation (3.94), leads to

$$p = \sigma_0 + \sigma_y\left(1 + \frac{2}{\sqrt{3}}\frac{(R-r)}{H}\right) \qquad P = \pi R^2\left(\sigma_0 + \sigma_y\left(1 + \frac{2}{\sqrt{3}}\frac{R}{3H}\right)\right) \tag{3.95}$$

$$H := \frac{h}{\cos\alpha} = h\sqrt{1 + ((\omega - \omega_{\mathrm{a}})h/\dot{h})^2} = h_0 \tag{3.96}$$

i.e. it is equivalent to the substitution of H for h. The equation $H = h_0$ follows from the conditions $P =$ constant and $\sigma_0 =$ constant. Equation (3.95) shows that at $P =$ constant due to $H =$ constant, the pressure distribution is independent of rotation, which corresponds to the experiments for NaCl [127,146] and X18H10T hardened steel [127].

Consequently, the rotation is equivalent to a *reduction* in *friction* in the radial direction and results in a *decrease* of the *disc thickness*. The greater the circumferential sliding along the anvil is, the greater the reduction in thickness is. The main task now is to find ω. We will use, for this purpose, the power balance

$$-P\dot{h} = 2\int_0^R \boldsymbol{\tau}\cdot\boldsymbol{v}(2\pi r\,\mathrm{d}r) + h\int_0^R \sigma_y\dot{q}(2\pi r\,\mathrm{d}r), \tag{3.97}$$

combined with these results. Here $\boldsymbol{v} = \{V_{\mathrm{r}}; \omega r/2\}$ is the material velocity at the contact surface (figure 3.35), and the terms on the right-hand side represent the power of the shear stresses at two contact surfaces and the plastic dissipation rate D, respectively. Calculations give:

$$\boldsymbol{\tau}\cdot\boldsymbol{v} = \frac{\sigma_y}{\sqrt{3}}\frac{\boldsymbol{v}_{\mathrm{s}}}{|\boldsymbol{v}_{\mathrm{s}}|}\cdot\boldsymbol{v} = \frac{\sigma_y r}{2\sqrt{3}}\frac{(\dot{h}/h)^2 + \omega^2 - \omega\omega_{\mathrm{a}}}{\sqrt{(\dot{h}/h)^2 + (\omega - \omega_{\mathrm{a}})^2}} \tag{3.98}$$

$$D := \sigma_y\dot{q} = \sigma_y\sqrt{\frac{2}{3}}\sqrt{e_z^2 + e_r^2 + e_\theta^2 + 2(\hat{\gamma}/2)^2} = \frac{\sigma_y}{h}\sqrt{\dot{h}^2 + \omega^2 r^2/3}. \tag{3.99}$$

Substituting equations (3.98) and (3.99) in equation (3.97), one obtains

$$-P\dot{h} = \frac{2\pi\sigma_y R^3}{3\sqrt{3}}\frac{(\dot{h}/h)^2 + \omega^2 - \omega\omega_{\mathrm{a}}}{\sqrt{(\dot{h}/h)^2 + (\omega - \omega_{\mathrm{a}})^2}} + \frac{2\pi\sigma_y}{3\omega^2}(3\dot{h}^3 + (\dot{h}^2 + \omega^2 R^2/3)^{3/2}). \tag{3.100}$$

One derives from equation (3.96)

$$\dot{h} = \frac{(\omega - \omega_{\mathrm{a}})h}{\sqrt{G^2 - 1}} \qquad G = \frac{h_0}{h} \geq 1 \tag{3.101}$$

where the negative signs of $\dot{h}$ and $\omega - \omega_{\mathrm{a}}$ are taken into account. Substituting equations (3.101) and (3.95) with $\sigma_0 = 0$ and $H = h_0$, $\omega = z\omega_{\mathrm{a}}$ $(0 \leq z \leq 1)$ in

equation (3.100), one obtains after some algebra

$$(1.5\sqrt{3}+m)(1-z) = m(1-G^2z) + \frac{3\sqrt{3}(z-1)^3 + (3(z-1)^2 + (G^2-1)G^2z^2m^2)^{3/2}}{(G^2-1)G^2m^2z^2}$$
$$m = \frac{R}{h_0}. \tag{3.102}$$

This is a highly nonlinear equation with respect to z depending on the two dimensionless parameters G and m. It is easy to show by constructing a Taylor series about the point $z = 0$, that $z = 0$ is one of the solutions of equation (3.102). This solution corresponds to the absence of material torsion and maximum possible sliding along the contact surface both in the circumferential and radial directions. Despite the absence of shear strain due to rotation, compressive strain is maximal for this case. Such a solution was assumed in [34, 164]; however, experiments exhibit significant material torsion [148,154]. Consequently, we will analyse a non-zero solution for Z.

Despite the complexity of equation (3.102), we were fortunate to find a very simple approximate solution. In fact, we found the solution for small G $(3(Z-1)^2 \gg (G^2-1)G^2Z^2m^2)$ and for large G $(3(Z-1)^2 \ll (G^2-1)G^2Z^2m^2)$ and it appears that the solutions do not differ significantly. Thus, for small and large G, after simplification of the last term, equation (3.102) has the solutions

$$Z_1 = \frac{1}{1+\sqrt{3}G^2m/8} \quad \text{and} \quad Z_2 = \frac{1}{1+2m\left(1-G^2+G\sqrt{G^2-1}\right)/(3\sqrt{3})} \tag{3.103}$$

respectively. We will substitute the smallest $G = 1$ in the expression for Z_1. Detailed numerical analysis of equation (3.102) shows that Z depends weakly on G. The expression for Z_2 gives the same three-digit precision for $G = 10$ and $G = 25$. If we substitute $G = 10$ in equation (3.103) for Z_2, we obtain a better agreement with the solution of equation (3.102) for $G < 10$ than by using equation (3.103) for the variable G. Then, instead of equation (3.103), we obtain

$$Z_1 = \frac{1}{1+0.216m} \quad \text{and} \quad Z_2 = \frac{1}{1+0.192m}. \tag{3.104}$$

The ratio Z_1/Z_2 varies from 1.08 for $m = 10$ to 1.25 for $m \to \infty$. If we assume $Z = 0.5(Z_1 + Z_2)$ or

$$Z = \frac{1}{1+0.204m} \quad \text{and, consequently,} \quad \omega - \omega_a = -\frac{0.204m}{1+0.204m}\omega_a \tag{3.105}$$

for any G, the discrepancy with the solution of equation (3.102) does not exceed 6.125%. This is acceptable, taking into account a number of simplifications in the

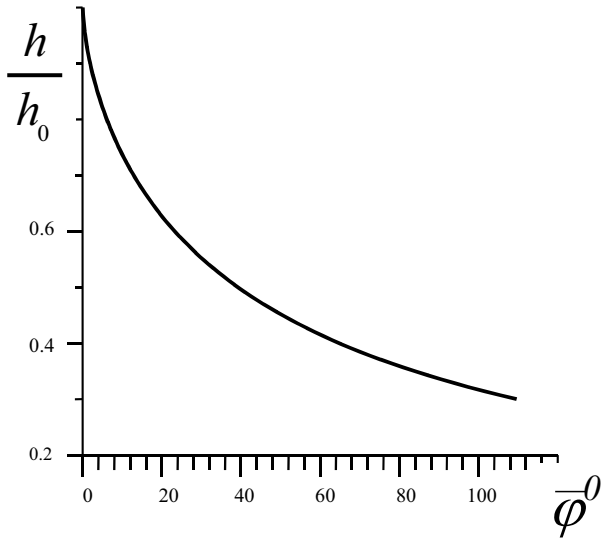

Figure 3.37. Plot of relative thickness of specimen h/h_0 *versus* the angle of relative sliding of an anvil with respect to material $\bar{\varphi}$.

model formulation. Substituting equation (3.105) into equation (3.96) results in the differential equation for the reduction in thickness:

$$\mathrm{d}\bar{\varphi} := \frac{0.204m}{1+0.204m}\,\mathrm{d}\varphi_{\mathrm{a}} = -\frac{\mathrm{d}h}{h}\sqrt{\left(\frac{h_0}{h}\right)^2 - 1} \tag{3.106}$$

which has the following solution

$$\bar{\varphi} = \sqrt{\frac{h_0^2}{h^2} - 1} - \arccos\frac{h}{h_0}. \tag{3.107}$$

Here $\bar{\varphi}$ is the angle of the relative sliding of an anvil with respect to the material. The plot of h/h_0 *versus* $\bar{\varphi}$ is shown in figure 3.37. This plot is in qualitative agreement with our experimental plot in [127] for KCl; however, it gives a smaller thickness reduction than the experiment. One of the possible reasons for this discrepancy (in addition to the approximate character of our model) is that elastic deformations of the system and the bending of plates for thickness measurement were not taken into account in [127] which led to an overestimation of the actual thickness reduction.

The obtained results explain the seeming contradiction: why does the rotation of the anvil reduce the PT pressure in the centre of the disc where plastic

shear is absent? The rotation induces a reduction in thickness and corresponding accumulated plastic strain $q = \ln(h/h_0)$ which, according to equation (3.84), induces the SC. The thickness reduction is remarkably large at small angles of twist (which agrees with experiments [127]); for $\bar{\varphi} \to 0$, $dh/d\bar{\varphi} \to \infty$. For small m, the relative sliding and the reduction in thickness is smaller than at large m. At $m = 5$–10 which is the smallest value for which our problem formulation is relevant and which is used in experiments, $\bar{\varphi} = (0.505\text{–}0.671)\varphi_a$. At $m \to \infty$, $\bar{\varphi} \to \varphi_a$, i.e. the torsion of the material is absent, but the reduction in thickness is the maximum possible. At large m and φ_a, both the shear and compressive plastic strains are small, i.e. rotation at a fixed force is not effective for inducing the SC.

To make the rotation effective again, the force P has to be increased. If the rotation stops at some thickness h, the plastic compression can start if the force increases to the value P determined by equation (3.90) (from the value P_0 determined by equation (3.90) for $h = h_0$). If the rotation starts at a force P and a thickness connected by equation (3.90), we can again apply all these equations starting with $\bar{\varphi} = 0$. There are three reasons for the intensification of SCs in this case: larger pressure, larger m and, consequently, a larger reduction in thickness, and a smaller $\bar{\varphi}$ and, consequently, a larger reduction in thickness. If the rotation starts at a force P smaller than necessary for plastic compression, then the new value of h_0 (and m) is determined from equations (3.95), (3.96) and the initial value $\bar{\varphi}_0$ is determined from equation (3.107). The thickness reduction during the rotation can be found from equation (3.107) with $\bar{\varphi}$ calculated from $\bar{\varphi}_0$.

In experiments [142], sometimes multiple rotations forward and back by an angle of order $\varphi_{ai} = 5^\circ$ are used. This results in more precise pressure measurements and the repeatability of results due to the smaller effect of the anvil's misalignment for small rotations. This theory gives the same results for monotonic and forward and back rotation for $\varphi_a = \sum |\varphi_{ai}|$. Indeed, if the rotation direction changes, compression does not start before the angle α has reached the same modulus (see equation (3.96)), because the compression under the larger value of τ_r is impossible.

There is one possible reason for the higher effectiveness of cycling rotation, which is the difference between plastic behaviour for monotonic and non-monotonic loading. The maximal difference is observed when the stress tensor changes sign. According to the Bauschienger effect, at a large strain, the yield stress at reverse loading for some metals is twice smaller than for monotonic loading and reaches the same value as for monotonic loading after the strain increment $\Delta q \simeq 0.1$ [40]. A similar effect with a smaller magnitude is observed at any change in the loading direction, the greater the angle between the stress and stress increment vector, the larger the effect is. The only deviatoric component of stress tensor is the shear stress τ. The angle of inclination of τ to the radius changes from α to $-\alpha$, so the angle between shear stress and stress increment vector, $\pi/2 + \alpha$, is large enough (for the maximal possible Bauschienger effect this angle is π). Consequently, the reduction in the yield stress is expected to be at least half the maximum possible reduction, i.e. of the order $0.25\sigma_y$. The yield

stress reaches its initial value after $\Delta q \simeq 0.05$ [40]. According to equation (3.95), the thickness will decrease down to a value of order $\Delta q \simeq 0.05$, necessary to reach the initial value of σ_y.

A similar phenomenon occurs for plastic contact friction [40]. It is probable that when the Bauschienger effect for the deformation disappears, the same effect for the friction does not, leading to the additional thickness reduction.

Consequently, forward and back rotation with small φ_{ai} leads to a more intensive thickness reduction, straining and SC. This result has to be checked quantitatively by experiments. Another conclusion is that the angle of material rotation rather than the anvil rotation determines the parameter q in the kinetic equation and, consequently, has to be measured.

Note that for a relatively large transformation shear, the change in the sign of the shear stresses suppresses direct SC and promotes reverse SC which is also observed experimentally [176]. This has to be taken into account for the analysis of SC and the development of the loading program to intensify SC.

3.5.6.2 Analysis of structural changes

We will limit ourselves to situations which can be analysed analytically.

SC in the centre of the disc. Interpretation of the measurements. Let us determine the pressure for the appearance of the first detectable amount, say $c_{\mathrm{d}} = 0.2$, of phase 2 in the centre of the disc as a function of strain q. We neglect stress redistribution and the reverse SC. In the centre $\hat{\gamma} = 0$, $\dot{q} = -\dot{h}/h$ and $q = \ln(h_0/h)$. First, we determine the volume fraction c_0 of phase 2 during the compression by integrating equation (3.86):

$$\begin{aligned} c_0 &= \frac{1}{a^{1/\chi}(p_{\mathrm{h}}^{\mathrm{d}} - p_{\varepsilon}^{\mathrm{d}})^{1/\chi}} \int_h^{h_1} \left(\sigma_y \left(1 + \frac{2}{\sqrt{3}}\frac{R}{\hat{h}}\right) - p_{\varepsilon}^{\mathrm{d}}\right)^{1/\chi} \frac{\mathrm{d}\hat{h}}{\hat{h}} \\ &= \frac{1}{a^{1/\chi}(p_{\mathrm{h}}^{\mathrm{d}} - p_{\varepsilon}^{\mathrm{d}})^{1/\chi}} \int_{p_{\varepsilon}^{\mathrm{d}}}^{p} \frac{(\hat{p} - p_{\varepsilon}^{\mathrm{d}})^{1/\chi}\,\mathrm{d}\hat{p}}{(\hat{p} - \sigma_y)} \end{aligned} \tag{3.108}$$

where equation (3.89) was used. Here h_1 is the thickness corresponding to pressure $p_{\varepsilon}^{\mathrm{d}}$. These integrals can be calculated using hypergeometric functions or numerically. The relation between the fixed pressure and the strain q necessary for the appearance of the first detectable amount c_{d} of phase 2 in the centre of a disc during the rotation of an anvil can be found by integrating equation (3.86) at a fixed pressure

$$\bar{p} = 1 + a\left(\frac{p_{\mathrm{h}}^{\mathrm{d}}}{p_{\varepsilon}^{\mathrm{d}}} - 1\right)\left(\frac{c_{\mathrm{d}} - c_0(p)}{\ln(h_0/h)}\right)^{\chi} \qquad \bar{p} := \frac{p}{p_{\varepsilon}^{\mathrm{d}}}. \tag{3.109}$$

For $p \gg \sigma_y$

$$c_0 = \left(\frac{p_{\varepsilon}^{\mathrm{d}}}{a(p_{\mathrm{h}}^{\mathrm{d}} - p_{\varepsilon}^{\mathrm{d}})}\right)^{1/\chi} \int_1^{\bar{p}} \frac{(p-1)^{1/\chi}\,\mathrm{d}p}{p}. \tag{3.110}$$

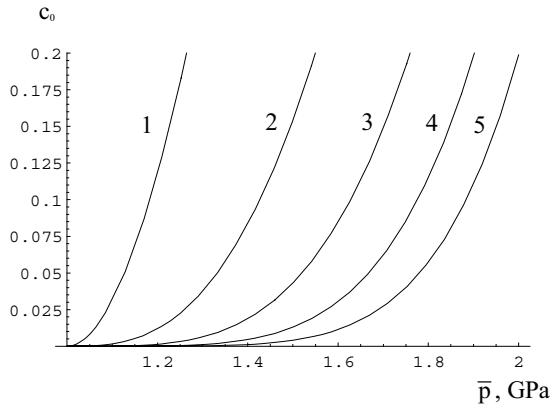

Figure 3.38. Relationship between the volume fraction of the product phase obtained during compression c_0 and the pressure $\bar{p}$ for various values of χ. The numbers near the curves designate the value of $1/\chi$.

This integral can be trivially calculated for the integer $1/\chi$. We assume $p_\varepsilon^{\mathrm{d}} = 1.25$ GPa, $p_{\mathrm{h}}^{\mathrm{d}} = 2.9$ GPa (i.e. $p_{\mathrm{h}}^{\mathrm{d}}/p_\varepsilon^{\mathrm{d}} = 2.32$), $\varepsilon_0 = 0.1133$ and $a = \varepsilon_0^\chi$, which is our very approximate estimate for the B1 $\rightarrow$ B2 PT in KCl. In figure 3.38, the relationship between the volume fraction of the product phase obtained during compression c_0 and the pressure $\bar{p}$ is plotted according to equation (3.108) for five values $0.2 \leq \chi \leq 1$. In figure 3.39, the relationship between the fixed pressure and the strain q necessary for the appearance of the first detectable amount $c_{\mathrm{d}} = 0.2$ of phase 2 in the centre of a disc is plotted according to equation (3.109) for the same χ. These results allow us to explain, why 'plastic shear' significantly reduces the PT pressure in comparison with hydrostatic experiments and plastic compression. Despite the fact that in both cases, namely under compression and twisting under constant pressure, strain-induced PT in the centre of the disc occurs under compression without shear, the trajectories of the loading in the $\bar{p}$–q plane are very different. This results in a different characterization of PT in terms of pressure. Under compression, pressure grows fast during the deformation process. That is why a detectable amount $c_{\mathrm{d}} = 0.2$ of phase 2 can be obtained under a relatively high pressure only, e.g. at $p = 2.375$ GPa for $\chi = 0.25$. If, e.g., compression stops at $p = 1.825$ GPa, when $c_0 = 0.009$ only, then $c_{\mathrm{d}} = 0.2$ can be reached after a rotation of an anvil resulting in $q = 1.47$. Traditionally, these results will be interpreted that the PT pressure under hydrostatic conditions is 2.9 GPa, for non-hydrostatic condition, it is 2.375 GPa and under large plastic shear, it is 1.825 GPa. Now we understand that the numbers 2.375 and 1.825 GPa do not characterize the 'PT pressures', because they depend significantly on the loading path in the $\bar{p}$–q plane.

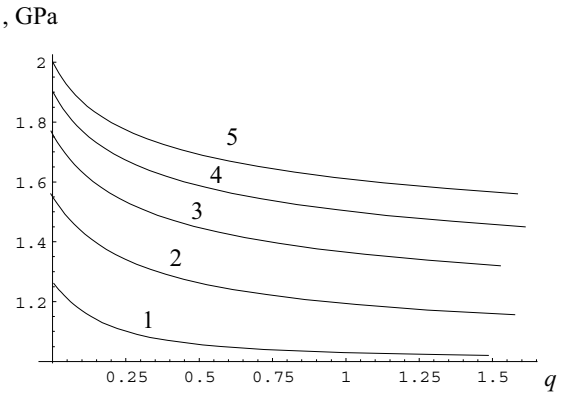

Figure 3.39. Relationship between fixed pressure $\bar{p}$ and the strain q necessary for the appearance of first detectable amount $c_{\mathrm{d}} = 0.2$ of phase 2 in the centre of the disc during anvil rotation. The numbers near the curves designate the value of $1/\chi$.

Kinematics. For the total strain rate, we put

$$e_z = -\frac{\dot{h}}{h} \qquad e_\theta = -\frac{V_{\mathrm{r}}}{r} \qquad e_r = \frac{\dot{h}}{h} + \frac{V_{\mathrm{r}}}{r} + \varepsilon_0 \dot{c} \qquad \hat{\gamma} = \frac{\partial V_\theta}{\partial z} = \frac{\omega r}{h}. \tag{3.111}$$

Let the transformation strain tensor consists of three equal, normal strains $1/3\varepsilon_0$ and transformation shear γ_{t} in the direction of torsion. The plastic strain rate is the difference between the total strain rate and the transformation strain rate:

$$e_z^p = -\frac{\dot{h}}{h} - 1/3\varepsilon_0 \dot{c} \qquad e_\theta^p = -\frac{V_{\mathrm{r}}}{r} - 1/3\varepsilon_0 \dot{c}$$
$$e_r^p = \frac{\dot{h}}{h} + \frac{V_{\mathrm{r}}}{r} + 2/3\varepsilon_0 \dot{c} \qquad \hat{\gamma}^p = \frac{\omega r}{h} - \gamma_{\mathrm{t}} \dot{c}. \tag{3.112}$$

Let $\dot{c} \neq 0$ in the ring $r_2 \leq r \leq r_1$, i.e. in the region $0 \leq r \leq r_2$, the SC into phase 2 is completed (in particular, $r_2 = 0$), and in the region $r \geq r_1$ the SC did not start yet. The continuity condition (3.88) can be satisfied by the following field:

$$V_{\mathrm{r}} = -\frac{\dot{h} r}{2h} - \frac{\varepsilon_0 \langle \dot{c} \rangle N r}{2} \qquad \text{for } r_2 \leq r \leq r_1 \qquad \langle \dot{c} \rangle := 2 \int_{r_2}^{r} \dot{c} \rho \, \mathrm{d}\rho / (r^2 - r_2^2) \tag{3.113}$$

$$V_{\mathrm{r}} = -\frac{\dot{h} r}{2h} \qquad \text{for } r \leq r_2 \qquad V_{\mathrm{r}} = -\frac{\dot{h} r}{2h} - \frac{\varepsilon_0 \langle \dot{c} \rangle (r_1^2 - r_2^2)}{2 r_1} \qquad \text{for } r \geq r_1 \tag{3.114}$$

where $\langle \dot{c} \rangle$ is the mean volume fraction rate in the ring $r_2 \leq \rho \leq r$, and $N = 1 - (r_2/r)^2$. In equation (3.114) $\langle \dot{c} \rangle$ is calculated for $r = r_1$. Then, in

the ring $r_2 \le r \le r_1$,

$$e_\theta = \frac{\dot{h}}{2h} + \frac{\varepsilon_0\langle\dot{c}\rangle N}{2} \qquad e_r = \frac{\dot{h}}{2h} - \frac{\varepsilon_0\langle\dot{c}\rangle N}{2} + \varepsilon_0\dot{c}$$
$$e_\theta^p = \frac{\dot{h}}{2h} + \frac{\varepsilon_0\langle\dot{c}\rangle N}{2} - \frac{1}{3}\varepsilon_0\dot{c} \qquad e_r^p = \frac{\dot{h}}{2h} - \frac{\varepsilon_0\langle\dot{c}\rangle N}{2} + \frac{2}{3}\varepsilon_0\dot{c}. \quad (3.115)$$

SC and pressure distribution in the central part of the disc. Let us analyse qualitatively the pressure redistribution during SC in the central part of the disc (figure 3.36) and its effect on SC. For $r_2 = 0$, equations (3.113) and (3.114) simplify to

$$V_\mathrm{r} = -(\dot{h}/h + \varepsilon_0\langle\dot{c}\rangle)r/2 \qquad \text{for } r \le r_1$$
$$V_\mathrm{r} = -1/2(\dot{h}r/h + \varepsilon_0\langle\dot{c}\rangle r_1) \qquad \text{for } r \ge r_1. \quad (3.116)$$

During intensive SC under compression without rotation under the prescribed load P increment, the thickness reduction can be relatively small ($-\dot{h}/h < \varepsilon_0\langle\dot{c}\rangle$) and some internal part of the disc material may move to the centre of the anvil due to a volume decrease. This is also observed experimentally [148, 154]. The radius of the neutral circle EF $r_n = -r_1 h\varepsilon_0\langle\dot{c}\rangle/\dot{h}$ is found from the condition $V_\mathrm{r} = 0$. Equation (3.87) is valid but the shear stress in the region EF changes sign and in the region A the yield stress of the two-phase mixture σ_y, which depends on c, should be used. In the simplest case, we can assume $\sigma_y = (1-c)\sigma_{y1} + c\sigma_{y2}$. We also assume that the pressure is continuous across the interface. Then

$$p_1(r) = \sigma_0 + \sigma_{y1}\left(1 + \frac{2}{\sqrt{3}}\frac{(R-r)}{h}\right) \qquad \text{for } r_n \le r \le R$$
$$p_{1n}(r) = p_1(r_n) - \frac{2\sigma_{y1}}{\sqrt{3}}\frac{(r_n - r)}{h} \qquad \text{for } r_1 \le r \le r_n$$
$$p_2(r) = p_{1n}(r_1) - \frac{2}{\sqrt{3}}\sigma_y\frac{(r_1 - r)}{h} \qquad \text{for } r \le r_1. \quad (3.117)$$

The pressure distribution is shown in figure 3.36(*a*). It is important to write that without rotation the pressure in the transforming region decreases significantly, which suppresses the SC. The higher σ_{y2} is, the larger the pressure reduction in the transforming region is.

The rotation of an anvil significantly reduces the thickness h and compensates the volume decrease due to SC, i.e. $-\dot{h}/h \ge \varepsilon_0\langle\dot{c}\rangle$. In this case material flows from the centre of the disc, shear stress does not change the sign and the pressure grows monotonically with the decreasing radius (figure 3.36(*b*)):

$$p_1(r) = \sigma_0 + \sigma_{y1}\left(1 + \frac{2}{\sqrt{3}}\frac{(R-r)}{H}\right) \qquad \text{for } r_1 \le r \le R$$
$$p_2(r) = p_1(r_1) + \frac{2}{\sqrt{3}}\sigma_y\frac{(r_1 - r)}{H} \qquad \text{for } r \le r_1. \quad (3.118)$$

Consequently, because of specific plastic flow, the pressure in the transforming region with rotation of the anvil is greater than without rotation. In addition, rotation increases the accumulated plastic strain. This is one of the macroscopic reasons why the rotation of an anvil promotes SC.

According to equation (3.118), if the yield stress of the product phase, σ_{y2}, exceeds the yield stress of the parent phase, σ_{y1}, the pressure increases in the transforming region (figure 3.36(b)), despite the volume decrease due to SC. This agrees with experiments exhibiting the effect of pressure self-multiplication in KCl [127, 146], C_{60} [127, 152] and PbTe [153]. In the opposite case, pressure decreases during the SC (figure 3.36(b)), which is also observed in experiments for the PT from semiconductor bcc (III) to the metal (weaker) tetragonal (II) phase in Ge under shear [144, 151]. This explains the pressure self-multiplication and self-demultiplication effects summarized in item 9 of section 3.5.2.

Further, if two alternative phases which differ by the yield stress only can appear as a result of SC, then the material with the smaller yield stress appears in the case without rotation (as pressure is higher at $\sigma_{y1} > \sigma_{y2}$) and the stronger phase will be obtained under compression with rotation (as pressure is higher at $\sigma_{y2} > \sigma_{y1}$). This is one of the macroscopic reasons why the rotation of an anvil leads to phases, especially to strong phases, which were not obtained under compression without rotation (see item 5 in section 3.5.2).

Note that the pressure distribution for the B1 $\rightarrow$ B2 PT in KCl without rotation of the anvil looks like in figure 3.36(b) rather than in figure 3.36(a) but with a much smaller (near-zero) pressure gradient in the transforming region [127, 146]. This means that the condition $-\dot{h}/h \geq \varepsilon_0\langle\dot{c}\rangle$ is fulfilled for the case without rotation of the anvil and material does not flow to the centre of the disc. Because $\sigma_{y2} > \sigma_{y1}$, the pressure gradient grows significantly during the PT under rotation and it is not clear why it decreases during the PT without rotation of the anvil.

One of the possible reasons for this phenomenon can be related to the well-known transition from the plastic to elastic state under axial compression in Bridgman anvils [40]. Namely, after the plastic compression of the thin disc, beginning with some value of a specific force (thickness), an elastic region arises at the centre of the disc and expands during further increase in applied force. This means that even an arbitrary large applied force cannot reduce the residual (after unloading) thickness of the disc below some critical value. One of the possible reasons suggested in [40] is related to the concave yield surface of the compressed material along the hydrostatic axis. This means that the yield stress grows with the pressure faster than a linear function, i.e. $\mathrm{d}\sigma_y/\mathrm{d}p$ is an increasing function of pressure. Such a pressure dependence of the yield stress was observed in numerous experiments by Bridgman and Vereschagin *et al* [177] summarized in [40].

The existence of a solution of the problem of plastic limit equilibrium can be proved for a non-concave yield surface only [178, 179]. Therefore, one can expect that for a concave yield surface, the solution may not exist and, in fact, the

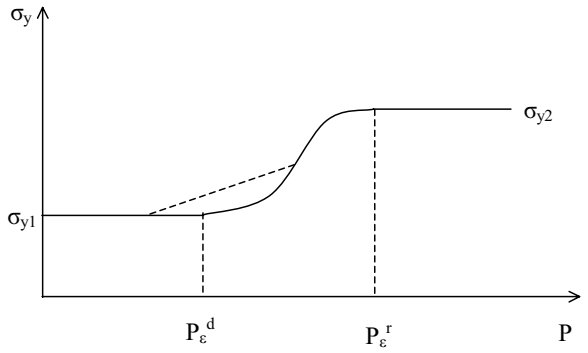

Figure 3.40. Example of the concave yield surface (curve) when a high-pressure phase has a greater yield stress than the low-pressure phase.

disc cannot be compressed plastically. In [40], an example of the impossibility of continuing a slip line field from the edges of the disc to its centre was demonstrated for a concave yield surface. It is related to the strong growth of the yield stress and the friction stress from the edges of the disc to its centre.

One of the reasons for the growth of $\mathrm{d}\sigma_y/\mathrm{d}p$ with pressure growth can be related to SC from a weaker to a stronger phase which is spread over some pressure range. If, e.g., $\sigma_y = (1-c)\sigma_{y1} + c\sigma_{y2}$, then according to stationary solution (3.85), the yield stress is pressure-independent for pressures corresponding to pure parent and product phase and grows with pressure between $p_\varepsilon^{\mathrm{d}}$ and $p_\varepsilon^{\mathrm{r}}$ (figure 3.40). Because there are straight lines connecting two points of the function $\sigma_y(p)$ which are located above the plot of $\sigma_y(p)$, the yield surface is concave and all arguments presented in [40] are valid. Consequently, after some SC in the centre of the disc, elastic deformation rather than plastic deformation takes place there. Then the friction shear stress is significantly smaller than the yield stress in shear and the pressure gradient is much smaller as well. Also pressure-induced SCs (which are less intensive) rather than strain-induced SCs can occur in elastically deformed regions which require $p \geq p_{\mathrm{h}}^{\mathrm{d}}$.

Under rotation of an anvil, the shear stress in a radial direction decreases significantly (see equation (3.94)), so the boundary conditions are less critical for the non-existence of a plastic solution discussed in [40]. That is why plastic flow and strain-induced SCs occur during the rotation of an anvil. The greater the yield stress of the second phase is, the greater the difference between compression and compression with rotation will be.

Let two alternative phases which differ by the yield stress only appear as a result of SC and the material with the smaller yield strength appears under compression without rotation. The material does not flow to the centre of the disc with or without rotation. The rotation can promote the appearance and growth of the high-strength phase, because rotation transforms stress-induced SC

to strain-induced SC (which can occur under a much smaller pressure), and causes significant pressure growth due to the pressure self-multiplication effect during the transformation. This is an additional argument why the rotation of an anvil is the perspective way of search for new superhard materials.

By calculating the force for the pressure distribution, equation (3.118), and making it equal to the force at the beginning of rotation,

$$P = \pi R^2 \left((\sigma_0 + \sigma_{y1}) + \frac{2}{3H\sqrt{3}} (R\sigma_{y1} + cr_1^3(\sigma_{y2} - \sigma_{y1})/R^2) \right)$$
$$= \pi R^2 \left(\sigma_0 + \sigma_{y1} \left(1 + \frac{2}{\sqrt{3}} \frac{R}{3h_0} \right) \right) \tag{3.119}$$

one finds

$$H = h_0 \left(1 + \left(\frac{r_1}{R} \right)^3 \left(\frac{\sigma_y}{\sigma_{y1}} - 1 \right) \right). \tag{3.120}$$

Even for $\sigma_y/\sigma_{y1} = 5$, if we limit ourselves to $r_1/R \leq 1/4$, we can neglect the last term with an error not exceeding 6.25%. So for a relatively small transforming region we can approximately use all equations (3.96)–(3.107).

For an approximate estimate of the maximum possible transformation rate, we assume that a volume decrease due to SC is completely compensated by (or infinitesimally smaller than) the reduction in h. In this case, when infinitesimal radial flow from the disc centre occurs, the shear stress does not change sign and the pressure grows monotonically with a decreasing radius. For a larger transformation rate, part of the material will move to the centre and the pressure will decrease (figure 3.36(a)), which will serve as negative feedback for a reduction in the transformation rate. The condition that $V_r = 0$ results in the equation

$$\dot{c}\varepsilon_0 = -\frac{\dot{h}}{h} = \dot{\tilde{\varphi}} \left(\left(\frac{h_0}{h} \right)^2 - 1 \right)^{-0.5} \tag{3.121}$$

which was used to estimate parameter $a = \varepsilon_0^{\chi}$ in kinetic equation (3.86). Equation (3.101) was used in the derivation of equation (3.121).

Possible reasons for 'steps' on the pressure distribution. As was mentioned in item 2 of section 3.5.2, a small region with almost constant (sometimes even decreasing) pressure (see figure 3.29) corresponds to a two-phase mixture where SC occurs. We will try to find possible explanations for this anomaly in the pressure distributions.

As follows from equilibrium condition (3.87), the radial component of the shear frictional stress has to be very small (or even directed from the centre of the disc). This is possible, in particular, when, for some r in the ring $r_2 \leq r \leq r_1$, one has $V_r = 0$ and

$$\langle \dot{c} \rangle = -\frac{\dot{h}}{h\varepsilon_0 N}. \tag{3.122}$$

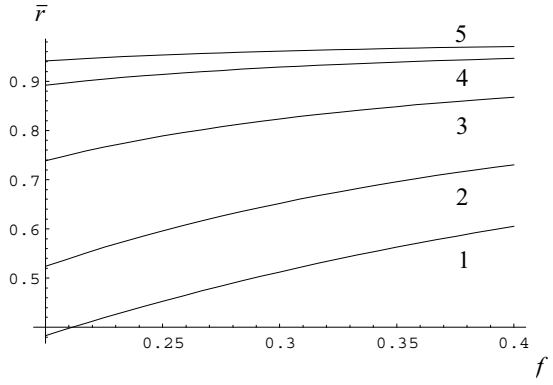

Figure 3.41. Relationship between $\bar{r} := r_2/r$ and $f := r/R$ obtained from the condition $\dot{c}\varepsilon_0/\dot{q} = 1$ for several values of $G := h_0/h$: 1–1.3; 2–1.5; 3–2; 4–3; 5–4.

The region near the neutral circle with $V_\mathrm{r} = 0$ is the stagnation region, where relative sliding with respect to the anvil is small and the shear stress grows slowly from zero at the neutral circle. The value of $\langle\dot{c}\rangle$ according to equation (3.122) is larger than in equation (3.121); however, because of shear strain, $-\dot{h}/h$ in equation (3.122) represents only part of $\dot{q}$. We will calculate $\dot{q}$ to be used in the kinetic equation (3.84) based on a solution without SCs, i.e. in equations (3.99), (3.101) and (3.105)

$$\omega = -\frac{\dot{h}}{0.204mh}\sqrt{G^2-1}$$
$$\dot{q} = \frac{1}{h}\sqrt{\dot{h}^2+\omega^2r^2/3} = \frac{\dot{h}}{h}\sqrt{1+8(G^2-1)(r/hm)^2}. \tag{3.123}$$

We estimate whether parameter

$$\langle\dot{c}\rangle\frac{\varepsilon_0}{\dot{q}} = \frac{1}{N\sqrt{1+8(G^2-1)(Gr/R)^2}} \tag{3.124}$$

can be equal to one, like in equation (3.121). In figure 3.41, the relationship $\bar{r} := r_2/r$ *versus* $f = r/R$ obtained from the condition $\dot{c}\varepsilon_0/\dot{q} = 1$ is plotted for several values of G. In experiments, the minimal reasonable value r_2/r exceeds 0.8. This value can be reached for $G > 2$ and $f > 0.3$ or for $G > 3$ for any f, which is realistic for some cases. However, this condition definitely cannot be fulfilled for small $G < 1.3$ and $f < 0.2$, when steps still can be observed experimentally. Consequently, the condition $V_\mathrm{r} = 0$ can be the reason for steps on a pressure distribution for a relatively large G and f and it cannot be the reason for a relatively small G and f.

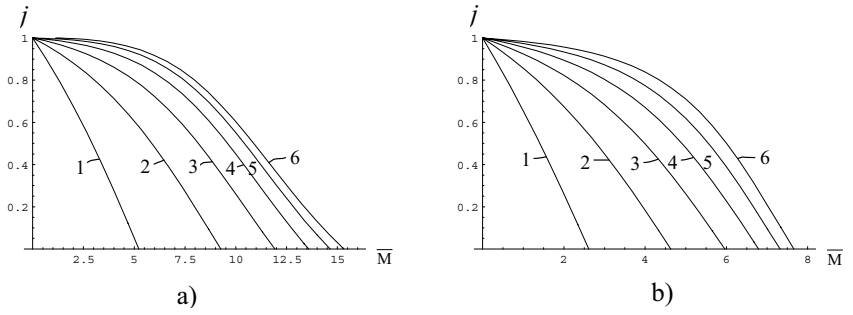

Figure 3.42. Plots $j := \tau/\tau_0$ *versus* $\bar{M}$ for several values of $u := r/h$: (*a*) $\gamma_t = 0.1$; (*b*) $\gamma_t = 0.2$. The numbers near the curves designate the value of u.

As an alternative (or additional) reason for steps in the pressure distribution, we will consider a reduction in shear stresses under a prescribed shear strain due to TRIP or RIP phenomena. The main idea of these phenomena is that the transformation strain produces huge internal stresses which in combination with external stresses (which can be significantly smaller than the yield stress) causes plastic flow. The total plastic deformation rate consists of contributions from traditional plasticity, which depends on stress (and on stress rate for hardening materials), and TRIP (RIP), which is proportional to the rate of the volume fraction. In particular, in equations (3.112) and (3.115), the terms proportional to $\dot{c}$ represent a contribution due to TRIP (RIP) and all other terms are due to classical plasticity.

In papers [6, 21, 26, 34], where analytical solutions for the problem for SC in a thin layer (e.g. surface layer, shear band or a layer at moving interface) were derived, an explicit expression for shear stress, plastic shear strain due to TRIP (RIP) and the transformation volume strain was obtained, see equation (3.41) and figure 3.8. One of the results was that when shear stress tends to the yield stress in shear, the plastic shear strain tends to infinity. Consequently, for any finite prescribed shear strain, the shear stress can be found which is smaller than the yield stress in shear. That is why TRIP is considered to be a mechanism of shear (deviatoric) stress relaxation. We expect that because, during rotation, the shear strain increment $\Delta\varphi_a r/h$ is prescribed, the shear stress at the contact surface will relax significantly due to TRIP (RIP). A similar situation may happen during compression without rotation. However, because our model operates with strains averaged over the thickness, shear strain γ_{rz} disappears from consideration. That is why we cannot check the validity of these reasons for steps for compression without rotation. We will now estimate the shear stress in the direction of rotation $\tau = \tau_{z\theta}$ and assuming $\tau_r = \operatorname{cotan}\alpha\,\tau_{z\theta}$ with the same α as for the regions without SC (see equation (3.93)), and will find how τ_r reduces due to TRIP (RIP). Consequently, it is sufficient to estimate τ/τ_0, where τ_0 is determined for the deformation without SC.

Using equation (3.99) for the dissipation rate, $D := \sigma_y \dot{q} = \sigma_y \sqrt{\frac{2}{3}} \sqrt{e_z^{p2} + e_r^{p2} + e_\theta^{p2} + 2(\hat{\gamma}^p/2)^2}$, one obtains, according to the associated flow rule [40, 178, 179],

$$\tau = \frac{\partial D}{\partial \hat{\gamma}^p} = \sigma_y \frac{\partial \dot{q}}{\partial \hat{\gamma}^p} = \frac{\sigma_y}{\sqrt{6}} \frac{\hat{\gamma}^p}{\dot{q}}. \tag{3.125}$$

To calculate $\dot{q}$, we assume for simplicity $\langle \dot{c} \rangle = \dot{c}$ which corresponds to a homogeneous distribution of $\dot{c}$ in the transforming region. Then, substituting equations (3.112) and (3.115) in equation (3.125), one obtains

$$\tau = \sigma_y \frac{\omega r - \gamma_t h \dot{c}}{\sqrt{\dot{c}^2(\varepsilon_0^2(4+3N(N-2))+3\gamma_t^2)h^2+6h\dot{c}(\varepsilon_0 \dot{h}-\gamma_t \omega r)+3(3\dot{h}^2+\omega^2 r^2)}}. \tag{3.126}$$

Now we express $\dot{h}$ from equation $(3.123)_1$, $\dot{h} = Ch\omega$, $C := -0.204m/\sqrt{G^2-1}$, express $\dot{c} = \bar{M}\dot{q}$ with $\bar{M}$ determined from kinetic equation (3.84), and use equation $(3.123)_2$ for $\dot{q}$. After the substitution of all of these results and $u = r/h$ in equation (3.126), we arrive at the following equation:

$$\tau = \sigma_y \frac{u - \bar{M}\gamma_t \bar{C}}{\sqrt{(\varepsilon_0^2(4+3N(N-2))+3\gamma_t^2)\bar{C}^2\bar{M}^2 + 6\bar{C}\bar{M}(\varepsilon_0 C - u\gamma_t) + 9\bar{C}^2}}$$

$$\bar{C} := \sqrt{u^2/3 + C^2}. \tag{3.127}$$

Putting $\bar{M} = 0$ in equation (3.127), we obtain

$$\tau_0 = \sigma_y u/(3\bar{C}). \tag{3.128}$$

Plots of $j := \tau/\tau_0$ *versus* $\bar{M}$ for several values u and $\gamma_t = 0.1$ and $\gamma_t = 0.2$ are presented in figure 3.42. Other parameters are: $\varepsilon_0 = 0.1$, $m = 10$ and $G = 1.5$ (i.e. $C = -1.82$). The results are weakly dependent on N for $0 \le N \le 0.36$ that is why we used the fixed value of $N = 0.19$. For both γ_t, parameter j reduces significantly with the growth of the parameter $\bar{M}$ which characterizes the intensity of SC kinetics. The closer SC region is to the centre of the disc, the more intensively the shear stress is reduced. Note that the estimated maximum value of $\bar{M}$ determined from equation (3.121) is $\bar{M} = 1/\varepsilon_0 = 10$. For $\gamma_t = 0.2$ and for all $u \le 6$, the shear stress reaches a zero value, i.e. friction and, consequently, the pressure gradient, are absent. For $\gamma_t = 0.1$, the same is valid for $u \le 2$. We did not continue the plots for a negative j, because for polycrystalline material for a small τ, the transformation shear γ_t is not a constant. It reduces with a reduction in τ and is zero for $\tau = 0$ (see, e.g., [30]).

Note that we took into account only part of the TRIP effect due to macroscopic (smeared) SCs. The contribution to TRIP from the discrete microheterogeneous distribution of transforming regions is usually included as

an additional term in the constitutive equation of type of $\boldsymbol{d}_p = \bar{\mu}\varepsilon_0 \boldsymbol{S}\dot{c}$, where $\bar{\mu}$ is some function of c and $\boldsymbol{S}$ is the stress deviator [17]. Consequently, we received a lower bound of the actual effect.

We can conclude that the relaxation in shear friction stresses due to TRIP (RIP) phenomenon can be partially or completely responsible for the appearance of small steps with almost constant pressure in the transforming zone.

Note that to integrate kinetic equation (3.121), one has to follow the material rather than the spatial points. This means that a Lagrangian rather than a Eulerian description has to be used. Even when $\sigma_{y1} = \sigma_{y2}$ and the pressure distribution is independent of rotation, the pressure in the material particles reduces because of radial flow. For some material particles after direct SC, this can cause the reverse SC. Probably, this is the case in the (or near) the regions where 'steps' in the pressure distributions are observed.

3.5.6.3 Alternative methods to promote structural changes

It follows from this analysis that one of the main macroscopic reasons for the promotion of SCs due to rotation of the anvil is related to the possibility of additional axial displacement, which compensates a volume decrease and increases the pressure and accumulated plastic strain. Based on this understanding, we can suggest some alternative ways to obtain additional displacement without rotation, see, in particular, [34].

(a) One possibility is to decrease the yield stress and σ_0 at a constant external force, e.g. due to the heating of the external part of the disc or of the whole disc.

By making the force before and during heating equal, from an equation similar to (3.119)

$$\begin{aligned} P/\pi R^2 = \sigma_0 + \sigma_{y1}\left(1 + \frac{2}{\sqrt{3}}\frac{R}{3h_0}\right) = (\sigma_0(1+\lambda_0\Delta\theta) + \sigma_{y1}(1+\lambda_1\Delta\theta)) \\ + \frac{2}{3h\sqrt{3}}\Bigg(R\sigma_{y1}(1+\lambda_1\Delta\theta) \\ + cr_1^3\frac{\sigma_{y2}(1+\lambda_2\Delta\theta) - \sigma_{y1}(1+\lambda_1\Delta\theta)}{R^2}\Bigg) \end{aligned} \tag{3.129}$$

one finds an explicit expression for h *versus* temperature rise $\Delta\theta$. In equation (3.129), the parameters λ_0, λ_1 and λ_2 characterize the temperature dependence of σ_0, σ_{y1} and σ_{y2}, respectively. Modification of all the equations in section 3.5.6.2 for this case is straightforward. As in the case with the rotating anvil, if a new phase is harder, the pressure increases in the centre of the disc. Such a situation is observed in [147]: the increase in pressure was caused by the B1 $\rightarrow$ B2 PT in KCl during heating from 300 up to 600 K and initial pressure 6 GPa at the centre was 30%.

Note that if the temperature is higher than the annealing temperature, then defect annihilation occurs, which eliminates strain hardening and leads to an

additional reduction in the yield stress by a factor of two to three and higher [40]. Also, the effect of temperature on $\Delta\psi$ and on nanoscale mechanisms (see section 3.5.4) has to be taken into account.

(b) The other possibility may be based on the use of TRIP (RIP). Let us consider a two-phase material consisting of inclusions in a plastic matrix. If under cyclic temperature variation, inclusions undergo a cyclic direct–reverse PT with a large enough volumetric transformation strain, then the matrix will be deformed plastically, even without external stresses. External stress produces plastic strain in the direction of its action which is proportional to the value of the applied stress and the number of thermal cycles, i.e. it is practically unlimited (see experiments in [18, 19] and our finite-element modelling in [35]). If we introduce the transforming particles into the disc compressed in the anvils, then it is possible to use thermal cycles instead of anvil rotation to get additional displacement and to promote the SC in the centre of the disc.

(c) The most impressive way to reduce the disc thickness, based on rotational plastic instability [128], which resulted in a reduction in the pressure to initiate a martensitic PT from rhombohedral rBN to cubic (diamond-like) cBN by one order of magnitude, will be described in section 3.5.9.

Note that because of a significant reduction in the thickness during anvil rotation, a relatively small (in comparison with compression without rotation) volume of the high-pressure phase can be obtained. This can be improved to some extent by constraining radial flow by an external ring, as in belt-type apparatuses. It will significantly increase σ_0 in the process of thickness reduction.

It is generally accepted that plasticity reduces stress concentration at the macroscale. The previous problem shows a good example of stress (pressure) concentration due to external friction during plastic loading. At large $R/h = 10$–100, the pressure in the disc centre exceeds the yield stress by a factor of $1.15 \times (10$–$100)$ and the specific applied force $P/(\pi R^2)$ by a factor of three. For materials with a pressure-dependent yield stress, these values can be several times higher [40].

The pressure dependence of the yield stress and elastic strain will be taken into account elsewhere. The problem of compression of a rigid-plastic disc for pressure-sensitive materials is solved numerically in [40].

3.5.7 Experimental characterization of strain-induced structural changes under high pressure

It is clear that pressure alone is not sufficient for the characterization of SC under non-hydrostatic conditions and plastic straining because it strongly depends on shear stresses and plastic strains. Even for hydrostatic conditions, the pressure hysteresis is quite high for materials with large volumetric transformation strain. This does not allow experimental determination of the thermodynamic equilibrium pressure and also reduces its significance. The equilibrium pressure can be determined theoretically using thermodynamic data or atomistic

calculations but the actual direct (reverse) SC occurs under much higher (lower) pressure.

Because shear straining in the RDAC reduces PT hysteresis (see item 3 in section 3.5.2), it was claimed that plastic shearing allows better localization of the phase equilibrium pressure. However, in some cases, the direct PT pressure under shear is lower than the equilibrium pressure and reverse PT pressure under hydrostatic conditions (see item 4 in section 3.5.2).

Local pressure in the transforming region varies significantly (even by several times) during the PT [34, 47, 128]. For example, if PT small spherical diamond nucleus appears in a large graphite sphere at applied pressure of 5 GPa, pressure in nucleus drops by a factor of 10 (if plastic deformation is taken into account) or even change of sign in the elastic regime [34], see equations in section 3.3.1. Pressure averaged over some gradually transforming volume varies with the change in volume fraction of the product phase. These changes depend on the mechanical behaviour of the transforming particle and its interaction with the surrounding materials. That is why SC pressure, under such conditions, strongly depends on the geometry and the structural materials of the high-pressure cell.

Note that in most cases, even in non-rotational DAC, when a high-pressure experiment is performed without hydrostatic media, the specimen undergoes large plastic deformations [3, 128, 172–174]. This is the case in experiments under megabar pressure, in particular with solid hydrogen [172–174]. PT conditions for such a case are characterized by pressure only and are compared with or led by atomistic calculations of the phase equilibrium pressure. We believe that this is conceptually wrong and even the term pressure-induced PT or CR is misleading in such a situation.

According to the classification, summarized in section 3.1, SCs in RDAC and in traditional DAC without hydrostatic media are strain-induced SCs. One of the key problems is to find a proper experimental and theoretical characterization of them. Let us analyse the characterization of temperature-, stress (pressure)- and strain-induced SC.

Temperature-induced SCs are characterized by a SC start temperature which depends on the volume fraction of the product phase. For a martensitic PT in steels, these temperatures are far from the equilibrium temperature. The equilibrium temperature cannot be determined in the transformation experiment but it can be calculated if the thermodynamic properties of the phases are known. Both temperatures also depend on the defect structure and, consequently, on the preliminary plastic strain [36]. This description is equivalent to the determination of volume fraction of the product phase as a function of temperature for direct and reverse SCs. For athermal martensitic PTs, the transformation is time- and rate-independent, i.e. time is not an essential parameter. There are a number of reasons for macroscopic time-independent kinetics, even when the microscale behaviour is thermally activated, see, e.g., [25]. For isothermal martensitic PTs, real time-dependent kinetics is used.

Similarly, it is possible to characterize pressure-induced SCs by the pressure necessary for direct and reverse SC. Both of them are functions of the fraction of the high-pressure phase and preliminary plastic deformation (due to the defect structure) [21, 34, 37, 39]. Note that PTs in elastic materials (e.g. in shape memory alloys) under general multiaxial loading (i.e. stress-induced PTs) are characterized with the help of the transformation surfaces in five-dimensional deviatoric stress space which depends on the volume fraction of the martensite and temperature [30, 32, 180–183]. The use of deviatoric space is related to a negligible volumetric transformation strain and the effect of pressure on PT. This representation is very similar to the yield surface in plasticity theory and its dependence on plastic strain [179]. A more detailed description includes, in addition to transformation surfaces for direct and reverse PT, surfaces for transformation between martensitic variants.

Such a multi-dimensional characterization in a space of stress tensor components is absent for high-pressure PTs and CRs. However, for a pressure which significantly exceeds the macroscopic yield stress in shear, τ_y, the effect of macroscopic shear stresses is negligible for a comparable volumetric and shear transformation strain. As mentioned in section 3.5.5, under the compression of materials in DAC, τ_y is smaller than the pressure in the centre of the disc by a factor of $2R/h = 10$–100.

Strain-induced kinetics in TRIP steels is described as a relationship between the volume fraction of the martensite and uniaxial or, more generally, the accumulated plastic strain q [14]. It is known that the strain-induced nucleation in TRIP steel occurs at the shear-band intersections. Based on such a model, the structure of the relationship between volume fraction of the martensite and the equivalent plastic strain was derived and the temperature-dependent coefficients were determined from experiments [14]. This model was not related to thermodynamics. It was generalized to the three-dimensional case and was used as a constitutive equation for modelling strain-induced PTs for various loadings [90, 91]. Reverse strain-induced martensitic PTs have not been considered in the available literature.

Similarly, the nucleation of the p-diamond at defects ('weak spots') generated during plastic flow at dynamic loading was assumed in [184].

As previously discussed, SCs occurring in RDAC and in non-rotational DAC during plastic compression are strain-induced SCs under high pressure rather than pressure-induced SCs. This is not a terminology problem: it defines a mechanism and a way to describe the SCs. In contrast to pressure-induced SCs which predominantly occur at pre-existing defects, strain-induced SCs occur at new defects generated during plastic flow. Since the strain-induced PTs in steels cannot be (and were not) characterized in terms of temperature, strain-induced PTs and CRs under high pressure cannot be characterized in terms of pressure. Similar to strain-induced PTs in TRIP steels, strain-induced SCs under high

pressure can be characterized by a strain-controlled kinetic equation of the type

$$\frac{\mathrm{d}c}{\mathrm{d}q} = f(p, q, \theta, c, \sigma_{y1}, \sigma_{y2}) = f_1(p, q, \theta, c) \tag{3.130}$$

where σ_{yi} were excluded as functions of p, q and θ. Kinetic equation (3.84) is an example of such a relationship. In the first approximation, the stress deviator (or shear stress) is not an explicit argument of equation (3.130), because its components are small in comparison with pressure. Also, its magnitude is equal to the yield stress, so its effect is included implicitly. For TRIP steels, the effect of the types of stress and strain states is observed [90, 91]. They could also affect strain-induced SCs at high pressure but it is unrealistic now to include additional arguments which are very difficult to determine experimentally.

There is a basic difference between traditional time-dependent kinetics and strain-controlled kinetics. For time-dependent kinetics, for infinitesimal $\mathrm{d}c/\mathrm{d}t$ and long enough experiments, it is possible, in some cases, to determine the thermodynamic equilibrium pressure *versus* temperature. A kinetic description, which depends upon many parameters, is an addition to the phase equilibrium diagram, which depends only on thermodynamic parameters. In contrast, strain-controlled kinetics is derived from the thermodynamic condition that the net thermodynamic driving force is equal to zero with an appropriate allowance for all dissipative forces. Because the thermodynamically equilibrium pressure does not characterize strain-induced SCs at all, a strain-controlled kinetic equation is not additional but the only way to characterize strain-induced SCs.

To determine all the parameters in equation (3.130) experimentally, one has to determine experimentally or calculate the small increment Δc corresponding to a small increment Δq and the current values of p, q, c and θ locally in some small volumes, in which the heterogeneity of these parameters is negligible. If the distributions of all of these fields can be determined, one can determine function f_1 (or f) from a few experiments.

The pressure distribution can be measured using a ruby sensor technique (see figure 3.29), the x-ray diffraction with synchrotron radiation (when the equations of state of the materials under study or sensor material are known) or Raman spectroscopy (after preliminary calibration). The measured force can be used to check the accuracy. Despite the recent progress in measurement of deviatoric stresses (see reviews [185, 186]), it is insufficient to measure deviatoric stresses distribution along the radius.

The displacement distribution at the contact surface between the sample and anvil can be measured by imaging the ruby particle positions [148, 154]. To measure the thickness of the compressed disc under load, a method based on the electric capacity sensor can be used [157]. To increase the accuracy of this method, the elastic deformation of the anvils and the support structure have to be taken into account using finite-element modelling [126, 187–190]. As a result, the entire profile of the specimen under the load can be obtained. An alternative method for the measurement of the entire profile of the specimen is

based on the measurement of the x-ray absorption [191]. When the displacement increment field during time Δt, the thickness and thickness increment are known, one can approximately determine the deformation rate fields (using the definitions in equation (3.92)) and calculate $\dot{q}$ (using equation $(3.99)_3$).

For the measurement of the phase distribution, x-ray diffraction with synchrotron radiation, Raman spectroscopy or Fourier transform infrared spectroscopy can be used. For high-pressure phases which are metastable at normal pressure, much more precise determination of the c field can be made on an unloaded specimen.

Note that one has to relate all parameters to the same material rather than spatial particles. That is why it is reasonable to 'personalize' ruby particles and relate all measurements to the neighbourhood of each (or some) particles.

This procedure can be used to check the validity and generalize or specify the kinetic equation (3.84). One of the possible procedures for parameter identification in equation (3.84) is described at the end of section 3.5.5.2.

In addition to a complete characterization in terms of the kinetic equation, partial characterization by the parameters $p_\varepsilon^{\mathrm{d}}$ and p_ε^r, function $c_s(p)$, and plots of the relationship between the fixed pressure and accumulated strain q, which is necessary for the appearance of several prescribed fractions c_i of phase 2 (both for direct and reverse SC) is very useful. The last relationship for the first detectable amount of phase 2 was determined experimentally for PTs in Si and Ge in [144]. A vivid representation of the solution of equation (3.130) can also be done by plotting $c(q)$ for a number of fixed pressures (both for direct and reverse SCs).

Note that the dependence $c(\gamma)$ for several fixed pressures was experimentally determined in [142] for the semiconductor $\rightarrow$ metal PT in InTe. We cannot use these results for the characterization of strain-induced PT because c was determined for the whole specimen and p was determined as the total force divided by the area of the specimen, rather than locally. Because of the heterogeneous and non-stationary distribution of the pressure and volume fraction, the error will be large. However, if such plots were to be determined for local values and in terms of q rather than γ, they would be exactly what we would need to determine function f.

Note that at the nanoscale, a condition of the type in equation (3.70), i.e. $p = \hat{f}(\tau, l, L, n, \theta)$, in principle, can be used for the experimental characterization of strain-induced SCs at high pressure. However, parameters l and L are too small to be measured *in situ*. A transmission electron microscopy study is needed to find the most potent nucleating defects and their characteristics for the SC under study.

3.5.8 Summary of the interpretation of experimental phenomena

In this section, we will summarize the results of our multiscale study in order to interpret the experimental phenomena enumerated in section 3.5.2.

1. The main nanoscale reason for the reduction of SC pressure due to plastic straining is related to the strain-induced rather than pressure- or stress-

induced SCs. A strain-induced SC occurs by nucleation on new defects generated by plastic flow. For strong enough defects, barrierless nucleation takes place which results in strain-controlled rather than time-controlled kinetics. For strain-induced defects of lower potency, thermal fluctuations are needed and the contribution of pre-existing defects has to be taken into account. This explains the effect of plastic straining on kinetics rather than on the thermodynamics of the PbO_2I $\leftrightarrow$ PbO_2II, calcite $\leftrightarrow$ aragonite and quartz $\leftrightarrow$ coesit PTs and the difference between these PTs and all other SCs mentioned in item I of section 3.5.2.

Estimates show that for strong defects, the direct SC pressure for strain-induced SCs can be lower than the equilibrium pressure and the reverse SC pressure under hydrostatic conditions. This does not mean that plastic straining reduces the phase equilibrium pressure significantly, because the phase equilibrium pressure does not appear in any equation for strain-induced nucleation and cannot be determined from the strain-induced experiment. Of course, the local pressure in the region of stress concentration near the defect is greater than the equilibrium pressure (for a given stress deviator). The pressure, averaged over some volume much greater than the nucleus, which is measured in experiments, can be much smaller than the equilibrium pressure. This explains the experimental results mentioned in item 4 of section 3.5.2.

Note that SC is promoted by plastic deformation at the pressure above $p_\varepsilon^{\mathrm{d}}$ only. A large plastic strain below $p_\varepsilon^{\mathrm{d}}$ suppresses SC because of strain hardening and growth of K_{d}. This explains why large plastic deformation during the compression of materials does not cause SC, while relatively small shear strain at relatively high pressure promotes SC significantly.

There is a macroscopic reason why 'plastic shear' significantly reduces the pressure for the appearance of the first detectable amount of the high-pressure phase in comparison with plastic compression. Despite the fact that in both cases, strain-induced SC in the centre of the disc occurs under compression without shear, the trajectory of the loading in the $\bar{p}$–q plane is very different. Under compression, the pressure grows fast during the deformation process. Under torsion, the pressure is constant.

There are several macroscopic reasons why anvil rotation intensifies the progress of SC in comparison with the case without rotation. Rotation, significantly reducing the disc thickness, compensates the volume decrease due to the SC and increases the pressure in the transforming region. It also increases the accumulated plastic strain. In the case without anvil rotation, the material deforms elastically during the SC in the central region of the disc and the rotation leads to plastic deformation. This transforms the stress-induced SC to strain-induced SC (which can occur under a much smaller pressure) and also causes significant pressure growth. The effect of rotation is much more pronounced if the high-pressure phase is stronger than the parent phase.

In a number of publications, the SC pressure is defined as the total force divided by the total area of a specimen rather than the local pressure (see, e.g., [125, 138, 142]). SC during anvil rotation may be caused by pressure growth in the centre of the disc at a fixed force, e.g. due to the pressure self-multiplication effect or substitution of elastic straining in the central part of the disc by plastic straining. Such a result does not indicate that rotation reduces the SC pressure. Consequently, it can be concluded that the reduction in SC pressure due to plastic straining can be made from local pressure measurements only.

For CRs, additional macroscopic reasons for intensification may be related to better mixing, fracture and the appearance of 'fresh' surfaces [124].

2. There are two possible reasons for the appearance of 'steps' in a pressure distribution. Both of them result in a small radial shear stress. One of the reasons is related to the flow of the material in the transforming ring to the centre of the disc and the formation of a stagnation zone. This can be the case for a relatively large reduction in thickness G and radius r. The second reason is connected to shear stress relaxation due to the TRIP (RIP) phenomenon. The meaning of the value of pressure at the 'step' is unclear but it has nothing to do with the phase equilibrium pressure.
3. The reduction in the pressure hysteresis is explained by the fact that the pressure for strain-induced direct (reverse) SC is always smaller (larger) than the pressure for stress-induced SC. Because anvil rotation causes more intensive plastic flow and straining at the initial stage of SC than for the case without rotation and SC can occur under constant pressure, the pressure hysteresis for the case with rotation is smaller than without rotation. However, pressure hysteresis is not a well-defined characteristic of strain-induced SC. Strain-induced defects cause simultaneous direct and reverse SC in different regions. It causes the necessity to consider both direct and reverse SC kinetics and results in the existence of the stationary solution $c_s(p)$. For example, if a system is in the stationary state under any pressure p with corresponding $c = c_s$, then any infinitesimal pressure increase (decrease) followed by plastic straining will cause a $1 \rightarrow 2$ ($2 \rightarrow 1$) SC, i.e. the pressure hysteresis is zero. This explains why zero pressure hysteresis is observed for the B1 $\leftrightarrow$ B2 PT in KCl [146] and demonstrates that the corresponding pressure is not a phase equilibrium pressure. Small plastic strain reduces the range of possible values of equilibrium pressure but it is absolutely unclear at which strain the direct (reverse) SC pressure is getting smaller (larger) than the phase equilibrium pressure.
4. Plastic strain leads to strain hardening and an increase in σ_y, K_{d} and K_{r}, i.e. to an increase in the pressure hysteresis for pressure(stress)-induced SCs. This explains why plastic straining under conditions which do not cause reverse SC, substitutes reversible SCs with irreversible ones (item 6 in section 3.5.2). For strain-induced SCs, the growth of K is more

than compensated by an increase in the driving force due to the stress concentration at defects generated during plastic flow. That is why pressure hysteresis decreases. So, there is no contradiction between the statements in items 3 and 6 of section 3.5.2. In item 3, both direct and reverse SCs are strain-induced, while in item 6 only direct SC is strain-induced.

Note that K also represents an additional heat source in the energy balance equation [21]. If it exceeds the SC heat at equilibrium conditions, then one will receive heat liberation with both direct and reverse SC. Such an experimental result was obtained for the B1 $\leftrightarrow$ B2 PT in RbCl and was also explained by the large pressure hysteresis [39].

5. The pressure self-multiplication (self-demultiplication) effect is explained by the appearance of phases with the higher (lower) yield stress, see equation (3.118). The necessary conditions for this effect are that the reduction in the thickness of the disc completely compensates the volume decrease due to SC and that plastic flow occurs rather than the elastic deformation of the central part of the disc. This is the case for RDAC and for a traditional DAC, when SC occurs under a fixed load due to the reduction in the yield stress by heating or rotational plastic instability [128]. This is not the case under compression in a traditional DAC.
6. Even without plastic deformations, the non-hydrostatic stress state can contribute differently to the driving force X for SC to two alternative phases if they have a different transformation strain deviator. Consequently, the non-hydrostatic stress state can lead to phases which are hidden in the hydrostatic experiment.

   Plastic straining, due to a change in K and the creation of new stress concentrators, provides many more opportunities for new phases, which not only were not but cannot be obtained under hydrostatic conditions. This is especially important for the appearance of alternative strong phases. At the nanoscale, stress concentration, due to new defects and, consequently, ΔX, are greater in the stronger phase. At the microscale, if a stronger phase appears, the deformation is more concentrated in the parent phase. This promotes direct SC and suppresses reverse SC, in comparison with the equal strength phases. If both strong and weak phases appear, again deformation is more concentrated in a weaker phase which may cause SC w $\rightarrow$ s.

   At the macroscale, when in a traditional DAC, the material flows to the centre of the disc, the material with the smaller yield stress appears in the case without rotation (as pressure is higher at $\sigma_{y1} > \sigma_{y2}$) and the stronger phase will be obtained under compression with rotation (as pressure is higher at $\sigma_{y2} > \sigma_{y1}$).

   Let the material not flow to the centre of the disc with and without rotation. Anvil rotation can promote the appearance and growth of the high-strength phase, because rotation transforms stress-induced SC to strain-induced SC (which can occur under a much smaller pressure) and causes significant pressure growth due to the pressure self-multiplication effect

during the SC. The pressure self-multiplication effect serves as a positive mechanochemical feedback.

7. At the nanoscale, barrierless nucleation at strong defects explains the strain-controlled rather than the time-controlled kinetics. The barrierless nucleus is the thermodynamically equilibrium one rather than the critical nucleus. That is why when straining stops, no new defects and nuclei appear and the growth of existing nuclei is thermodynamically prohibited. For weaker defects, thermally activated kinetics is observed (see item 1 in section 3.5.2). At the macroscale, if the anvil stops rotating and the SC continues, then the pressure drops because of a volume decrease and a flow to the centre of the disc. As follows from section 3.5.7, the pressure–shear diagram suggested in [144, 151] represents useful but limited information about strain-induced SC.
8. We did not explicitly analyse the reasons why the rate of strain-induced CR in some polymers increases by a factor of 10^2–10^5 with shear strain compared with the liquid-phase reaction, see item 8 in section 3.5.2. It cannot be done quantitatively because of insufficient information. Qualitatively, we see several possible reasons for this effect. Defects induced by plastic flow create stress concentration and a much higher driving force for SC than in a liquid at the same macroscopic pressure. Under the same applied force, the pressure gradient and a possible pressure self-multiplication effect also create a much higher local pressure in the central part of the disc than in a liquid. The mixing of components during plastic flow may be comparable with mixing in a liquid phase. For strain-controlled kinetics, $\dot{c}$ is proportional to $\dot{q}$ which could be very high for a thin disc. However, it is not clear whether these reasons are sufficient for the quantitative explanation.
9. There are two possible reasons for the phenomenon summarized in item 10 of section 3.5.2. A matrix with a yield stress higher (lower) than that for reagents significantly promotes (suppresses) the CRs, because the plastic strain is concentrated in the reacting material (matrix). Moreover, the pressure gradient and pressure in the central part of the disc is higher (lower) for the stronger (softer) matrix at the same applied load.
10. The reduction in SC pressure with an increase in strain rate can be explained by the competition between the product phase nucleation and dislocation slip activation at defects like a dislocation pile-up. For slip, higher shear stress is necessary for a higher strain-rate, which increases τ in equations (3.70)–(3.72). Pressure redistribution at the macroscale may also play a role because of an increase in macroscopic yield stress. Because strain rate grows with the growing radius, it will lead to a smaller pressure gradient and a smaller pressure in the centre of the disc. The interplay of these two factors determines the resulting effect of strain rate. For polymers studied in [125, 138], the independence of the volume fraction of product phase on strain rate may be related to the mutual compensation of both reasons.

This is a very preliminary assumption, because neither the condition of the experiments in [125, 138] nor the nature of the nucleating defects and data on material rate sensitivity are known.

11. It was explained in item 6 why plastic straining may lead to new phases. If alternative phases were known, this means that the plastic straining changes the transformation path, as described in item 12 of section 3.5.2. The appearance of some phases at the pressure release in an indentation test rather than at a pressure increase can be related to a specific internal stress field created by defects induced during loading.
12. The proportionality of the pressure hysteresis for the PT after preliminary plastic deformation and the yield stress is related to the fact that parameter K, which characterizes the pressure hysteresis, and the yield stress are determined by an interaction of a moving interface and dislocations through the same obstacles (point, linear and other defects). This proportionality was used in [21, 34] to derive the equation $K = L\sigma_y\varepsilon_0$.
13. The regularity summarized in item 14 of section 3.5.2 demonstrates the universal character of strain-induced nucleation at various loading schemes. There are no data on specific loading parameters, so quantitative comparison is impossible. However, it allows us to assume that our theory will be applicable to various materials and deformation processes, which occur under static and shock loading, in material synthesis, geophysics, mechanosynthesis, and shear ignition of explosives.
14. The independence of the pressure distribution from anvil rotation was obtained in our macroscopic approach using a model of perfectly plastic material. It is definitely not true for hardening or softening material [40]. This, in particular, confirms a postulate about the existence of the limiting surface of the perfect plasticity [40]: above some (rather large) level of plastic strain, the initially isotropic polycrystalline materials are deformed as perfectly plastic and isotropic with a strain-history-independent limiting surface of perfect plasticity. This means that the strain hardening is saturated and plastic properties reached their steady state.
15. We can also answer the question why anvil rotation reduces the SC pressure in the centre of the disc where plastic shear and shear stresses are absent. Rotation induces a significant reduction in the thickness and a corresponding accumulated plastic strain $q = \ln(h/h_0)$, which, according to equation (3.84), induces the SC.

3.5.9 Low-pressure phase transformation from rhombohedral to cubic BN: experiment and theory

This section is based on papers [128, 129, 157] and represents one of the most exciting examples of the interaction between plasticity and PTs. An abrupt martensitic PT from rhombohedral rBN to cBN was recorded at a pressure 5.6 GPa before the PT. In comparison, under hydrostatic loading the irreversible

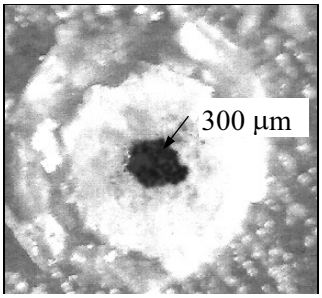

Figure 3.43. View of a sample at the diamond anvils. The black region represents cBN transformed from rBN at the pressure 5.6 GPa at the beginning of transformation.

rBN $\rightarrow$ cBN PT has been reported to occur at a pressure of 55 GPa [192]. Thus a reduction in PT pressure, *by one order of magnitude has been achieved*. We concluded in [128] that a new phenomenon occurs, namely a *PT induced by a rotational plastic instability*.

3.5.9.1 Experimental results

We describe the experimental results obtained in [129] and our additional experiments, which are necessary to verify our theory. A very high-textured rhombohedral phase of BN, with disorientation of the C-axes of crystallites of about $\pm 3^\circ$ with respect to the [0001] rBN texture axis, was compressed in diamond anvils along the [0001] rBN direction. The disc-shape samples of a pyrolytic material containing up to 95 mass% rBN, 3 mm in diameter were used. The ruby fluorescence technique was used to measure the pressure in the centre of the sample [193]. It allows fast pressure measurements in a DAC *in situ* from a shift in the ruby luminescence line R1. The method consists in the following. A tiny ruby chip 3.5 μm in size was placed on a sample surface at the centre of the sample. During the experiment, ruby fluorescence is excited by an argon laser. The fluorescence spectrum is registered by a spectrophotometer and is transmitted to a computer. The pressure is determined from the known shift of the ruby luminescence line R1 [193]. The time of pressure determination at a point does not exceed 20 s. The basic difficulty consisted in registration of the ruby fluorescence spectra ($l = 0.6942$ μm) because rBN has a strong luminescence in this spectral range. By choosing both the laser beam diameter and the ruby chip dimensions (3.5 μm), we recorded sharp ruby fluorescence spectra. A detailed description of the DAC and the measurement technique can be found in [127].

Up to about 3.5 GPa, the material was deformed elastically, because on unloading there was practically no anvil indent on the sample surface. At recompression in a range 4.2–5.6 GPa, small strips 10 μm $\times$ 80 μm in size, well visible in transmitted light, appeared on the sample surface. In [129], these

strips were interpreted as cracks; however, there was no evidence of crack at unloading. Now we believe that reorientation of crystallites under an applied load takes place and these strips represent the boundary between differently oriented crystal regions.

When the pressure reached 5.6 GPa and the load was fixed, an amount of chaotically located strips increased quickly. After 5–7 s, an abrupt irreversible martensitic PT from rhombohedral rBN to cubic cBN was recorded at the sample centre, accompanied by a distinct acoustic emission signal, a significant reduction in the disc thickness and dynamic loading.

The as-recovered sample of the produced bulk material looked like a plate of black colour with mirror-smooth plane-parallel surfaces (figure 3.43). When the anvils were aligned well, the shape of the transforming region was close to a circle. The microhardness of the transformed material defined by Knoop microindentation was 49.6 GPa, which is typical of cBN. The analysis of electron-diffraction patterns of spalled particles of the sample uniquely shows the presence of a fair quantity of cBN. All measured geometric parameters of compressed disc and pressure at the beginning of the PT for several experiments are summarized in table 3.3. The parameters given in brackets were used in our calculations. Experiment 3, which corresponds to a small initial disc thickness, was accompanied by the spalling of the non-loaded disc part (at a radius greater than anvil radius R). In experiment 4, one of the anvils received a ring crack. Its position approximately corresponds to the boundary between the rBN and cBN phases. This anvil was polished to remove the crack. However, in the next experiment, after dynamic loading during the PT from rBN to cBN, it was broken into dust.

3.5.9.2 Phase transformation criterion

We will need to use our PT criterion formulated for finite strain [21]. The main difference is in the expression for the transformation work. Also, because the volume of the nucleus depends on stress, parameters X and K are determined per

Table 3.3. Measured geometric parameters of compressed disc and axial stresses at the beginning of the PT.

	Radius of anvil R (μm)	Radius of cBN phase r_0 (μm)	Final thickness h (μm)	PT start pressure σ_{zi} (GPa)	Initial thickness h_i (μm)
1	250	100	26	5.6	310
2	375	∼150	∼50	∼5.6	∼450
3	375	70–105 (70)	∼20	>5 (5.6)	∼175
4	375	100–160 (100)	30–35 (30)	∼5.5	380

unit mass rather than per unit volume. In [128], strain-induced kinetics was not considered because it had not yet been developed. The PT criterion $X = K$ was applied to the appearance of the whole transformed region of cBN. It is still a reasonable approximation: strain-induced defect concentrators effectively reduce the threshold K.

For a martensitic PT, the transformation deformation gradient $\boldsymbol{F}_t$ (Bain strain) transforms a crystal lattice of the parent phase into a crystal lattice of the product phase. For small strain $\boldsymbol{F}_t = \boldsymbol{I} + \varepsilon_t + \boldsymbol{\omega}$, where $\boldsymbol{I}$ is the unit tensor and $\boldsymbol{\omega}$ is the rotation tensor. Below $\boldsymbol{\omega} = \boldsymbol{0}$. As the behaviour of inelastic materials is history dependent, consideration of the entire process of the growth of transformation deformation gradient $\boldsymbol{F}_t$ from unit tensor $\boldsymbol{I}$ to the final value $\boldsymbol{F}_{t2}$ in the transforming region is necessary. Transformation of the crystal lattice with the rBN $\rightarrow$ cBN PT consists of 1.596-fold compression in the [0001] direction and an extension by a factor of 1.02 in the basal plane (orthogonal direction). Consequently, the three principal values of transformation deformation gradient $\boldsymbol{F}_{t2}$ are $F^z_{t2} = 1/1.596 = 0.627$; $F^r_{t2} = F^\theta_{t2} = 1.02$. In the simplest case, when the temperature is fixed and homogeneous in the transforming volume and elastic strains are small, our thermodynamic criterion for PTs in the region with a mass m_n looks as follows:

$$X := -\frac{1}{m_n}\int_{m_n}\int_{\boldsymbol{I}}^{\boldsymbol{F}_{t2}} \frac{1}{\rho}\boldsymbol{T} : (\mathrm{d}\boldsymbol{F}_t \cdot \boldsymbol{F}_t^{-1})\,\mathrm{d}m_n - \frac{1}{2m_n}\int_{m_n}\int_{\boldsymbol{E}_1}^{\boldsymbol{E}_2} \frac{1}{\rho}\boldsymbol{\varepsilon}_\mathrm{e} : \mathrm{d}\boldsymbol{E} : \boldsymbol{\varepsilon}_\mathrm{e}\,\mathrm{d}m_n - \Delta\psi(\theta) = K. \quad (3.131)$$

Here $\boldsymbol{T}$ is the true Cauchy stress, calculated per unit deformed area, ρ is the variable mass density during the PT and $\boldsymbol{\varepsilon}_\mathrm{e}$ is the elastic strain. The minus sign before the transformation work is used because the compressive stresses are considered as positive, but the sign of $\boldsymbol{F}_t$ cannot be changed, as the sign of ε_t.

When all parameters are homogeneously distributed in the transforming region and the stress tensor reduces to the hydrostatic pressure p, $\boldsymbol{T} = p\boldsymbol{I}$, then using known kinematic relations [40], we obtain

$$\frac{1}{\rho}\boldsymbol{T} : (\mathrm{d}\boldsymbol{F}_t \cdot \boldsymbol{F}_t^{-1}) = \frac{p}{\rho}\,\mathrm{d}\boldsymbol{F}_t : \boldsymbol{F}_t^{-1} = \frac{p}{\rho}\,\mathrm{d}\ln\frac{\rho_1}{\rho} = p\,\mathrm{d}\frac{1}{\rho} = \frac{1}{m}p\,\mathrm{d}V = \frac{1}{\rho_1}p\,\mathrm{d}\frac{V}{V_1}$$

where m is the mass of small transforming particle, V_1 and V is its volume before and during the PT. If the pressure and elastic strains are fixed during the PT, equation (3.131) can be transformed to the form

$$\rho_1 X = p\left|\frac{V_2}{V_1} - 1\right| - \frac{1}{2}\boldsymbol{\varepsilon}_\mathrm{e} : \left(\frac{\rho_1}{\rho_2}\boldsymbol{E}_2 - \boldsymbol{E}_1\right) : \boldsymbol{\varepsilon}_\mathrm{e} - \rho_1\Delta\psi(\theta) = \rho_1 K. \quad (3.132)$$

If $K = 0$, equation (3.132) describes the standard equilibrium line $p(\theta)$, which can be expressed as $p = A + B\theta$ with $A = -6.5$ GPa and $B =$

0.00354 GPa K^{-1} [194]. Comparison of these two equations allows us to express the two last terms in the expression for X through known material parameters. Then equation (3.132) can be transformed to

$$\rho_1 X = \frac{\rho_1}{m_n}\int_{m_n}\int_{\boldsymbol{I}}^{\boldsymbol{F}_{t2}} \frac{1}{\rho}\boldsymbol{T} : (\mathrm{d}\boldsymbol{F}_t \cdot \boldsymbol{F}_t^{-1})\,\mathrm{d}m_n - a - b\theta = \rho_1 K \qquad (3.133)$$

with

$$a = A\left|\frac{V_2}{V_1} - 1\right| = -4.24\ \text{GPa}$$

and

$$b = B\left|\frac{V_2}{V_1} - 1\right| = 0.002\,31\ \text{GPa K}^{-1}.$$

3.5.9.3 Phase transformation scenario

We consider the following PT scenario. Before the PT, a sample is compressed elastically and stresses are distributed homogeneously. During the PT, the axial load is fixed. According to Schmid's law, the compressive yield stress in the axial direction (the z direction), when the c-axis makes an angle of 3° with respect to the z-axis, is an order of magnitude higher than the yield stress $\sigma_{y\perp}$ for the optimal orientation of the crystal. With the rotation of a single crystal with respect to the uniaxial stress, the yield stress varies from its maximum to its minimum values. If such a single crystal in diamond anvils is compressed in the axial direction, due to friction stresses, the rotation of the anisotropy axis will occur. This will lead to a reduction in the yield stress in the direction of compression (rotational softening). After some critical reorientation, the carrying capacity (limit load) of the sample becomes smaller than the applied load and continues to reduce with further thickening. Due to such a rotational softening, dynamic compression occurs with a constant force up to the thickness at which the carrying capacity of the sample becomes equal to the applied load.

In the case of perfectly plastic or hardening media and a PT in the central part of the disc, due to compressive volumetric transformation strain, the pressure in the PT region and the transformation work in equation (3.133) decrease significantly, which makes the PT condition worse, see [34] and figure 3.36(*a*). For the softening material described earlier, the decrease in thickness due to rotational plastic instability completely compensates the volume decrease due to the PT and increases the stresses in the transforming region and transformation work. One more very significant contribution to the transformation work is related to stress redistribution. Plastic flow during the PT causes a significant pressure gradient from the periphery to the centre (figures 3.36 and 3.44). Due to the higher yield strength of cBN in comparison with rBN, the pressure self-multiplication effect is also expected [34]. So, the pressure in the transforming region during the PT is much higher than before, which is in agreement with cracking in the anvil. As the reduction in the thickness is much higher than the compression due

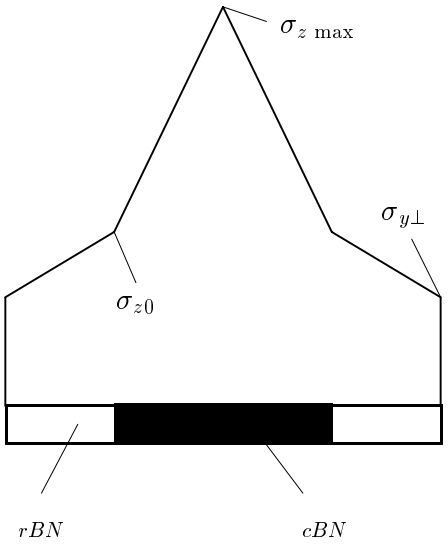

Figure 3.44. Axial stress distribution after the rBN → cBN PT.

to the transformation by a factor of 1.596, then the transforming region undergoes a significant plastic compression. This is also in agreement with the compact structures, high hardness and mirror-smooth surfaces of obtained cBN phase. Consequently, a strain-induced PT takes place.

We conclude that a new phenomenon occurs, namely a PT induced by a rotational plastic instability. The pressure growth and defect generation with the simultaneous occurrence of a rotational plastic instability and PT allows for the fulfilment of the PT criterion at a significantly lower initial pressure than is usually observed. We will confirm this scenario by simple estimates.

3.5.9.4 Stress field in the process of phase transformation

We consider the initial state before the PT as a homogeneous stress state with axial stress $\sigma_{\mathrm{zi}} = P/\pi R^2$, where P is the axial force which will be considered as constant during the PT. After the dynamic PT and plastic flow are combined and equilibrium is reached, the external ring consists of rBN with the yield stress $\sigma_{y\perp}$, the internal ring is cBN with a yield stress σ_{yc} (figure 3.44). We will not consider the entire deformation process, only the final equilibrium state and then assume that the stresses vary linearly with variation in the transformation strain F_t^z during the transformation process.

We will slightly extend our solution of the axisymmetric problem of the PT in a disc compressed in a DAC (see section 3.5.6) for the case of large strain and

an anisotropic transformation strain. We will use the Tresca rather than the von Mises yield condition, as in [128], which does not change the results significantly. Thus, instead of $\tau_{\mathrm{r}} = \sigma_y/\sqrt{3}$ and equation (3.87), we obtain $\tau_{\mathrm{r}} = \sigma_y/2$ and

$$\frac{\partial p}{\partial r} = -\frac{2\tau_{\mathrm{r}}}{h} = -\frac{\sigma_y}{h}. \tag{3.134}$$

Combining this condition with the von Mises or Tresca yield conditions (or their pressure-dependent generalizations) results in the equality of all normal stresses $\sigma_z = \sigma_r = \sigma_\theta = p$ at the contact surface, which conforms with slip line [40] and finite-element [126] modelling. Using the pressure continuity condition at the boundary $r = r_0$ between rBN and cBN while solving equation (3.87), we obtain the pressure (or axial stress σ_z) distribution at the contact surface S (figure 3.44):

$$\sigma_z = \sigma_{y\perp}\left(1 + \frac{R-r}{h}\right) \qquad \text{at } r_0 \le r \le R$$
$$\sigma_z = \sigma_{z0} + \sigma_{yc}\left(\frac{r_0 - r}{h}\right) \qquad \text{at } r \le r_0$$

where

$$\sigma_{z0} = \sigma_{y\perp}\left(1 + \frac{R-r_0}{h}\right) \tag{3.135}$$

is the σ_z at $r = r_0$ and boundary condition $\sigma_z = \sigma_{y\perp}$ at the external radius of anvil $r = R$ is taken into account. The applied load is determined by integrating $\sigma_z(r)$ over S:

$$P = \pi R^2\left(\sigma_{y\perp}\left(1 + \frac{R}{3h}\right) + \frac{\pi r_0^3}{3h}(\sigma_{yc} - \sigma_{y\perp})\right) = \sigma_{\mathrm{zi}}\pi R^2 \tag{3.136}$$

where the equality of the applied force before and after transformation is taken into account.

3.5.9.5 *Determination of the PT condition*

As we now know the stress distribution, we can evaluate the PT conditions using the PT criterion (3.133). For our transformation deformation gradient, the transformation work is

$$\int_{\boldsymbol{I}}^{\boldsymbol{F}_{t2}} \frac{1}{\rho}\boldsymbol{T} : (\mathrm{d}\boldsymbol{F}_t \cdot \boldsymbol{F}_t^{-1}) = \frac{1}{\rho^*}\boldsymbol{T}^* : \ln \boldsymbol{F}_{t2} = \frac{1}{\rho^*}(\sigma_z^* \ln F_{t2}^z + (\sigma_r^* + \sigma_\theta^*)\ln F_{t2}^r) \tag{3.137}$$

where the superscript $*$ designates some intermediate value of the parameters as the transformation deformation gradient is varied from $\boldsymbol{I}$ to $\boldsymbol{F}_{t2}$. As $\ln F_{t2}^z = -0.468$, $\ln F_{t2}^r = 0.020$ and $\sigma_z^* \ge \sigma_r^*$ and $\sigma_z^* \ge \sigma_\theta^*$ [40, 126], then even with equal normal components of the stress tensor, the second term in equation (3.137)

is one order of magnitude smaller than the first term. As follows from slip line [40] and finite element [126] solutions in the absence of PTs, $\sigma_r = \sigma_\theta$ almost everywhere. At the contact surface $\sigma_r = \sigma_z$: while moving to the symmetry plane, σ_z becomes larger than σ_r, with the maximum difference at the symmetry plane equal to the yield stress. Consequently, the ratio of the first and second terms in equation (3.137) averaged over the disc thickness (such terms contribute to the PT criterion (3.133)) is even larger than ten and we can neglect the second term. Neglecting F^r_{t2}, we obtain

$$\frac{1}{\rho} = \frac{1}{\rho_1} \det \boldsymbol{F}_t = \frac{F^z_t}{\rho_1} \qquad \left(\text{as } \det \boldsymbol{F}_t = \frac{V}{V_1}\right)$$

and

$$\int_{\boldsymbol{I}}^{\boldsymbol{F}_{t2}} \frac{1}{\rho}\boldsymbol{T} : (\mathrm{d}\boldsymbol{F}_t \cdot \boldsymbol{F}_t^{-1}) = \int_1^{F^z_{t2}} \frac{F^z_t}{\rho_1}\sigma_z(r)\frac{\mathrm{d}F^z_t}{F^z_t} = \frac{1}{\rho_1}\sigma^*_z(r)(F^z_{t2} - 1). \quad (3.138)$$

The stress σ^*_z represents the local stress in each point averaged over the transformation process. We define $\sigma^*_z(r)$ as the semi-sum of the stress before and after the PT $\sigma^*_z(r) = 0.5(\sigma_{zi} + \sigma_z(r))$, where $\sigma_z(r)$ is defined by equation (3.135). Substituting equation (3.138) into equation (3.133), expressing $\mathrm{d}m_n = \rho_2\,\mathrm{d}V_{n2}$ and integrating over the final transformed volume $V_{n2} = \pi r_0^2 h$, we obtain

$$\begin{aligned}
&\frac{1}{m_n}\int_{m_n}\int_{\boldsymbol{I}}^{\boldsymbol{F}_{t2}} \frac{1}{\rho}\boldsymbol{T} : (\mathrm{d}\boldsymbol{F}_t \cdot \boldsymbol{F}_t^{-1})\,\mathrm{d}m_n \\
&\quad = \frac{\rho_2}{\rho_1 m_n}(F^z_{t2} - 1)\int_{V_{n2}} \sigma^*_z(r)\,\mathrm{d}V_{n2} \\
&\quad = \frac{2\pi h}{\rho_1 V_{n2}}(F^z_{t2} - 1)\int_0^{r_0} \sigma^*_z(r) r\,\mathrm{d}r = \frac{1}{2\rho_1}(F^z_{t2} - 1)\left(\sigma_{zi} + \sigma_{z0} + \sigma_{yc}\frac{r_0}{3h}\right) \\
&\quad = \frac{1}{\rho_1}\sigma_{ef}(F^z_{t2} - 1). \qquad (3.139)
\end{aligned}$$

If we compare the transformation work in equation (3.139) and under hydrostatic condition in equation (3.132), then the terms $(\frac{V_2}{V_1} - 1)$ and $(F^z_{t2} - 1)$ are approximately the same and the term

$$\sigma_{ef} := \frac{1}{2}\left(\sigma_{zi} + \sigma_{z0} + \sigma_{yc}\frac{r_0}{3h}\right) \qquad (3.140)$$

which we will call the effective stress, plays a role similar to the PT pressure. Then we represent the final expression for the PT criterion for our problem in the following form:

$$\rho_1 X = \sigma_{ef}|F^z_{t2} - 1| - a - b\theta = \rho_1 K. \qquad (3.141)$$

Table 3.4. Calculated values of stresses and dissipative threshold.

	σ_{z0} (GPa)	$\sigma_{\rm ef}$ (GPa)	$\sigma_{z\,\max}$ (GPa)	$\sigma_z(h)$ (GPa)	$\rho_1 K$ (GPa)
1	3.05	16.50	76.13	57.12	9.70
2	2.48	13.54	59.48	40.48	8.60
3	7.31	17.54	73.81	54.81	10.09
4	4.58	15.60	67.91	48.91	9.37

3.5.9.6 Parameters estimation

To use this theory quantitatively, we need to know two material parameters: σ_{yc} and $\sigma_{y\perp}$. The yield stress of cBN at compression can be estimated using the known relation $\sigma_{yc} = 0.383H = 19$ GPa [40], where $H = 49.6$ GPa is the hardness. Substituting this value and all parameters from the first line of table 3.3 in equation (3.136), we obtain $\sigma_{y\perp} = 0.45$ GPa.

Substituting the values of σ_{yc}, $\sigma_{y\perp}$ and all parameters from table 3.3 in equations (3.135), (3.140) and (3.141), we obtain the values of σ_{z0}, $\sigma_{\rm ef}$, $\sigma_{\rm z\,max}$, and $\sigma_z(h)$ at $r = h$, as well as $\rho_1 K$ at $\theta = 300$ K for all four cases, which are put in table 3.4.

Let us analyse them. During the transformation event, the axial stress at the external boundary $r = R$ decreases from its initial value ∼5.6 to 0.45 GPa. The axial stress at the final boundary between rBN and cBN slightly decreases from ∼5.6 GPa by several GPa for cases 1, 2 and 4 and increases for case 3. The axial stress in the centre of the disc increases drastically to 60–76 GPa. These values are probably overestimated, because at a distance from the disc centre of order h, the shear stress reduces from its maximum value to zero at the centre and solution of equation (3.87) results in a smaller axial stress [40, 126]. For this reason, the values of $\sigma_z(h)$ at $r = h$ are also given in table 3.4 and they are of the order 40–57 GPa. However, due to the small radius, the contribution of such an error to effective stress is not high. However, allowing for the effect of high pressure on σ_{yc} may compensate this error.

In fact, the pressure self-multiplication effect during the PT is well known with compression with shear in diamond anvils [127, 145, 146, 148, 151–153, 157] and with heating at a fixed axial force [147] (see section 3.5.6). Such an effect with compression without rotation of one anvil was not observed experimentally and contradicted existing theory [34]. In our paper [128], the pressure (stress) self-multiplication effect with compression without rotation was predicted for the first time and is in agreement with a low initial PT pressure. The first reason is that the transformation compression in the axial direction is compensated by a reduction in thickness due to rotational softening. The second reason is related to the anisotropic character of the transformation strain and the transformational extension (rather than compression) in the radial direction. For chaotically distributed crystal orientations, the compression occurs in the radial direction,

the pressure reduces due to the PT and a higher initial pressure will be required to receive the same effective stress. As soon as both of these reasons provide complete compensation of the volume reduction due to the PT, the pressure (stress) self-multiplication effect occurs as a result (a) of pressure redistribution from a homogeneous one before the PT one to strongly growing at the centre of the disc; and (b) a higher yield stress of cBN.

According to the PT criterion and the solution obtained, the pressure growth during the PT is one of the main reasons that the PT starts at a relatively low initial pressure of 5.6 GPa. In fact, the effective stress, which according to our theory, affects the PT rather than the initial stress, is much higher, namely 13.54–17.54 GPa. These values are comparable with the value of the pressure at which the reversible PT from rBN to cBN occurs at hydrostatic conditions [192].

According to the data reported in [192], the rBN-to-cBN transformation process occurs as the pressure grows from 8 to 20 GPa. *In situ* x-ray-diffraction measurements demonstrated that a cBN(111) reflection appears at 8 GPa; however, the rBN(003) reflection persists up to 20 GPa. At pressure up to 15 GPa, no traces of cBN are observed after unloading. At least above 55 GPa, the PT from rBN to cBN is irreversible and small 300 Å particles of cBN were retrieved.

Analysis of equation (3.140) shows that due to a high $\sigma_{z\,\max}$, the initial stress σ_{zi} does not significantly influence the effective stress and the PT condition. At the same time, the rotational instability starts at some critical stresses independent of the final or effective stresses. Therefore, for all experiments, almost the same initial stress σ_{zi} is the stress at which the rotational instability starts rather than the PT start pressure.

3.5.9.7 Comparison with a PT under hydrostatic conditions

A comparison of the results obtained in [129] and here with [192] is not straightforward due to different spatial scales. In our case, the PT occurs in a macroscopic region, the surface energy can be neglected and the dissipative threshold K represents some averaged characteristic of interaction between numerous interfaces, defects and plastic flow. The PT in our case represents a combination of a stress- and strain-induced PT, when the plastic flow generates new nucleation sites and promotes the transformation, which is effectively reflected in lowering the calculated value K. Similarly, nucleation of p-diamond at defects ('weak spots') generated during the plastic flow at dynamic loading was assumed in [184]. Similar processes in steels are described in [94].

At unloading $\sigma_z = 0$ and $\rho_1 X = 3.55$ GPa > 0 and the criterion for the reverse PT $X \leq -K_{2\to1} < 0$ cannot be satisfied. This is clear because according to the new BN equilibrium diagram [195], we are in the stability region for cBN.

For experiments described in [192], due to the very small transforming volume, the situation is qualitatively different. Due to the smaller scale, the probability that the interface intersects the dislocation and the point defect is much

smaller than for the macroscopic transforming region. Therefore, both $K_{1\to2}$ and $K_{2\to1}$ are related to the activation barrier at the atomistic scale [150, 166] and to the Peierls barrier and are much smaller than for the macroscopic case. However, the change in surface energy per unit transforming mass, $\Delta\Gamma$, which makes a negative contribution to the driving force has to be taken into account. The direct PT criterion looks like $X - \Delta\Gamma = K_{1\to2}$. The sum $K_{1\to2} + \Delta\Gamma$ has the same order of magnitude, as the estimated dissipative threshold, because the PT occurs at a similar pressure range 15–20 GPa. However, the change in surface energy is a reversible process in contrast to the irreversible processes reflected in K and it makes the same negative contribution to the driving force for the reverse PT. Therefore, the reverse PT criterion $X - \Delta\Gamma = K_{2\to1} < 0$ can be satisfied at unloading. Consequently, at unloading, reverse interface motion and the disappearance of cBN nucleus occur (as for shape memory alloys with pseudoelastic behaviour), despite the fact that the cBN nucleus is in the cBN stability region. Due to the reversible interface motion, it is very likely that heterogeneous nucleation near some defects (stress concentrators) occurs, in this case the nucleus is stable and increases (decreases) its size with the pressure growth (reduction) [56]. For a homogeneous nucleation, the critical nucleus is unstable and spontaneously grows until it is arrested by a subgrain or grain boundary.

We see two possible reasons why the PT from rBN to cBN becomes irreversible under some critical pressure between 20 and 55 GPa. The first one is that the nucleus becomes large enough to reach and be arrested by the nearest defect (dislocation, subgrain or grain boundary). In this case, the reverse interface motion is arrested as well. The second reason is that in the framework of linear elasticity, the internal stresses due to a jump in the elastic moduli grow proportionally with the pressure growth (internal stresses due to transformational strain are independent of applied pressure) [47]. Under some critical applied pressure they become high enough to generate dislocations and initiate plastic flow. Then K grows drastically or the interface is arrested by these dislocations.

3.5.9.8 Concluding remarks

A simple analytical model, based on the new thermodynamic criterion for the PT in plastic materials and the solution of the corresponding large strain plastic problem, suggests a very unexpected explanation of the low PT start pressure of 5.6 GPa of the irreversible rBN $\to$ cBN PT. A new phenomenon, namely a PT induced by rotational plastic instability, is revealed.

In our thermodynamic criterion, the effective stress, which, in the case under the study, is the axial stress averaged over the transforming region and transformation process, is substituted for the pressure in the classical approach. Due to drastic axial stress growth in the transforming region during the transformation process, the effective stress is of the order 13.54–17.54 GPa.

There are the following reasons for the stress increase.

1. The main phenomenon is related to the rotational plastic instability of rBN and a drastic softening (a reduction in the yield stress) due to reorientation of the rBN crystals. This leads to a significant reduction in disc thickness which compensates for the volume decrease due to the PT.
2. The second reason is related to the anisotropic character of the transformation strain and transformational extension (rather than compression) in the radial direction.
3. As soon as both of these reasons provide complete compensation of the volume reduction due to the PT, the stress self-multiplication effect occurs as a result of (a) pressure redistribution from the homogeneous one before the PT to a strongly growing to the centre of the disc one; and (b) the higher yield stress of cBN.

The fact that the calculated values of the dissipative threshold $\rho_1 K$ for four very different experiments is almost the same (see table 3.4) strongly supports our theory. The averaged value over four experiments $\rho_1 K = 9.44$ GPa, substituted into equation (3.141) completes this equation. Now equations (3.135), (3.136) and (3.141) can be used to predict the PT conditions, the geometry of the transformed region and the stress distribution for various experiments.

One of the conclusions of this analysis is that the initial pressure before the PT (5.6 GPa) does not characterize the PT conditions, rather it is the stress of the onset of rotational plastic instability. By changing the initial disorientation of the C-axes of the crystallites with respect to the compression direction and/or using some gaskets, the stress for the onset of rotational softening and, consequently, the stress when the PT starts, can be changed significantly without changing the effective stress. However, there is no practical reason to reduce the σ_{zi}, because the stresses after the PT are much higher and they determine the strength and durability of diamond anvils or other types of high-pressure apparatuses which may be used for the industrial application of the effects described here. In contrast, it is necessary to increase σ_{zi}, to reduce $\sigma_{z\,max}$ at the same effective stress and to avoid a strong dynamic instability in order to optimize the strength and durability of the loading device. This solution in combination with the strength calculation methods and optimal design [189,190] can be used for these purposes. After finding the optimal way to produce cBN in a controlled quasi-static process without fracture of an anvil, a similar method can be applied to obtain a graphite $\rightarrow$ diamond PT, as well as to seek new superhard phases, e.g. in a B–C–N system.

3.5.10 Possible ways to control structural change conditions

Let us summarize our analysis of various examples which we considered as possible ways of controlling SCs by the purposeful control of the thermomechanical loading process and microstructure.

1. The trivial contribution of shear stresses to the force driving SC is connected with the work of shear stresses along the transformation shear strains. This

contribution is extremely important for SCs in the elastic regime (stress-induced SCs) when the volumetric transformation strain is negligible and the transformation shear is 0.1–0.2. It may also be important for SC under indentation (see section 3.6). When the pressure exceeds the yield stress in shear by a factor of 10–100, as in diamond anvils, the contribution of macroscopic shear stress to the driving force is negligible in comparison with the pressure contribution. However, even in this case, the thermodynamic effect of macroscopic shear stress may be important:

(a) to choose alternative phases (may be new phases) or alternative mechanisms which have the same (or almost the same) volumetric transformation strain and different transformation shear; e.g. rBN transforms to a zinc-blende structure under hydrostatic conditions by 'a layer puckering' mechanism and to a wurtzite structure by 'a layer buckling' mechanism under non-hydrostatic conditions [196]; and
(b) to choose different martensitic variants (which have the same volumetric transformation strain) and microstructure.

2. Shear stress causes the TRIP (RIP) phenomenon. If the shear stress exceeds the yield stress, then classical plastic flow occurs as well. Both TRIP and classical plasticity generate defects (stress concentrators) which serve as nucleation sites for strain-induced SCs. As local, normal and shear stresses near the strong defect can be by a factor of 10–1000 higher than the macroscopic shear stresses, the main nanoscale effect of plastic straining is related to the contribution of local stresses to the thermodynamic driving force. Pure hydrostatic pressure does not cause plastic flow and the appearance of strong stress concentrators, which explains the unique role of shear stresses and strains on SC. Even for zero transformation shear, i.e. when the macroscopic shear stress does not contribute to transformation work, equations (3.70) and (3.75) exhibit the significant effect of τ on p because of the pressure concentration at the tip of the pile-up (see equation (3.64)).
3. Because defects like dislocation pile-ups generate both a compressive and tensile pressure with the same magnitude, they simultaneously promote both direct and reverse SC in different regions. This results in the existence of a stationary value of the product phase fraction which depends on pressure (figure 3.34) and in some limitation to the intensification of SC by plastic straining. As it follows from figure 3.34, a significant quantity of the high-pressure phase or complete SC can be induced by a large strain at a low pressure for a small M only, i.e. if the kinetics of the reverse PT is suppressed or the product phase is much stronger. However, even for a large M, a detectable amount of the product phase can be obtained at a low pressure, which is important for the search for new phases.
4. According to the equation $K = L\sigma_y\varepsilon_0$, preliminary plastic deformation suppresses SCs and increases pressure hysteresis. The plastic deformation

of a high-pressure phase, under a pressure slightly above p_ε^r, can be used to reduce the reverse SC pressure and keep the high-pressure phase under room pressure. By finding an unloading path which minimizes or avoids plastic straining, one can avoid or minimize strain-induced reverse SC. It allows the use of a high-pressure phase in engineering applications. One of the possible ways to reduce plastic strain during unloading is to make the unloading as fast as possible (quenching from a high-pressure state).

With a the large strain of order 0.4 (for rocks)–1.5 (for metals), according to the regularity revealed in [40], σ_y and, consequently, K have to be strain and strain-history independent. That is why it is desirable to exceed this strain before SC if one wants to exclude the effect of strain and strain history on the yield stress and K. Based on known data for the strain hardening of metals [40], the value of K and pressure hysteresis in the maximum hardened state can be, by a factor of two to four, higher than in annealed state, see also [37–39].

5. SC is promoted by plastic deformation at a pressure above $p_\varepsilon^{\mathrm{d}}$ only. A large plastic strain below $p_\varepsilon^{\mathrm{d}}$ suppresses PTs because of strain hardening and the growth of K_{d}. Any action, which increases the local plastic strain at $p > p_\varepsilon^{\mathrm{d}}$ and pressure, promotes SCc. As an example, we can mention mixing the material under study with strong particles or using a matrix made of a stronger material. Adding weaker particles suppresses SC. In particular, mixing with ruby particles for pressure measurement may reduce SC pressure.
6. Because the length of the dislocation pile-up and, consequently, the stress concentration is limited by the grain size, one way to intensify (suppress) the SC is related to an increase (decrease) in grain size. This can be done by avoiding plastic straining below $p_\varepsilon^{\mathrm{d}}$ (see item 7) or by annealing and re-crystallization after the compression of the disc at a pressure below $p_\varepsilon^{\mathrm{d}}$. Annealing under a pressure slightly below $p_\varepsilon^{\mathrm{d}}$ also reduces the yield stress σ_y, K_{d} and the direct PT pressure. Annealing under room pressure (if this does not cause a reverse SC) decreases σ_y, K_{d} and internal stresses and can lead to an increase in the net driving force and to the growth of a high-pressure phase.
7. Note that a thin specimen can be used in a DAC experiment to avoid plastic straining in the central part of the disc during the compression stage. The applied force P has to be smaller than that defined by equation (3.90). One of the reasons to use a thin specimen and to avoid plastic straining may be that to obtain pressure(stress)-induced rather than strain-induced SC even without hydrostatic media. Another reason is to avoid preliminary plastic deformation, which causes a decrease in grain size, strain hardening and an increase in K: this can reduce the SC pressure and pressure hysteresis. For a single crystal, a thin specimen will avoid the formation of a subgrain structure, disorientation of material regions and will keep the specimen as a single crystal. A very small pressure gradient in the central part of the disc

is a signature of elastic deformation rather than plastic flow.

8. Additional axial displacements, compensating volume decrease and causing plastic straining under a fixed load, promote SC. They can be obtained by
   - reducing the contact friction in the radial direction due to anvil rotation or using some other methods;
   - reducing the yield stress and supporting pressure σ_0 under a fixed applied load, e.g. due to the heating of the whole or external part of a specimen;
   - using the TRIP (RIP) phenomenon during temperature cycling; and
   - using the rotational plastic instability for highly anisotropic materials.

   These methods are especially effective for producing high strength materials. They are opposite to the methods in item 7 and can also be used to avoid elastic straining and stimulate plastic straining in the centre of the disc.
9. A reduction in the dissipative threshold K can be achieved, in addition to the reduction of the yield stress (e.g. by annealing or increasing the grain and subgrain size) by
   - replacing a *martensitic* PT with a *diffusive* PT; and
   - by performing the SC through a liquid phase.
10. A decrease in the energy of internal stresses and, consequently, an increase in the driving force can be achieved by
    - using intermediate liquids or materials with a small yield limit;
    - reducing the interface shear strength τ_s to promote semicoherence or incoherence;
    - reducing the interface tensile strength σ_c or use of intermediate materials (layers) around the places of expected nucleation, e.g. brittle materials with small σ_c or without cohesion to the parent phase or liquid; and
    - choosing parameters such that solid–solid SC occurs near the melting point. In our recent work, we predicted theoretically a new phenomenon, namely that solid–solid transformation with a relatively large transformation strain can occur through virtual melting along the interface at temperatures significantly (more than 100 K) below the melting temperature. Energy of elastic stresses, induced by transformation strain, increases the driving force for melting and reduces the melting temperature. Immediately after melting, stresses relax and unstable melt solidifies. Melt exists during extremely short time sufficient for stress relaxation; we called this state the virtual melt. Thus, virtual melting represents a new mechanism of stress relaxation and loss of coherency at moving solid–solid interface; the threshold $K = 0$ for this mechanism. Theoretical predictions are in agreement with experiments on the $\beta \rightarrow \delta$ transformation in HMX energetic crystal [197], for which $\varepsilon_0 = -0.08$.
11. Macroscopic ways to intensify the SCs include:

- increasing the axial force after some rotation, i.e. search for a loading $P - \varphi_a$ programs;
- using cyclic back-forward rotation;
- using lateral support (e.g. as in belt-type apparatuses) (this will increase σ_0 and the thickness and, consequently, the volume of the transformed material); and
- an increase of deformation rate.

12. For stress-induced SC in a shear band (or surface layer) [6,21,22,26,34] and inclined layer [34] (sections 3.3.2 and 3.3.3), the following regularities have to be taken into account:
    - Applied shear stresses contribute to the yield condition in a way equivalent to the *decrease* in the yield limit and this is one of the mechanisms of an additional increase in the driving force of SC.
    - If a new phase has a yield stress $\sigma_{y2} \geq 2\sigma_{y1}$, shear stresses practically do *not affect* the SC condition.
    - Shear stresses can render the SC *impossible*, if due to the necessity of fulfilling the yield condition for a parent phase, a PT criterion is violated.

    This is in contrast to experiments in RDAC, where the appearance of a strong phase is promoted.

    For strain-induced SC, the additional contribution of defects generated during plastic flow has to be taken into account, e.g. in terms of the strain-controlled kinetics developed in section 3.5.5. Even for stress-induced SC, TRIP or RIP produces a strain-induced contribution. Classical plasticity and RIP (TRIP) can significantly increase the temperature, driving force (if it grows with temperature increase), and accelerate the SC kinetics. If the temperature exceeds the melting temperature, then the appearance of a strong phase through melting can be promoted by shear stresses and strains.
13. Macroscopic stress (pressure) concentrations in the transformation zone can be created:
    - by the compression of a thin layer in Bridgman anvils or DAC;
    - by using another SC with a corresponding transformation strain (e.g. metal melting at PT G–D [34], see section 3.3.1); and
    - by using intermediate materials with a higher elastic moduli (the problem of the G–D PT [34], see section 3.3.1).
14. SC can cause mechanochemical feedback which can be used to control SC. The pressure self-multiplication (self-demultiplication) effect represents positive (negative) mechanochemical feedback which promotes (suppresses) SC. RIP and TRIP induce new nucleation sites which, in turn, promotes SC (autocatalytic effect). They also increase the temperature and represent positive (negative) feedback, if the driving force for SC grows (reduces) with temperature growth. Volume decrease during SC to a high-pressure phase leads to pressure reduction and negative feedback. This may cause the self-regulation phenomenon, similar to that which we revealed for

diamond synthesis [34], see section 3.4.6. Rotational plastic instability [128] causes positive mechanochemical feedback by intensifying plastic flow, compensating volume decrease due to SC, and by increasing the pressure (see section 3.5.9).

15. High pressure allows the plastic straining of materials which are brittle at normal pressure. It also increases the critical stress for dislocation slip. That is why mechanochemical effects may start at some critical pressure and temperature, when SCs is a more preferable relaxation mechanism than fracture and plasticity. Plastic straining creates strong compressive and tensile stress concentrators which can induce both direct and reverse SCs. In such a way, high pressure can promote SCs to low-pressure phases, as in the case with the diamond-to-graphite PT [170]. Strain-induced SC can occur during loading or unloading (at defects created during loading); e.g., PT from phase II to III in Ge and Si occurs during indentation under unloading [171].
16. One of the ways to promote (suppress) strain-induced SC is related to the creation of a microstructure which is favourable (unfavourable) to the appearance of strong defects during plastic deformation. Such a microstructure has to be determined in connection with the mechanism of plastic deformation.

3.6 Concluding remarks

In this chapter, fundamentals of continuum mechanochemistry were conceptually developed. The results obtained are independent of concrete atomistic mechanisms of SC, i.e. they have a universal continuum nature. No one atomistic theory can explain these results, because they are related to the mechanical behaviour of the system of the transforming particle and surrounding materials at the micrometre and larger scale. The continuum approach plays a supplementary role to atomistic theories and reveals new opportunities in the characterization and intensification of SC, as well as the production of new materials.

The first-principles study, which allows us to find energetic barriers and to choose the transformation path at the atomistic level [198, 199], usually uses a constant pressure (or constant volume) approximation. First, non-hydrostatic applied stresses are of interest. Second, stress variation in the transforming region obtained in this chapter (see [34, 128]) can be used in such calculations as input data to find a transformation path for cases which correspond to real experimental situations.

One of the possible ways to bridge atomistic and continuum scales in study of stress- and strain-induced SCs is outlined in the following. The results of atomistic calculations can be used to find parameters for Landau-type theory which then can be used to study the interaction between defects and SCs. In particular, the recently developed Landau theory for a stress-induced martensitic PT [180] was calibrated by known molecular dynamics calculations. Nucleation

on dislocations based on previous versions of the Landau theory were studied in [56, 57].

It is clear that the obtained solutions represent the first approximation only. More detailed finite-element solutions of the same problems will be done in the near future. Macroscopic flow theory has to be substituted by continuum and discrete dislocation theories, depending on the scale. Also, other loading schemes, which are used in practice or physical experiments, have to be analysed. For example, PTs under indentation [170, 171] have the following peculiarities: the averaged plastic strain is relatively small ($q = 0.05$–0.1 for a spherical indenter and $q = 0.02$–0.3 for a conical indenter [40]), so a significant reduction in the PT pressure and a significant amount of a high-pressure phase cannot be expected. As the mean contact pressure $p \simeq 3\sigma_y \simeq 5\tau_y$, then the effect of the macroscopic shear stress is more significant than that in RDAC. One would expect a combination of strain-induced PTs and stress-induced PTs in different regions.

It is evident that there are a number of mechanisms for strain-induced SCs which were not analysed in this chapter. For example, plastic flow can also facilitate PTs due to some dislocation mechanisms of martensite nucleation [13, 15, 54]. For some PTs (e.g. for a bcc–hcp reconstructive PT), the transformation strain is the secondary effect [200]. The primary effect is atomic displacements (shuffles) resulting in a change in the stacking sequence, which can be produced by the dislocations, see, e.g., [13, 15, 54].

We see new perspectives in a combined multiscale experimental and theoretical study of PTs and CRs for various materials in terms of the entire stress and plastic strain tensor history rather than the pressure at the beginning of the PT. The results can be used to find methods to control and facilitate (or suppress) SCs and to synthesize new materials. In addition, specific physical mechanisms of the creation of stress concentrators and nucleation sites in specific materials at various spatial scales have to be studied both experimentally and theoretically.

Acknowledgments

This work was performed by the author during last ten years. In Germany, this work was supported by the Alexander von Humboldt Foundation and Volkswagen Foundation, as well as by German Research Society (DFG), during the work of the author at the Institute for Structural and Computational Mechanics (University of Hannover, Germany). In the USA, the support was obtained from the Texas Tech University, Los Alamos National Laboratory (consulting agreement C-8060 and contract 52844), NSF (CMS-02011108), as well as visiting grants from the Institute for Mechanics and Materials (University of California San Diego). Current collaboration with the author's former group at the Institute for Superhard Materials (Kiev, Ukraine) is supported by the US Department of State through the Science and Technology Center in Ukraine (STCU project 1565). All these supports are very much appreciated.

The author is very much indebted to Professors N V Novikov, E Stein, A V Idesman, G B Olson, M A Meyers and V F Nesterenko, as well as to Drs D L Preston, L N Shvedov, A A Leshchuk and S B Polotnyak for fruitful collaboration and discussions. Discussions with Professors J Hashemi and Y Ma and Drs S G Buga, I A Petrusha and V V Solozhenko were very important for this work. I also would like to thank Professor T D Burton for creating the most favourable environment for my research at TTU.

References

[1] Green H W and Burnley P C 1989 *Nature* **341** 733–737
[2] Kirby S W 1987 *J. Geophys. Res.* **92** 13789–800
[3] Wu T C, Basset W A, Burnley P C and Weathers M S 1993 *J. Geophys. Res.* **98** 19767–76
[4] Boyle V, Frey R and Blake O 1989 *Ninth Symposium (International) on Detonation 1 (OCNR 113291-7, Portland, OR, August 28–September 1)* (Arlington: Naval Research Office)
[5] Coffey C S and Sharma J 2001 *Proc. 11th Int. Detonation Symposium (Snowmass Village, CO)* (Arlington: Naval Research Office) pp 751–7
[6] Levitas V I, Nesterenko V F and Meyers M A 1998 *Acta Mater.* **46** 5929–63
[7] Koch C C 1993 *Nanostruct. Mater.* **2** 109–29
[8] Matteazzi P, Basset D, Miani F and Caer G Le 1993 *Nanostruct. Mater.* **2** 217–29
[9] Bhattacharyya K and Kohn R V 1996 *Acta Mater.* **4** 529–42
[10] Pitteri M and Zanzotto G 2003 *Continuum Models for Phase Transformations and Twinning in Crystals* (New York: Chapman and Hall)
[11] Lin M, Olson G B and Cohen M 1993 *Acta Metall. Mater.* **41** 253–63
[12] Olson G B 1984 *Deformation, Processing and Structure* ed G Krauss (Warrendale, PA: ASM International) pp 391–424
[13] Olson G B and Cohen M 1972 *J. Less-Common Metals* **28** 107
[14] Olson G B and Cohen M 1975 *Metall. Trans.* A **6** 791
[15] Olson G B and Cohen M 1986 *Dislocations in Solids* vol 7, ed F R N Nabarro (Amsterdam: Elsevier Science) pp 297–407
[16] Wayman C M 1964 *Introduction to the Crystallography of Martensitic Transformation* (New York: Macmillan)
[17] Fischer F D, Sun Q-P and Tanaka K 1996 *Appl. Mech. Rev.* **49** 317–64
[18] Mitter W 1987 *Umwandlungsplastizität und ihre Berücksichtigung bei der Berechnung von Eigenspannungen* (Stuttgart, Berlin: Gebrüder Bornträger)
[19] Padmanabhan K A and Dabies G J 1980 *Superplasticity* (Berlin: Springer)
[20] Zackay V F, Parker E R, Fahr D and Busch R 1967 *Trans. Am. Soc. Mater.* **7** 252–9
[21] Levitas V I 1998 *Int. J. Solids Structures* **35** 889–940
[22] Levitas V I 2000 *Int. J. Plasticity* **16** 805–49, 851–92
[23] Idesman A V, Levitas V I and Stein E 1999 *Comput. Meth. Appl. Mech. Eng.* **173** 71–98
[24] Idesman A V, Levitas V I and Stein E 2000 *Int. J. Plasticity* **16** 893–949
[25] Levitas V I, Idesman A V, Olson G B and Stein E 2002 *Phil. Mag.* A **82** 429–62
[26] Levitas V I 1998 *ZAMM Suppl.* **78** S117–20

[27] Levitas V I 1992 *Post-Bifurcation Behaviour in Finite Elastoplasticity. Applications to Strain Localization and Phase Transitions* (Hannover: Universität Hannover. Institut für Baumechanik und Numerische Mechanik, IBNM-Bericht 92/5)
[28] Levitas V I 1995 *Int. J. Eng. Sci.* **33** 921–71
[29] Levitas V I 1998 *J. Mech. Phys. Solids* **46** 557–90
[30] Levitas V I and Stein E 1997 *Mech. Res. Commun.* **24** 309–18
[31] Levitas V I, Idesman A V and Olson G B 1999 *Acta Mater.* **47** 219–33
[32] Levitas V I, Idesman A V and Stein E 2000 *J. Intell. Mater. Syst. Structures* **10** 983–96
[33] Mielke A, Theil F and Levitas V I 2002 *Arch. Rat. Mech. Anal.* **162** 137–77
[34] Levitas V I 1997 *J. Mech. Phys. Solids* **45** 923–47, 1203–22
[35] Levitas V I, Idesman A V and Stein E 1998 *Int. J. Solids Structures* **35** 855–87
[36] Ghosh G and Olson G B 1994 *Acta Metall. Mater.* **42** 3361–70, 3371–9
[37] Blank V D, Konyaev Yu S and Estrin E I 1982 *Zhurnal Tekhnicheskoi Fiziki* **52** 1418–19
[38] Blank V D, Konyaev Y S, Osipova V T and Estrin E I 1983 *Inorg. Mater.* **19** 72–6
[39] Estrin E I 1993 *Phase Transformation of Martensitic Type*, ed V V Nemoshkalenko (Kiev: Naukova Dumka) pp 110–39
[40] Levitas V I 1996 *Large Deformation of Materials with Complex Rheological Properties at Normal and High Pressure* (New York: Nova Science)
[41] Hornbogen E 1997 *Int. Conf. on Displacive Phase Transitions and their Application in Material Engineering* ed K Mukherjee *et al* (TMS) pp 27–35
[42] Spielfeld J and Hornbogen E 1998 *IUTAM Symposium 1997* ed O T Bruhns and E Stein (Bochum: Kluwer Academic) pp 325–34
[43] Spielfeld J, Hornbogen E and Franz M 1998 *Proc. European Symposium on Martensitic Transformation. ESOMAT 1997* ed J Beyer, A Böttger and J Muller (Enschede) pp 239–44
[44] Treppmann D and Hornbogen E 1998 *European Symposium on Martensitic Transformation. ESOMAT 1997* ed J Beyer, A Böttger and J Muller (Eschede: J. de Physique IV) pp 211–20
[45] Theil F and Levitas V I 2000 *Math. Mech. Solids* **5** 337–68
[46] Lifshitz I M and Gulida L S 1952 *Dokl. Akad. Nauk SSSR* **87** 377–80
[47] Roitburd A L and Temkin D E 1986 *Sov. Phys. Solid State* **28** 432–6
[48] Bar'yachtar V G, Enilevskiy S G, Tokiy V V and Jablonsky D A 1986 *Sov. Phys. Solid State* **28** 1303–10
[49] Kaganova I M and Roitburd A L 1989 *Sov. Phys. Solid State* **31** 545–50
[50] Fischer F D, Berveiller M, Tanaka K and Oberaigner E 1994 *Arch. Appl. Mech.* **64** 54–85
[51] Marketz F and Fischer F D 1994 *Modelling Simul. Mater. Sci. Eng.* **2** 1017–46
[52] Marketz F and Fischer F D 1994 *Comput. Mater. Sci.* **3** 307
[53] Marketz F and Fischer F D 1995 *Metall. Mater. Trans.* A **26** 267–78
[54] Olson G B and Cohen M 1976 *Metall. Trans.* A **7** 1897–904
[55] Olson G B and Roytburd A L 1995 *Martensite* ed G B Olson and W S Owen (The Materials Information Society) ch 9, pp 149–74
[56] Boulbitch A A and Toledano P 1998 *Phys. Rev. Lett.* **81** 838
[57] Reid A C E, Olson G B and Moran B 1998 *Phase Trans.* **69** 309–28
[58] Levitas V I 1995 *J. Physique III* **5** 173–8
[59] Levitas V I 1995 *Mech. Res. Commun.* **22** 87-94

[60] Levitas V I 1995 *J. Physique III* **5** 41–6
[61] Levitas V I 1996 *Mech. Res. Commun.* **23** 495–503
[62] Levitas V I 1996 *J. Physique III* **6** 55–64
[63] Haezebrouck D M 1987 *Doctoral Thesis* (Evanston: Northwestern University, Materials Research Center, Steel Research Group)
[64] Kaganova I M and Roitburd A L 1987 *Sov. Phys. Solid. State* **29** 800–3
[65] Arutyunyan N Kh and Drosdov A D 1992 *Int. J. Solids Structures* **29** 783–97
[66] Kondaurov V I and Nikitin L V 1986 *Mech. Solids* **21** 130–9
[67] Eshelby J D 1970 *Inelastic Behaviour of Solids* ed M F Kanninen *et al* (New York: McGraw-Hill) pp 77–115
[68] Levitas V I 1992 *Thermomechanics of Phase Transformations and Inelastic Deformations in Microinhomogeneous Materials* (Kiev: Naukova Dumka)
[69] Cherkaoui M, Berveiller M and Sabar H 1998 *Int. J. Plasticity* **14** 597–626
[70] Cherkaoui M and Berveiller M 2000 *Arch. Appl. Mech.* **70** 159–81
[71] Fischer F D and Reisner G 1998 *Acta Mater.* **46** 2095–102
[72] Fischer F D, Reisner G, Werner E, Tanaka K, Cailletaud G and Antretter T 2000 *Int. J. Plasticity* **16** 723–48
[73] Levitas V I 2002 *Int. J. Plasticity* **18** 1499–525
[74] Patel J R and Cohen M 1953 *Acta Metall.* **43** 531–8
[75] Ganghoffer J F, Denis S, Gautier E, Simon A, Simonsson K and Sjöström S 1991 *J. Physique III* **1** 83–8
[76] Wen Y H, Denis S and Gautier E 1999 *Proc. IUTAM Symposium on Micro- and Macrostructural Aspects of Thermoplasticity (Bochum, 25–29 August 1997)* ed O T Bruhns and E Stein, pp 335–44
[77] Boguslavskiy Yu Ya 1985 *Solid State. Phys.* **27** 140–3
[78] Christian J W 1965 *The Theory of Transformation in Metals and Alloys* (Oxford: Pergamon)
[79] Roitburd A L 1972 *Sov. Phys.–JEPT* **15** 300–2
[80] Grinfeld M A 1991 *Thermodynamic Methods in the Theory of Heterogeneous Systems* (Sussex: Longman)
[81] Leo P H and Sekerka R F 1989 *Acta. Metall.* **37** 3119–38
[82] Cermelli P and Gurtin M E 1994 *Acta Metall. Mater.* **42** 3349–59
[83] Levitas V I 1990 *Ukrainian SSR Acad. Sci.* A **8** 41–6
[84] Raniecki B and Bruhns O 1991 *Arch. Mech.* **43** 343–76
[85] Bhattacharyya A and Weng G J 1994 *J. Mech. Phys. Solids* **42** 1699–724
[86] Levitas V I 1996 *Proc. IUTAM Symposium (Paris)* ed A Pineau and A Zaoui (Boston and London: Kluwer Academic Publishers) pp 313–20
[87] Petryk H 1998 *J. Mech. Phys. Solids* **46** 873–94
[88] Leblond J B, Devaux J and Devaux J C 1989 *Int. J. Plasticity* **5** 551–91
[89] Simonsson K 1995 *Micromechanical FE-Simulations of the Plastic Behaviour of Steels Undergoing Martensitic Transformation* (Linköping: Dissertation no 362)
[90] Stringfellow R G, Parks D M and Olson G B 1992 *Acta Metall. Mater.* **40** 1703–16
[91] Diani J M and Parks D M 1998 *J. Mech. Phys. Solids* **46** 1613–35
[92] Cherkaoui M and Berveiller M 2000 *Smart Mater. Structures* **9** 592–603
[93] Olson G B 1996 *J. Physique III* **6** 407–18
[94] Levitas V I and Stein E (ed) 2000 Phase transitions and other structural changes in inelastic materials *Int. J. Plasticity* **16** special issue

[95] Levitas V I and Cherkaoui M (ed) 2002 Physics and mechanics of phase transformations *Int. J. Plasticity* **18** special issue
[96] Bundy F P 1989 Behaviour of elemental carbon up to very high temperatures and pressures *High Pressure Science and Technology, Proc. XI AIRAPT Int. Conf.* vol 1, ed N V Novikov (Kiev: Naukova Dumka) pp 326–36
[97] Kurdyumov A V 1980 *Superhard Materials* ed I N Franzevich (Kiev: Naukova Dumka) pp 131–66
[98] Novikov N V, Fedoseev D V, Shul'zhenko A A and Bogatireva G P 1987 *Diamond Synthesis* (Kiev: Naukova Dumka)
[99] Bell J F 1973 *The Experimental Foundations of Solid Mechanics (Handbuch der Physik VIa/1)* (Berlin: Springer)
[100] Vereshchagin L F and Zubova E V 1960 *Dokl. Acad. Sci. USSR* **134** 787–8
[101] Shul'zhenko A A *et al* 1977 *Effect of High Pressure on Substances* (Kiev: Institute of Problems of Materials Science) pp 113–17
[102] Leshchuk A A, Novikov N V and Levitas V I 2002 *J. Superhard Mater.* **1** 49–57
[103] Nesterenko V F, Meyers M A, Chen H C and LaSalvia J C 1994 *Appl. Phys. Lett.* **65** 3069–71
[104] Nesterenko V F, Meyers M A, Chen H C and LaSalvia J C 1995 *Metall. Mater. Trans.* A **26** 2511–19
[105] Thadhani N N, Graham R A, Royal T, Dunbar E, Anderson M U and Holman G T 1997 *J. Appl. Phys.* **82** 1113–28
[106] Mura T 1987 *Micromechanics of Defects in Solids* (Dordrecht: Martinus Nijhoff)
[107] Datta R, Ghosh G and Raghavan V 1986 *Scripta Metall.* **20** 559–63
[108] Ghosh G and Raghavan V 1986 *Mater. Sci. Eng.* **79** 223–31
[109] Novikov N V, Levitas V I, Leshchuk A A and Idesman A V 1991 *High Pressure Res.* **7** 195–7
[110] Novikov N V, Levitas V. I and Shestakov S I 1991 *Strength Mater.* **6** 635–52
[111] Prikhna A I, Maslenko Y S, Myasnikov E P and Belousov I S 1978 *Effect of High Pressure on Substance* (Kiev: Naukova Dumka) pp 103–8
[112] Idesman A V and Levitas V I 1995 *Comput. Meth. Appl. Mech. Eng.* **126** 39–66
[113] Levitas V I, Idesman A V, Leshchuk A A and Polotnyak S B 1989 *High Pressure Science and Technology, Proc. XI AIRAPT Int. Conf.* vol 4, ed N V Novikov (Kiev: Naukova Dumka) pp 38–40
[114] Novikov N V, Levitas V I, Leshchuk A A and Idesman A V 1988 *Dokl. Ukrainian SSR Acad. Sci.* A **7** 40–3
[115] Novikov N V, Levitas V I and Idesman A V 1990 *High Pressure Res.* **5** 868–70
[116] Leshchuk A A, Novikov N V and Levitas V I 2001 *Strength Mater.* **33** 277–92
[117] Panin V E, Likhachev V A and Grinjaev J V 1985 *Structural Levels of Deformation of Solids* (Novosibirsk: Nauka)
[118] Gilman J J 1994 *High Pressure Science and Technology—1993*, ed S C Schmidt *et al* (New York: AIP) pp 1349–52
[119] Gilman J J 1995 *Phil. Mag.* B **71** 1057–68
[120] Gilman J J 1995 *Metal–Insulator Transitions Revisited* ed P P Edwards and C N R Rao (London: Taylor and Francis) pp 269–84
[121] Gilman J J 1996 *Science* **274** 65
[122] Dremin A N and Bruesov O N 1968 *Russ. Chem. Rev.* **37** 392–402
[123] Graham R A 1989 *Proc. 3rd Int. Symposium on Dynamic Pressures* (France: La Grande Motte)

[124] Boldyrev V V 1993 *Solid State Ionics* **63–65** 537–43
[125] Zharov A A 1984 *Usp. Khimii* **53** 236–50
[126] Levitas V I, Polotnyak S B and Idesman A V 1996 *Strength Mater.* **3** 221–7
[127] Novikov N V, Polotnyak S B, Shvedov L K and Levitas V I 1999 *Superhard Mater.* **3** 39–51
[128] Levitas V I and Shvedov L K 2002 *Phys. Rev.* B **65** 104109
[129] Novikov N V, Petrusha I A, Shvedov L K, Polotnyak S B, Dub S N and Shevchenko S A 1999 *Diamond Related Mater.* **8** 361–3
[130] Levitas V I 2003 *Phys. Rev.* B submitted
[131] Bridgman P W 1935 *Phys. Rev.* **48** 825–47
[132] Bridgman P W 1937 *Proc. Am. Acad. Arts Sci.* **71** 387
[133] Bridgman P W 1947 *J. Chem. Phys.* **15** 311–13
[134] Enikolopyan N S 1985 *Pure Appl. Chem.* **57** 1707
[135] Enikolopyan N S, Mkhitaryan A A, Karagezyan A S and Khzardzhya A A 1987 *Dokl. Akad. Nauk SSSR* **292** 887
[136] Enikolopyan N S 1989 *Russ. J. Phys. Chem.* **63** 1261
[137] Zharov A A 1989 *High Pressure Science and Technology, Proc. XI AIRAPT Int. Conf.* vol 1, ed N V Novikov (Kiev: Naukova Dumka) pp 377–80
[138] Zharov A A 1994 *High Pressure Chemistry and Physics of Polymers* ed A L Kovarskii (Boca Raton, FL: Chemical Rubber Company) ch 7, pp 267–301
[139] Vereschagin L F, Zubova E V, Burdina K P and Aparnikov G L 1971 *Dokl. Akad. Nauk SSSR* **196** 81–2
[140] Aksenenkov V V, Blank V D, Golubev A S, Konyaev Yu S, Kuznetsov A I and Estrin E I 1980 *Diamonds Superhard Mater.* **7** 3–5
[141] Aksenenkov V V, Blank V D, Borovikov N F, Danilov V G and Kozorezov K I 1994 *Dokl. Akad. Nauk. SSSR* **338** 472–6
[142] Aleksandrova M M, Blank V D, Golobokov A E, Konyaev Yu S and Estrin E I 1987 *Solid State Phys.* **29** 2573–8
[143] Alexandrova M M, Blank V D, Golobokov A E and Konyaev Yu S 1988 *Sov. Phys. Solid State* **30** 577–9
[144] Alexandrova M M, Blank V D and Buga S G 1993 *Solid State Phys.* **35** 1308–17
[145] Batsanov S S, Serebryanaya N R, Blank V D and Ivdenko V A 1995 *Crystallography Rep.* **40** 598–603
[146] Blank V D, Boguslavski Yu Ya, Eremetz M I, Izkevich E S, Konyaev Yu S, Shirokov A M and Estrin E I 1984 *Sov. Phys.–JEPT* **87** 922–6
[147] Blank V D, Boguslavski Yu Ya, Buga S G, Itskevich E S, Konyaev Yu S and Shirokov A M 1989 *High Pressure Science and Technology, Proc. XI AIRAPT Int. Conf.* vol 4, ed N V Novikov (Kiev: Naukova Dumka) pp 64–6
[148] Blank V D and Buga S G 1993 *Instrum. Exp. Techniques* **36** 149
[149] Blank V D, Buga S G, Serebryanaya N R, Denisov V N, Dubitsky G A, Ivlev A N, Mavrin B N and Popov M Yu 1995 *Phys. Lett.* A **205** 208–16
[150] Blank V D, Dubitsky G A, Plotyanskaya S A 1995 High pressure science and technology *Proc. Joint XV AIRAPT and XXXIII EHPRG International Conf. (Warsaw)* ed W A Trzeciakowski (London: World Scientific Publishing) pp 325–7
[151] Blank V D, Malyushitska Z H and Kulnitskiy B A 1993 *High Pressure Phys. Eng.* **3** 28–35
[152] Blank V D, Popov M, Buga S G, Davydov V, Denisov V N, Ivlev A N, Mavrin B N, Agafonov V, Ceolin R, Szwarc H and Passat A 1994 *Phys. Lett.* A **188** 281–6

[153] Blank V D, Serebryanaya N R, Vorontsov A A and Zerr A Yu 1993 *High Pressure Phys. Eng.* **3** 36–9
[154] Buga S G and Blank V D 1993 *High Pressure Phys. Eng.* **3** 40–6
[155] Levitas V I, Hashemi J, Mathis W, Holtz M and Ma Y 2002 *Brookhaven National Laboratory Year Book*
[156] Ma Y, Levitas V I, Hashemi J, Mathis W and Holtz M 2002 *Brookhaven National Laboratory Year Book*
[157] Novikov N V, Shvedov L K, Levitas V I, Petrusha I A and Polotnyak S B 2000 *Synthesis, Sintering and Properties of Superhard Materials* ed A A Shulzhenko (Kiev: Material Science Serial, Institute for Superhard Materials) pp 131–44
[158] Pruzan Ph, Chervin J C, Thiery M M, Itie J P, Besson J M, Forgerit J P and Revault M 1990 *J. Chem. Phys.* **92** 6910–15
[159] Chistotina N P, Zharov A A, Kissin Yu V and Enikolopyan N S 1970 *Dokl. Akad. Nauk. SSSR* **191** 632–4
[160] Chistotina N P, Zharov A A, Matveev M G and Zhulin V M 1983 *Dokl. Akad. Nauk. SSSR* **269** 648–51
[161] Dachille F and Roy R 1964 *Modern High Pressure Technique* (Moscow: Mir) pp 256–83
[162] Moffitt C E, Chen B, Wieliczka D M and Kruger M B 2000 *Solid State Commun.* **116** 631–6
[163] Tang Z P, Li X Z, Zhou G Q and Lin S B 1993 *High Pressure Science and Technology* Part 1, ed S C Schmidt *et al* (New York: AIP) pp 327–9
[164] Ogibalov P M and Kiyko I A 1962 *Notes on High Parameters Mechanics* (Moscow University)
[165] Serebryanaya N R, Blank V D and Ivdenko V A 1995 *Phys. Lett.* A **197** 63–6
[166] Bokarev V P, Bokareva O M, Tempizky I I and Batsanov S S 1986 *Solid State Phys.* **28** 813–16
[167] Matveev M G, Zharov A A, Zhulin V M and Zhuravleva E B 1983 *Sov. Phys. Dokl.* **270** 1156–9
[168] Hirth J P and Lothe J 1992 *Theory of Dislocations* (Malabar, FL: Krieger)
[169] Meyers M A, Vohringer O and Lubarda V A 2001 *Acta Mater.* **49** 4025–39
[170] Gogotsi Y G, Kailer A and Nickel K G 1999 *Nature* **401** 663–4
[171] Kailer A, Gogotsi Y G and Nickel K G 1997 *J. Appl. Phys.* **81** 3057–63
[172] Goncharov A F, Gregoryanz E, Hemley R J and Mao H K 2001 *Proc. National Academy of Sciences of the United States of America* **98** pp 14234–7
[173] Loubeyre P, Occelli F and LeToullec R 2002 *Nature* **416** 613–17
[174] Narayana C, Luo H, Orloff J and Ruoff A L 1998 *Nature* **393** 46–9
[175] Thomsen E G, Yang Ch T and Kobayashi Sh 1965 *Mechanics of Plastic Deformation in Metal Processing* (New York: Macmillan)
[176] Buga S G 2002 Private communication
[177] Bridgman P W 1952 *Studies in Large Plastic Flow and Fracture* (New York)
[178] Hill R 1950 *Mathematical Theory of Plasticity* (Oxford: Clarendon)
[179] Lubliner J 1990 *Plasticity Theory* (New York: Macmillan)
[180] Levitas V I and Preston D L 2002 *Phys. Rev.* B **66** 134206 (9) and 134206 (15)
[181] Rogueda C, Lexcellent C and Bocher L 1996 *Arch. Mech.* **48** 1025–45
[182] Sun Q P and Hwang K C 1993 *J. Mech. Phys. Solids* **41** 1–33
[183] Tanaka K and Nishimura F 1998 *Metals Mater.* **4** 554–61
[184] Yamada K, Burkhard G, Tanabe Y, Sawaoka A B 1999 *Carbon* **37** 275

[185] Mao Ho-kwang and Hemley R J 1998 *Ultrahigh-Pressure Mineralogy: Physics and Chemistry of the Earth's Deep Interior. Reviews in Mineralogy* vol 37, ed R J Hemley (Washington, DC: Mineralogical Society of America) pp 1–32
[186] Weidner D J 1998 *Ultrahigh-Pressure Mineralogy: Physics and Chemistry of the Earth's Deep Interior. Reviews in Mineralogy* vol 37, ed R J Hemley (Washington, DC: Mineralogical Society of America) pp 493–524
[187] Merkel S, Hemley R J and Mao H K 1999 *Appl. Phys. Lett.* **74** 656–8
[188] Moss W C, Hallquist J O, Reichlin R, Goettel K A and Martin S 1986 *Appl. Phys. Lett.* **48** 1258–60
[189] Novikov N V, Levitas V I, Polotnyak S B and Potyomkin M M 1991 *High Pressure Res.* **8** 507–9
[190] Novikov N V, Levitas V I, Polotnyak S B and Potyomkin M M 1994 *Strength Mater.* **26** 64–9
[191] Hemley R J, Mao H K, Shen G, Bardo J, Gillet Ph, Hanfland M and Häusermann D 1997 *Science* **276** 1242–5
[192] Ueno M, Hasegawa K, Oshima R, Onodera A, Shimomura O, Takemura K, Nakae H, Matsuda T and Hirai T 1992 *Phys. Rev.* B **45** 10226
[193] Piermarini G J, Block S, Barnett J D and Forman R A 1975 *J. Appl. Phys.* **46** 2774
[194] Solozhenko V L 2000 Private communication
[195] Solozhenko V L 1995 *High Pressure Res.* **13** 199
[196] Britun V F and Kurdyumov A V 2000 *High Pressure Res.* **17** 101–11
[197] Henson B F, Smilowitz L, Asay B W and Dickson P M 2002 *J. Chem. Phys.* **117** 3780–8
[198] Tateyama Y, Ogitsu T, Kusakabe K, Tsuneyuki S 1996 *Phys. Rev.* B **54** 14994
[199] Tateyama Y, Ogitsu T, Kusakabe K, Tsuneyuki S, Itoh S 1997 *Phys. Rev.* B **55** 10161
[200] Sanati M, Saxena A, Lookman T and Alberts R C 2001 *Phys. Rev.* B **63** 224114